EFFECTS OF PORE-SCALE VELOCITY AND PORE-SCALE PHYSICAL PROCESSES ON CONTAMINANT BIODEGRADATION DURING TRANSPORT IN GROUNDWATER: MODELING AND EXPERIMENTS

A Dissertation

by

ITZA MENDOZA SANCHEZ

Submitted to the Office of Graduate Studies of
Texas A&M University
in partial fulfillment of the requirements for the degree of

DOCTOR OF PHILOSOPHY

December 2007

Major Subject: Civil Engineering

EFFECTS OF PORE-SCALE VELOCITY AND PORE-SCALE PHYSICAL PROCESSES ON CONTAMINANT BIODEGRADATION DURING TRANSPORT IN GROUNDWATER: MODELING AND EXPERIMENTS

A Dissertation

by

ITZA MENDOZA SANCHEZ

Submitted to the Office of Graduate Studies of
Texas A&M University
in partial fulfillment of the requirements for the degree of

DOCTOR OF PHILOSOPHY

Approved by:

Co-Chairs of Committee,	Robin L. Autenrieth
	Jeffrey A. Cunningham
Committee Members,	Jennifer T. McGuire
	Hongbin Zhan
Head of Department,	David Rosowsky

December 2007

Major Subject: Civil Engineering

ABSTRACT

Effects of Pore-Scale Velocity and Pore-Scale Physical Processes on Contaminant Biodegradation during Transport in Groundwater: Modeling and Experiments. (December 2007)

Itza Mendoza Sanchez, B.S., Instituto Politécnico Nacional;

M.S., Texas A&M University

Co-Chairs of Advisory Committee: Dr. Robin L. Autenrieth
Dr. Jeffrey A. Cunningham

Contamination of surface and ground water has emerged as one of the most important environmental issues in developed and developing countries. Bioremediation of groundwater takes advantage of bacteria present in the environment to transform toxic compounds to non-toxic metabolites. This biotechnology holds the potential for fast, inexpensive, and effective water decontamination. However, it is still poorly understood and usually not fully controlled due to the lack of information describing the natural phenomena involved. Therefore, a better understanding of the phenomena involved during bioremediation of groundwater could help in the design and implementation of more efficient technologies.

The main objective of the present research is to assess how pore-scale physical factors, such as pore-scale velocity, affect the degradation potential of contaminants

during transport in groundwater. The target chemicals studied were chlorinated ethenes because they are commonly found in contaminated groundwater sites.

To achieve the research objective, the following were employed: a mathematical model that links pore scale processes to the macro-scale representation of contaminant transport; development of numerical tools to solve the mathematical model; and experimental elucidation of the influence of pore-scale flow velocity on the biodegradation of contaminants using column experiments. Results from the mathematical model and experiments were used to elucidate the inter-relationship between physical and biological phenomena at the micro scale. The influence of flow velocity through the porous media (a physical factor) on the biological structure (microbial community in the porous media) was assessed.

The results of this investigation contribute to the bioremediation of contaminated groundwater understanding with new insights on the importance of physical transport factors on the biodegradation potential. For example, flow velocity is shown to have an important effect on the degradation potential of chlorinated ethenes. Additionally, the mathematical model and numerical tools have potential application to many other reactive transport problems, including: adsorption onto activated carbon, reaction in packed beds of catalyst, chemical transport in streambeds, and separation in chromatographic columns.

DEDICATION

A Elvis por poseer el arte de reconstruir mis silencios.

A Susana, Abel y Pablo por estar siempre presentes.

ACKNOWLEDGMENTS

I would like to thank Dr. Cunningham under whose direction this research was possible. Even though he was appointed at the University of South Florida, I was never left without his support and guidance. I would like to extend my gratitude to Dr. Autenrieth for her professional guidance along with a number of pleasant conversations ranging from environmental issues to personal objectives in life.

I want to extend my appreciation to: Dr. McDonald for providing many valuable insights on the development of analytical techniques; Dr. McGuire and Erik W. Smith who provided crucial assistance during the experimental phase of this project; Dr. Zhan for helpful discussions that guided the proposal of this research; and Dr. Chang-Ping who offered priceless laboratory supervision for the DNA extraction.

The author would like to thank SiREM Labs for providing the KB-1® culture used in this research. Special thanks go to Sandra Dworatzek, Phil Dennis, and Elizabeth Ney for their technical advice and assistance in the DGGE and quantitative PCR analysis.

I would like to thank to the following sources for their financial support: Consejo Nacional de Ciencia y Tecnología (CONACYT), México; Instituto Politécnico Nacional (IPN), Ciudad de México, México; and the U. S. Geological Survey (USGS) through the Texas Water Resources Institute (TWRI).

TABLE OF CONTENTS

Page

CHAPTER Page

CHAPTER Page

LIST OF FIGURES

FIGURE Page

FIGURE Page

FIGURE Page

LIST OF TABLES

CHAPTER I

INTRODUCTION

Problem Description

Contamination of groundwater has emerged as one of the most important environmental issues in developed and developing countries (N.A.S. 1999, 2000). To guarantee water supply for both urban and rural areas, it is necessary to develop cost-effective remediation technologies (N.R.C. 2000). Cost-effective bioremediation technologies are of potential interest to guarantee a sustainable supply of clean water in the future (Singleton 1994; Suflita et al. 1988). Many bioremediation technologies are relatively inexpensive (Okoh and Trejo-Hernandez 2006); however, they remain empirically controlled due to a lack of understanding of the phenomena involved (E.P.A. 1998). Therefore, a better understanding of the processes controlling biodegradation in porous media could improve the design and implementation of more efficient technologies.

Physical and biological processes interact at the pore scale to control biodegradation in groundwater (Hall et al. 2005). Biological processes may include microbial attachment to the solid grains (Gargiulo et al. 2007), growth, and decay (Sandrin et al. 2001, Horn et al. 2003). Physical processes at the pore scale may include diffusion of the target contaminant from the mobile fluid through biofilm-coated aquifer solids (Cabirol et al. 1998; Overmiere et al. 1994) and sorption/desorption of contaminants into or out of aquifer solids (Karapanagioti et al. 2001). Transport factors at the pore scale, such as groundwater pore flow velocity, affect some physical and

---

This dissertation follows the style of Transport in Porous Media.

biological processes, and consequently may influence the biodegradation potential of contaminants in groundwater. Thus it is necessary to develop an effective way to evaluate the interaction of physical factors with physical and biological processes at the pore scale.

Groundwater flow velocity is an important physical factor that could control biodegradation potential of contaminants. It is well known that the flow velocity can change due to heterogeneity of the soils at scales that are small relative to the overall spatial scale of the aquifer. It is also known that the microbial composition could have a great variation along small spatial and temporal scales, leading to changes in biodegradation potential over time and space. However it is not known what effect flow velocity can have on the biodegradation potential of contaminants in the groundwater. Filling this gap is a requisite to better understand the phenomenon of biodegradation in groundwater, and therefore attain more efficient bioremediation technologies in groundwater.

In order to determine the effect of flow velocity or other physical factors on biodegradation, we must have a conceptual and/or mathematical framework to interpret experimental observations. Therefore, development and solution of mathematical models that account for pore-scale physical and biological processes during contaminant transport and biodegradation are necessary. Unfortunately, most existing mathematical models for contaminant fate and transport in groundwater are defined at the macro-scale, i.e., at spatial scales larger than a single pore or grain of aquifer material. In such models, mathematical descriptions of chemical reactions depend upon concentrations

defined at similar scales. For contaminants that undergo biologically-mediated degradation, the actual reaction process depends upon diffusion and reaction in pore-scale biofilms or bacterial colonies (Williamson and McCarty 1976). Thus, existing models for contaminant fate and transport are not sufficient to determine how flow velocity or other physical factors affect biodegradation. There remains a need to evaluate how we can or should account for biodegradation in macroscopic models of contaminant transport. By providing such a modeling framework, the effect of physical transport factors on pore-scale physical and biological processes can then be more easily evaluated.

Hypothesis, Objective, and Goals

The present research sought to improve understanding of the processes controlling biodegradation in groundwater. The **main objective** of the present research was ***to elucidate the degree to which physical and biological phenomena interact at the pore scale during bioremediation of groundwater***. With this main objective, one important goal was to evaluate if the pore flow velocity is a controlling process on the degradation potential of contaminants in groundwater. The rationale for asking this question is that biodegradation in groundwater occurs inside biofilms that coat the aquifer grains (Rittmann 1993). Accordingly, the degree of contaminant degradation is likely to be a function of both the chemical mass transfer from the bulk solution to the surface of the biofilm and the structure of the active biofilm layer. Chemical mass transfer depends on the thickness of a stagnant layer formed immediately adjacent to the surface of the

biofilm, the diffusion layer. The structure of the active biofilm layer will depend on the chemical bioavailability and bacterial adherence characteristics. The physical factor of groundwater flow velocity may control the degradation potential of contaminants because it influences two important structures at the microscopic (biofilm) scale: 1) the thickness of the diffusion layer, and 2) the biofilm structure. Therefore one *hypothesis* of the research project is that ***flow velocity is an important factor controlling the biodegradation potential of groundwater systems.***

The main objective of this research will be accomplished through the three following *specific goals*:

1. **Development of a mathematical model that links pore-scale processes to the macro-scale representation of contaminant transport.**
2. **Development of efficient numerical approaches to solve the mathematical model.**
3. **Experimental elucidation of the influence of pore-scale flow velocity on the biodegradation of contaminants using column experiments.**

Dissertation Overview

This dissertation is composed of six chapters. Two of them have already been published as papers in peer-reviewed journals; two more will be submitted for publication; and two of them comprise an introduction and a summary and conclusions of the research. The content of each chapter is summarized below.

Chapter I introduces the problem description and states the hypothesis, objective, and goals of the research.

Chapter II, "Equivalence of two models for biodegradation during contaminant transport in groundwater," was published by Jeff Cunningham and Itza Mendoza-Sanchez in *Water Resources Research* 42, W02416, doi: 10.1029/2005WR004205.2006. This chapter is reproduced by permission of American Geophysical Union. It provides a theoretical foundation for how we can account for biodegradation in macroscopic models of contaminant transport, under certain conditions.

Chapter III, "Efficient algorithm for modeling transport in porous media with mass exchange between mobile fluid and reactive stationary media," was published by Itza Mendoza-Sanchez and Jeff Cunningham in *Transport in Porous Media* 68, 285-300, doi: 10.1007/s11242-006-9047-6 2007. This chapter is reproduced with kind permission of Springer Science and Business Media. It describes an algorithm for efficient numerical solution of the mathematical model when biodegradation kinetics are linear.

Chapter IV, "Modeling multispecies non-linear reactive transport in porous media with mass exchange between mobile fluid and stationary medium," will be submitted for publication. This chapter evaluates the applicability of a novel numerical approach to solve the mathematical model when biodegradation kinetics are nonlinear.

Chapter V, "Pore velocity effect on contaminant transport and degradation in porous media," will be submitted for publication. This chapter evaluates the effect of flow velocity on the degradation potential of chlorinated ethenes. Chlorinated ethenes have been chosen because they are common groundwater contaminants. Another reason for

the use of chlorinated ethenes is that incomplete dechlorination is commonly found at contaminated sites. In this chapter, the effects of flow velocity on the potential for dechlorination of cis-dichloroethene have been evaluated.

Chapter VI provides a summary and conclusions of the overall research, discusses the importance of this research in the understanding of bioremediation of groundwater, and provides suggestions for recommended future research.

CHAPTER II

EQUIVALENCE OF TWO MODELS FOR BIODEGRADATION DURING CONTAMINANT TRANSPORT IN GROUNDWATER*

Overview

In this chapter, two models are compared that have been used frequently for describing biodegradation during contaminant transport in groundwater. One is a "simple" model based upon macroscopic properties only, and the other is a "biofilm" model that accounts for contaminant diffusion and reaction in biofilms. Although the simple model has been used frequently, its mathematical formulation appears inadequate to describe the physics of the biodegradation process. Hence, it is unclear when the simple model should be considered valid, and analyses predicated upon the simple model are called into question. This issue is resolved by arguing that the simple model should be considered valid when it is mathematically equivalent to the conceptually superior biofilm model. It is demonstrated that the two models are exactly equivalent at the macroscopic scale when steady-state conditions prevail. Under these conditions, the equivalent macroscopic degradation rate coefficient k can be related to microscopic rate parameters that describe mass transfer across a boundary layer, diffusion within the biofilm, and reaction within the biofilm. Under transient (non-steady-state) conditions, the two models are not strictly equivalent. However, the error between the two models is negligible in certain cases. In particular, when the rate-limiting step for

* Reproduced by permission of American Geophysical Union. Cunningham J.A. and Mendoza-Sanchez I., Equivalence of two models for biodegradation during contaminant transport in groundwater, Water Resources Research, 42, 2, W02416, 2006.

biodegradation is either mass transfer across the boundary layer or diffusion within the biofilm, there is no distinguishable difference between the predictions of the two models. Thus, this chapter can be considered a theoretical foundation for use of the commonly-employed simple biodegradation model, as well as an elucidation of the conditions for its validity.

Introduction

Biodegradation is one of the most important processes affecting contaminant fate and transport in groundwater. Not surprisingly, then, numerous models have been developed for describing or modeling biodegradation during contaminant transport. For example, consider the equation

$$n\frac{\partial C(x,t)}{\partial t} = nD\frac{\partial^2 C(x,t)}{\partial x^2} - nv\frac{\partial C(x,t)}{\partial x} - nk_{\max}\frac{C(x,t)}{C(x,t)+K_M} \qquad (1)$$

which describes the transport of a contaminant subject to the processes of dispersion, advection, and biodegradation (the three terms on the right-hand side, respectively). In this equation, it is assumed that the rate of contaminant biodegradation follows a Michaelis-Menten kinetic expression (similar to a Monod kinetic expression [cf. Michaelis and Menten 1913; Monod 1949; see also El-Farhan et al. 1998]). The parameter n is porosity, C is the concentration of the contaminant in the groundwater, D is a dispersion coefficient, v is the groundwater velocity, and k_{max} and K_M are parameters of the Michaelis-Menten rate expression. For simplicity, in Eq. 1 it is assumed that transport is primarily one-dimensional in the x-direction. Equation 1 could be modified

to include, for instance, the dependence of the biodegradation kinetics on the concentration of an electron acceptor or electron donor [e.g., Celia et al. 1989; MacQuarrie et al. 1990; Murphy et al. 1997; Oya and Valocchi 1997; Brusseau et al. 1999]. Here it is assumed that such a modification is not needed; this assumption is valid if, for instance, the contaminant is the rate-limiting substrate of the biodegradation process.

In the commonly-occurring case that contaminant concentrations are relatively low, that is, $C(x,t) << K_M$, Eq. 1 simplifies to

$$n\frac{\partial C(x,t)}{\partial t} = nD\frac{\partial^2 C(x,t)}{\partial x^2} - nv\frac{\partial C(x,t)}{\partial x} - nkC(x,t) \qquad (2)$$

where the parameter k is a first-order biodegradation rate constant, equal to k_{max}/K_M. Eqs. 1 and 2, or close analogs thereof, have been used countless times to describe or predict contaminant transport with biodegradation (Brusseau et al. 1992; Bekins et al. 1998; Bjerg et al. 1996; Chang et al. 1999; Fry and Istok 1994; Miralles-Wilhem and Gelhar 1996; Sun and Lu 2005; Sun et al. 2004; Zhang and Woodbury 2002).

There is a potential problem with this approach. In Eqs. 1 and 2, the rate of contaminant degradation is considered proportional to the aqueous concentration $C(x,t)$. The problem with this representation is that, in most cases, biodegradation occurs not in the bulk aqueous phase, but rather inside an active biofilm or bacterial colony. That is, active bacteria grow in an aquifer and form colonies or biofilms, usually attached to the grains of geologic material that comprise the aquifer (Rittmann 1993). Biodegradation is a relatively complicated process that depends, in part, upon contaminant transport to and

within the biofilms, mechanisms that are not represented in Eqs. 1 and 2. Therefore, the conditions are not apparent under which Eqs. 1 or 2 are legitimate mathematical representations of transport with biodegradation (Baveye and Valochi 1989). One could therefore question if research predicated upon Eqs. 1 or 2 is suspect, because those equations are insufficient representations of the biodegradation process. To resolve this issue, there must be stipulated the conditions under which Eqs. 1 and 2 may be considered acceptable.

In recognition of the complexity of the biodegradation process, a second class of conceptual and mathematical models has been developed that attempts to account for the most important microscopic processes. In this chapter this class of models are termed "idealized biofilm" models, after Rittmann and McCarty (2001). Details of these models will be provided in a subsequent section; here it is noted only that idealized biofilm models account for contaminant mass transfer from the bulk groundwater to the surface of a biofilm, contaminant diffusion through the biofilm, and degradation within the biofilm. Hence, these biofilm models appear to be quite different, both conceptually and mathematically, from the simpler models (Eqs. 1 and 2) (Rittmann and McCarty 1980; Suidan and Wang 1985; Williamson and McCarty 1976).

The problem with the idealized biofilm models is that, because of their increased complexity, they do not lend themselves well to certain types of investigations. For example, the analyses of Chang et al. (1999); Fry and Istok (1994); Miralles-Wilhem and Gelhar (1996) would likely not be possible if a biofilm model were used in place of a simple first-order kinetic model. In fact, much or most of the previous research that has

been predicated on Eq. 1 or 2 might not be possible if a biofilm model were invoked instead. Thus we are faced with the dilemma that Eq. 1 and 2 might be inadequate representations of biodegradation, but a more realistic representation of biodegradation might be too mathematically cumbersome to be useful in many applications.

In this chapter, the dilemma is resolved by determining when the simple model (Eq. 2) is mathematically equivalent to a more sophisticated biofilm model. When the two models are equivalent, the simple model (Eq. 2) may be considered valid, because the first-order kinetic representation is adequate to describe the underlying microscopic processes. Thus, the work presented in this chapter can be considered a theoretical foundation for use of the commonly-employed model (Eq. 2), as well as an elucidation of the conditions for its validity. Furthermore, this work implies that, in cases where the two models are equivalent, the more complicated biofilm model can be discarded in favor of a simpler model.

To achieve this goal, this chapter proceeds as follows: (1) A mathematical model is presented that accounts for contaminant advection and dispersion in the bulk aqueous phase, with diffusion and biodegradation occurring in continuous biofilms that coat the surfaces of the grains of aquifer material. (2) It is demonstrated that, when steady-state conditions are reached, the biofilm model predicts a concentration profile at the macroscopic scale that is, in fact, exactly equivalent to the profile predicted by the simple model (Eq. 2). Under these conditions, the apparent first-order degradation rate k can be considered as a macroscopic parameter that is a function of three microscopic rate parameters: an external mass transfer rate, a biofilm diffusion rate, and a degradation

rate within the biofilm. (3) It is demonstrated that, under transient conditions, the simple model (Eq. 2) is not strictly valid, but that it may be applied at the macroscopic scale with negligible error under certain circumstances. (4) The implications of these findings are discussed with regard to selecting an appropriate model for biodegradation during contaminant transport.

Biofilm Model

Here the biofilm model is presented to which Eq. 2 will be compared in order to determine the conditions under which Eq. 2 is valid. The biofilm model is based on similar models proposed earlier by Williamson and McCarty (1976), Rittman and McCarty (1980), and Suidan and Wang (1985). These models differ somewhat from the "microcolony"' model used by Molz (1986). The relation of the "biofilm" model to the "microcolony" model has been discussed by Baveye and Valocchi (1989) and by Rittmann (1993).

Figure 1 shows schematically the conceptual model for the biofilm. Contaminant biodegradation takes place when the contaminant diffuses from the bulk solution through the boundary layer (also called the diffusion layer) to the biofilm, then diffuses through the biofilm. Active bacteria within the biofilm degrade the contaminant. The radius of the aquifer grain is R_1, and the thickness of the biofilm is denoted L_f. The total radius of the coated grain is R_2, i.e., $R_2 = R_1 + L_f$. Contaminant diffusion and reaction within the biofilm are described by the following equation:

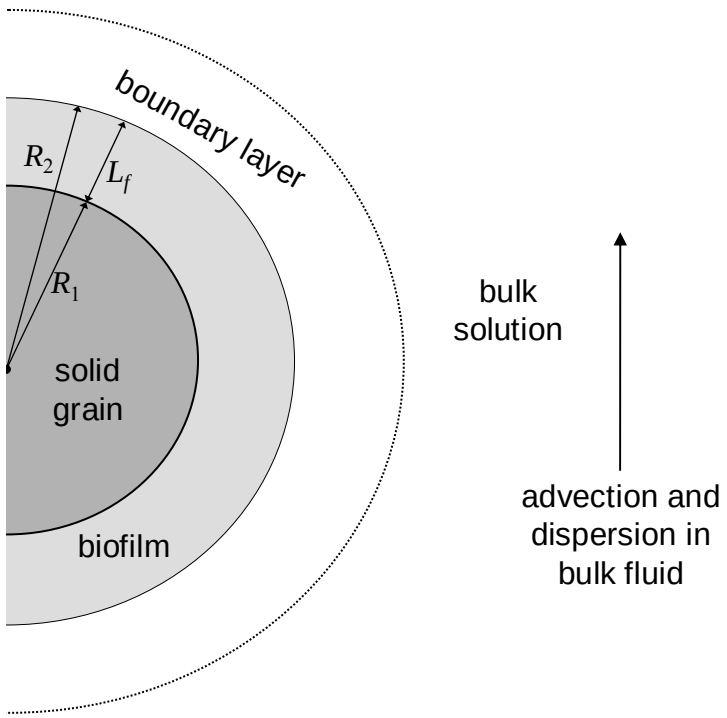

Fig. 1 Conceptual diagram of a biofilm coating a grain of aquifer material. Contaminant biodegradation takes place when the contaminant diffuses from the bulk solution through the boundary layer to the biofilm then diffuses through the biofilm. The thickness of the biofilm is denoted L_f, the radius of the aquifer grain excluding the biofilm is denoted R_1, and the radius of the grain including the biofilm coating is denoted R_2.

$$n_f \frac{\partial C_f(x,r,t)}{\partial t} = n_f D_f \frac{1}{r^2}\frac{\partial}{\partial r}\left[r^2 \frac{\partial C_f(x,r,t)}{\partial r}\right] - n_f k_f C_f(x,r,t) \quad \text{for } R_1 \le r \le R_2 \qquad (3)$$

where $C_f(x,r,t)$ is the chemical concentration within the pore space of the reactive film, n_f is the porosity of the reactive film, D_f is the diffusion coefficient within the reactive film, and k_f is the reaction rate constant inside the reactive film. Here it has been assumed first-order reaction kinetics within the biofilm. This requires that the contaminant concentration C_f in the biofilm is low enough that a Michaelis-Menten kinetic expression can be reduced to a first-order expression (e.g. Rittmann and McCarty 2001), in the same manner that Eq. 1 was reduced to Eq. 2.

Within the mobile (bulk) groundwater, the contaminant undergoes advection, dispersion, and mass transfer through the diffusive layer to the biofilm:

$$n \frac{\partial C(x,t)}{\partial t} = n D \frac{\partial^2 C(x,t)}{\partial x^2} - n v \frac{\partial C(x,t)}{\partial x} - 3(1-n)\frac{\omega}{R_2}\left[C(x,t) - C_f(x, r = R_2, t)\right] \qquad (4)$$

where ω is the mass-transfer coefficient (length/time) describing transport through the diffusive boundary layer. Eq. 4 has been presented and discussed in the literature previously (e.g., Crittenden et al. 1986; Cunningham et al. 1997; Kasten et al. 1952b; Miller and Webber 1986; Rasmuson and Neretniecks 1981; Rosen 1952), and is therefore not derived here.

The biofilm transport equation (Eq. 3) and the bulk transport equation (Eq. 4) are coupled through the boundary condition at the surface of the biofilm:

$$n_f D_f \frac{\partial C_f(x, r = R_2, t)}{\partial x} = \omega\left[C(x,t) - C_f(x, r = R_2, t)\right] \qquad (5)$$

which states that the flux to the surface of the biofilm equals the flux into the biofilm, i.e., there is no build-up of contaminant mass right at the biofilm surface. Finally, a boundary condition is needed at the interface of the grain surface and the biofilm:

$$\frac{\partial C_f(x, r = R_1, t)}{\partial r} = 0 \qquad (6)$$

which indicates that there is no contaminant flux into the grain (Rittmann and McCarty 1980).

Equations 3 – 6 comprise what will be called the "biofilm model." To be sure, this model still invokes a number of simplifications. For instance, first-order kinetics are used for the biodegradation rate; growth and death of the biofilm bacteria are not considered; the biodegradation kinetics are assumed to depend only upon the concentration of the contaminant, not upon the concentration of oxygen (or other electron acceptor or donor); it is assumed that biofilms exist as continuous coatings of uniform thickness; and it is assumed that the biodegradation rate is uniform within the biofilm. Despite these assumptions, the biofilm model is a significant improvement upon the simple model of Eq. 2: the biofilm model accounts for the processes of mass transfer across a boundary layer, diffusion through a biofilm, and reaction within the biofilm. Rittmann and McCarty (2001, p. 208) note that the idealized biofilm model describes concentration gradients within the biofilm in a "tractable, yet realistic way." Thus, for the purposes of this chapter, it is considered that the biofilm model is sufficiently realistic to be acceptable as a basis of comparison for the simple model

(Eq. 2). When the simple model (Eq. 2) is equivalent to the biofilm model (Eqs. 3 – 6), it shall be considered that such equivalence validates the use of the simple model (Eq. 2).

Models in Dimensionless Forms

To facilitate the analysis and discussion in the remainder of this chapter, the non-dimensional form of both the simple model and the biofilm model is obtained. Subsequent sections are presented primarily in terms of the dimensionless variables and parameters. Dimensionless variables are defined as follows.

$$\overline{C} = \frac{C}{C_0} \qquad \overline{C}_f = \frac{C_f}{C_0} \qquad \overline{x} = \frac{x}{L} \qquad \overline{t} = \frac{v\,t}{L} \qquad \overline{r} = \frac{r}{R_2} \tag{7}$$

where C_0 is a characteristic concentration of the contaminant in question, L is a characteristic length scale of the transport problem, and other variables have been defined previously. Non-dimensionalization of the simple model (Eq. 2) results in the following:

$$\frac{\partial \overline{C}(\overline{x},\overline{t})}{\partial t} = \frac{1}{Pe}\,\frac{\partial^2 \overline{C}(\overline{x},\overline{t})}{\partial \overline{x}^2} - \frac{\partial \overline{C}(\overline{x},\overline{t})}{\partial \overline{x}} - Da\;\overline{C}(\overline{x},\overline{t}) \tag{8}$$

where Pe is the well-known Peclet number, and Da is a Damköhler number, defined as follows.

$$Pe = \frac{vL}{D} \qquad Da = \frac{kL}{v} \tag{9}$$

The Damköhler number is the ratio of the contaminant reaction rate to the rate of advection, i.e., a dimensionless measure of the contaminant biodegradation rate (cf. Bahr and Rubin 1987; Dykaar and Kitanidis 1996; Quindoz and Valocchi 1993). The

Damköhler number *Da* should be thought of as the dimensionless analog to the first-order reaction rate *k*.

Non-dimensionalization of the biofilm model results in the following system of equations, the dimensionless analogs to (Eqs. 3 – 6).

$$\frac{\partial \overline{C}(\bar{x},\bar{t})}{\partial \bar{t}} = \frac{1}{Pe}\frac{\partial^2 \overline{C}(\bar{x},\bar{t})}{\partial \bar{x}^2} - \frac{\partial \overline{C}(\bar{x},\bar{t})}{\partial \bar{x}} - 3\,\kappa\, St\left[\overline{C}(\bar{x},\bar{t}) - \overline{C}_f(\bar{x},\bar{r}=1,\bar{t})\right] \tag{10}$$

$$\frac{\partial \overline{C}_f(\bar{x},\bar{r},\bar{t})}{\partial t} = Ed\,\frac{1}{\bar{r}^2}\frac{\partial}{\partial \bar{r}}\left[\bar{r}^2\,\frac{\partial \overline{C}_f(\bar{x},\bar{r},\bar{t})}{\partial \bar{r}}\right] - Da_f\,\overline{C}_f(\bar{x},\bar{r},\bar{t}) \tag{11}$$

$$Ed\,\frac{\partial \overline{C}_f(\bar{x},\bar{r}=1,\bar{t})}{\partial \bar{x}} = St\left[\overline{C}(\bar{x},\bar{t}) - \overline{C}_f(\bar{x},\bar{r}=1,\bar{t})\right] \tag{12}$$

$$\frac{\partial \overline{C}_f(\bar{x},\bar{r}=r^*,\bar{t})}{\partial \bar{r}} = 0 \tag{13}$$

This system of dimensionless equations depends on a total of six dimensionless groups.

$$\kappa = \frac{1-n}{n}n_f \qquad r^* = \frac{R_1}{R_2} \qquad Pe = \frac{v\,L}{D}$$

$$St = \frac{\omega/R_2}{n_f v/L} \qquad Ed = \frac{D_f/R_2^{\,2}}{v/L} \qquad Da_f = \frac{k}{v/L} \tag{14}$$

The parameter κ is a capacity factor, indicating the capacity of the biofilms to store the contaminant. The parameter r^* is the dimensionless radius of the interface between the aquifer grain and the biofilm. The Stanton number *St* (following the notation of Crittenden et al. 1986) is a measure of the external mass transfer rate, i.e., the rate of contaminant mass transfer from the bulk groundwater to the biofilm across the diffusion layer (boundary layer). The parameter *Ed* (again following Crittenden et al. 1986) is a measure of the internal mass transfer rate, i.e., the rate of contaminant

diffusion inside the biofilm. Finally, the parameter Da_f is a Damköhler number for inside the biofilm, i.e., a measure of the contaminant degradation rate inside the biofilm. The Sherwood number, $Sh=St/Ed$, is sometimes used to quantify the external mass transfer rate; however, in this case, the Stanton number is preferable, because *St*, *Ed*, and Da_f are all defined relative to the rate of advection, whereas the Sherwood number is not.

The non-dimensionalization has reduced the number of parameters in the biofilm model from ten original parameters to six dimensionless parameters. Therefore, in the sections that follow, the dimensionless form of both the simple model and the biofilm model is used. Equation 8 is the dimensionless form of the simple model; Eqs. 10-13 are the dimensionless form of the biofilm model. In subsequent sections, these two models are compared, demonstrating the conditions under which they are equivalent, and thereby determining the validity of the simple model. The three parameters *St*, *Ed*, and Da_f are dimensionless rate parameters, quantifying the rates of mass transfer across the boundary layer, diffusion within the biofilm, and reaction with the biofilm, respectively.

Model Equivalence at Steady State

In certain cases, the contaminant concentration profile in an aquifer will approach a steady state, i.e., the concentration profile will be changing only very slowly in time. Consider, for instance, the following initial and boundary conditions:

$$C\left(x,t=0\right)=0 \tag{15}$$

$$C\left(x=0,t\right)=C_0 \qquad C\left(x\to\infty,t\right)=0 \tag{16}$$

which would represent a large, initially clean aquifer with a continuous source of contamination located at $x = 0$. These conditions would be a decent approximation to describe, for instance, the plume emanating from a leaking underground storage tank. In dimensionless variables, these initial and boundary conditions would be written as follows.

$$\bar{C}\left(\bar{x}, \bar{t} = 0\right) = 0 \qquad \bar{C}\left(\bar{x} = 0, \bar{t}\right) = 1 \qquad \bar{C}\left(\bar{x} \to \infty, \bar{t}\right) = 0 \tag{17}$$

If applied to the simple model (Eq. 8), the initial and boundary conditions (Eqs. 17) result in the following concentration profile at steady state:

$$\bar{C}\left(\bar{x}\right) = \exp\left[\bar{x}\frac{Pe}{2}\left(1 - \sqrt{1 + 4\frac{Da}{Pe}}\right)\right] \tag{18}$$

Equation 18 is derived by setting the time derivative in Eq. 8 equal to zero, then applying the boundary conditions (Eqs. 17). An approximation to Eq. 18 is noted that is valid when *Da*/*Pe* is small (less than about 0.1), which will typically be the case at high Peclet number:

$$\bar{C}\left(\bar{x}\right) \approx \exp\left[-\bar{x}Da\left(1 - \frac{Da}{Pe}\right)\right] \tag{19}$$

If the boundary conditions (Eqs. 17) are applied instead to the biofilm model (i.e., Eqs. 10 - 13), then the following steady-state concentration profile is derived:

$$\bar{C}\left(\bar{x}\right) = \exp\left[\bar{x}\frac{Pe}{2}\left(1 - \sqrt{1 + 4\frac{Da_{equiv}}{Pe}}\right)\right] \tag{20}$$

where Da_{equiv} is an equivalent macroscopic Damköhler number, equal to the following:

$$Da_{equiv} = 3\kappa St \frac{Ed\left(z_2 \cosh z_2 - \sinh z_2 + \gamma z_2 \sinh z_2 - \gamma z_2 \cosh z_2\right)}{Ed\left(z_2 \cosh z_2 - \sinh z_2 + \gamma z_2 \sinh z_2 - \gamma z_2 \cosh z_2\right) + St\left(\gamma z_2 \cosh z_2 + \sinh z_2\right)} \tag{21}$$

where

$$z_2 = \sqrt{\frac{Da_f}{Ed}} \tag{22}$$

$$\gamma = \frac{\sinh z_1 - z_1 \cosh z_1}{z_1 \sinh z_1 - \cosh z_1} \tag{23}$$

$$z_1 = r^* z_2 = r^* \sqrt{\frac{Da_f}{Ed}} \tag{24}$$

Equations 20 through 24 are derived by setting the time derivatives equal to zero in the biofilm model, then applying the boundary conditions.

The essential point is that Eqs. 18 and 20 are of exactly the same form, and, therefore, can make exactly equivalent predictions for $\bar{C}(\bar{x})$. The only restriction for equivalence is that the simple macroscopic Damköhler number, *Da*, must be made equal to Da_{equiv}; or, in other words, *Da* must be related to the parameters of the biofilm model according to Eq. 21. Under this restriction, the "simple" model (Eq. 8) yields an estimate of contaminant concentration profile that is exactly equal to that of the more sophisticated biofilm model. Hence, it is concluded that the simple model (Eqs. 2 or 8) is valid under steady-state conditions, as long as the parameter *k* or *Da* is chosen appropriately.

Simplified Steady State Cases

Equation 21 indicates that the equivalent macroscopic Damköhler number, Da_{equiv}, is a somewhat complicated function of the three dimensionless groups *St*, *Ed*, and Da_f. These are, respectively, the rate of contaminant mass transfer across the diffusive boundary layer, the rate of contaminant diffusion in the biofilm, and the rate of chemical reaction in the biofilm. In some cases, one of these processes will be the controlling (rate-limiting) process for the overall contaminant biodegradation. In these cases, it is possible to simplify equation 21. In the sub-sections below, three regimes of control for degradation in the biofilm are explored: external mass-transfer control, internal mass-transfer control, and chemical reaction control.

External Mass Transfer Control

Consider the case where contaminant mass transfer through the diffusive boundary layer (i.e., "external" mass transfer) is slow relative to the other processes. That is, $St \ll Ed$ and $St \ll Da_f$. Physically, this might occur, for instance, if the active biofilm is surrounded by a relatively thick inactive polysaccharide matrix that comprises the diffusive boundary layer (Baveye and Valocchi, 1993). In this case, it can be seen that

$$\frac{Ed\left(z_2\cosh z_2-\sinh z_2+\gamma z_2\sinh z_2-\gamma z_2\cosh z_2\right)}{Ed\left(z_2\cosh z_2-\sinh z_2+\gamma z_2\sinh z_2-\gamma z_2\cosh z_2\right)+St\left(\gamma z_2\cosh z_2+\sinh z_2\right)}\approx 1 \qquad (25)$$

which, from Eq. 21, implies that

$$Da_{equiv}\approx 3\kappa St \qquad (26)$$

The approximation shown in Eq. 26 could also be derived from Eq. 10 by noting that, when external mass transfer is slow, $\bar{C}_f(\bar{x},\bar{r}=1,\bar{t}) \ll \bar{C}(\bar{x},\bar{t})$.

Equation 26 indicates that the effective macroscopic degradation rate does not depend upon the diffusion rate or the degradation rate within the biofilm, but only upon the rate of mass transfer across the diffusive boundary layer. This is consistent with the approximation made above that the external mass transfer rate is slow compared to processes occurring within the biofilm. As soon as contaminant diffuses across the external boundary layer, it quickly diffuses into the active biofilm and is degraded. External mass transfer is the rate-limiting step, and therefore controls the overall biodegradation rate.

Biofilm Diffusion Control

Consider the case where contaminant diffusion within the active biofilm (internal mass transfer) is slow relative to external mass transfer. That is, $Ed \ll St$. In this case, Eq. 21 reduces to

$$Da_{equiv} \approx 3\kappa Ed \frac{z_2 \cosh z_2 - \sinh z_2 + \gamma z_2 \sinh z_2 - \gamma z_2 \cosh z_2}{\gamma \cosh z_2 + \sinh z_2} \tag{27}$$

$$= 3\kappa Ed \left(z_2 \frac{\gamma \sinh z_2 + \cosh z_2}{\gamma \cosh z_2 + \sinh z_2} - 1 \right) \tag{28}$$

Further suppose that the contaminant diffusion rate inside the biofilm is slow compared to the degradation rate inside the biofilm, i.e., $Ed \ll Da_f$. This situation has previously been termed a "diffusion-limited" situation (Williamson and McCarty 1976). In this

case, the terms z_1 and z_2 are both large. Then, Eq.28 can be simplified further, finally yielding the following approximation:

$$Da_{equiv} = 3\kappa\left(\sqrt{Da_f}\sqrt{Ed} - Ed\right) \tag{29}$$

It is interesting to compare the results from internal diffusion control and external mass transfer control. In the case of external mass transfer control (Eq. 26), the external mass transfer is the rate-limiting step for the whole process, and the equivalent macroscopic Damköhler number depends only on *St*, but not on *Ed* or Da_f. However, in the case of biofilm diffusion control (Eq. 29), the equivalent macroscopic Damköhler number depends on both the biofilm diffusion rate, *Ed*, and the degradation rate within the biofilm, *Daf*. This difference makes sense because, within the biofilm, diffusion and degradation are not strictly sequential; they occur simultaneously, as shown in Eqs. 3 and 10. Therefore, even if diffusion within the biofilm is the rate-limiting step, the equivalent macroscopic degradation rate still depends on the biofilm degradation rate Da_f.

Biofilm Reaction Control

Consider the case where degradation within the active biofilm is slow compared to both diffusion across the boundary layer and diffusion within the biofilm. This situation has previously been called metabolism limited (Williamson and McCarty 1976). This might occur, for instance, if the intra-cellular metabolic processes of the active bacteria are slow compared to diffusion through the boundary layer and the biofilm. In this case,

$Da_f \ll St$ and $Da_f \ll Ed$. Thus, $z_2 = \sqrt{Da_f / Ed}$ and $z_1 = r^* \sqrt{Da_f / Ed}$ are both small, and the hyperbolic trigonometric functions in Eqs. 21 and 23 can be approximated with the first few terms of their Taylor (Maclaurin) series. After some considerable algebra, this leads to the approximation that, for biofilm reaction control,

$$Da_{equiv} \approx \kappa \left[1 - \left(r^* \right)^3 \right] Da_f \tag{30}$$

The macroscopic equivalent biodegradation rate is directly proportional to the microscopic degradation rate within the biofilm. This makes sense because, in this case, the degradation rate within the biofilm is the rate-limiting step for the entire biodegradation process.

The three different approximations to Eq. 21 are summarized in Table 1.

Summary of Steady-State Equivalence

For boundary conditions under which the contaminant concentration profile reaches a steady state, the simple model (Eq. 8) and the more sophisticated biofilm model (Eqs. 10-13) both predict the same steady-state profile for the macroscropic contaminant concentration. This can be seen by comparing Eqs. 18 and 20. Therefore, the two models can be made exactly equivalent by the proper selection of the macroscopic biodegradation rate, *Da*. By choosing *Da* according to Eq. 21, the macroscopic degradation rate is expressed in terms of the microscopic rate parameters that correspond

Table 1. Summary of approximation for Da_{equiv} under limiting conditions

Limiting conditions	Criteria for validity	Approximation of Da_{equiv}
External mass transfer control	$St \ll Ed,\ St \ll Da_f$	$Da_{equiv} \approx 3\kappa St$
Biofilm diffusion control	$Ed \ll St,\ Ed \ll Da_f$	$Da_{equiv} \approx 3\kappa Ed\left(\sqrt{\frac{Da_f}{Ed}}-1\right)$
Biofilm reaction control	$Da_f \ll St,\ Da_f \ll Ed$	$Da_{equiv} \approx \kappa\left[1-(r^*)^3\right]Da_f$

to the processes of diffusion across a boundary layer, diffusion within the biofilm, and reaction within the biofilm. Although the simple model given in Eqs. 2 and 8 does not explicitly account for the true physics of the biodegradation process, those equations are mathematically sufficient under steady-state conditions. The transient (early-time) conditions under which Eq. 2 or 8 might also be valid is addressed in the following section.

Transient Conditions

To determine when Eq. 2 or 8 might be valid under transient (early-time) conditions, the initial and boundary conditions given by Eqs. 15-17 were again applied. However, the development that follows does not depend strongly on the choice of initial or boundary conditions; these are chosen only for expediency. Equation 8 was solved by use of Laplace transforms. Transforming Eq. 8 to the Laplace domain under initial condition of Eq. 17 gives

$$s\hat{C}(\overline{x},s) = \frac{1}{Pe}\frac{d^2\hat{C}(\overline{x},s)}{d\overline{x}^2} - \frac{d\hat{C}(\overline{x},s)}{d\overline{x}} - Da\hat{C}(\overline{x},s) \tag{31}$$

where $\hat{C}(\overline{x},s)$ is the Laplace transform of $\overline{C}\left(\overline{x},\overline{t}\right)$, and s is the Laplace variable. With boundary conditions of Eq. 17, this equation has the following solution in the Laplace domain:

$$\hat{C}\left(\overline{x},s\right) = \frac{1}{s}\exp\left[\overline{x}\frac{Pe}{2}\left(1-\sqrt{1+\frac{4\left(Da+s\right)}{Pe}}\right)\right] \tag{32}$$

Equation 32 can be transformed from the Laplace domain back to the time domain numerically, thereby providing an estimate of $\bar{C}(\bar{x},\bar{t})$. For instance, suppose it is desired to determine the contaminant breakthrough curve at a location L = 10 m, with groundwater velocity v = 0.1 m/day, dispersion coefficient D = 0.02 m^2/day, and first-order degradation rate k = 0.01 day^{-1}. These values of L, v, D, and k correspond to a Peclet number Pe = 50 and a Damköhler number Da = 1. The Crump algorithm (Crump 1976) was applied to Eq. 32, and the resultant breakthrough curve is shown in Fig. 2 . Figure 2 shows that the contaminant concentration at L = 10 m approaches a steady-state concentration of $\bar{C} = C/C_0 = 0.375$. This is correctly predicted by Eqs. 18 and 19. Thus we see how the steady-state solution presented in the section of Model Equivalence at Steady State is related to the transient solution presented here.

The biofilm model, Eqs. 10-13, can be solved by the same procedure. Transforming to the Laplace domain and solving, we determine

$$\hat{C}(\bar{x},s) = \frac{1}{s}\exp\left[\bar{x}\frac{Pe}{2}\left(1-\sqrt{1+\frac{4(\beta(s)+s)}{Pe}}\right)\right] \tag{33}$$

where $\beta(s)$ is a complicated function of s, St, Ed, and Da_f, which is not presented here in the interest of space.

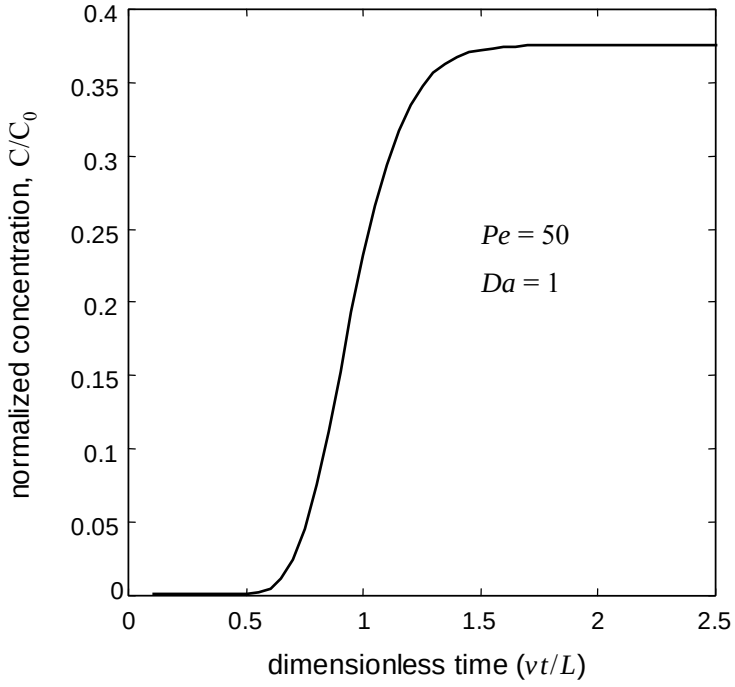

Fig. 2 Contaminant breakthrough curve at $L = 10$ m with groundwater velocity $v = 0.1$ m/day, dispersion coefficient $D = 0.02\text{m}^2/\text{d}$, and macroscopic degradation rate constant $k = 0.01$ d^{-1}. The contaminant concentration approaches a normalized value of $\overline{C} = C/C_0 = 0.375$ as predicted by Eqs. 18 and 19.

Equations 32 and 33 are almost identical, but with one very important difference. Whereas Eq. 32 depends upon the constant biodegradation rate parameter *Da*, Eq. 33 depends upon the function $\beta(s)$, which is not a constant. In other words, under transient conditions, the biofilm model (Eqs. 10-13) can not be made equivalent to the simple model (Eq. 8).

However, despite the fact that the simple model and the biofilm model cannot be made exactly equivalent under transient conditions, it is still possible that the simple model might provide an acceptable approximation to the more sophisticated biofilm model under many circumstances. To determine the conditions under which the "simple" model (Eq. 8) is an adequate approximation of the more sophisticated biofilm model, this chapter proceeds as follows. Twelve sets of conditions are chosen for input to the biofilm model: these conditions are shown in Table 2. For each set of conditions, the breakthrough curve $\overline{C}(\overline{x}=1,\overline{t})$ as predicted by the biofilm model is determined by numerically inverting Eq. 33. Then, the equivalent value of *Da* for the simple model is determined according to Eq. 21, and the breakthrough curve is determined for the simple model by numerically inverting Eq. 32. The two breakthrough curves are then compared graphically to determine if the simple model is an adequate approximation to the biofilm model. The twelve sets of conditions were chosen to span the range of reasonable possibilities: cases 1-3 where external mass transfer controls, cases 4-6 where internal mass transfer controls, cases 7-9 where the biofilm reaction rate controls, and cases 10 - 12 where all of these processes are significant.

Table 2. Values for 12 Breakthrough Curve Simulations[a]

Case	*St*	*Ed*	Da_f	Controlling Process	Da_{equiv}[b]
1	0.50	1000.	100.	external mass transfer	2.17
2	0.15	1000	100	external mass transfer	0.70
3	0.05	1000	100	external mass transfer	0.24
4	1000	2.5×10^{-3}	100	internal mass transfer	2.39
5	1000	2.5×10^{-4}	100	internal mass transfer	0.76
6	1000	2.5×10^{-5}	100	internal mass transfer	0.24
7	1000	1000	10	reaction	2.28
8	1000	1000	3	reaction	0.69
9	1000	1000	1	reaction	0.23
10	1.25	0.10	20	all three	2.39
11	0.38	0.05	6	all three	0.74
12	0.13	0.03	2	all three	0.25

[a] For all 12 simulations, $r^* = 0.95$, $\kappa = 1.6$, and $Pe = 100$.

[b] Equation 21 is used to calculate Da_{equiv}

Results are shown in Figs. 3, 4, 5, and 6. The rather remarkable result is that, for six of the 12 cases considered (cases 1-6), the breakthrough curves are indistinguishable between the simple model and the biofilm model. In other words, the simple model is able to reproduce almost exactly the macroscopic concentrations predicted by the biofilm model, as long as Eq. 21 is used to compute the macroscopic rate constant *Da*. From the mathematical development above, it is known that the final (steady-state) concentration predicted by the two models is exactly equivalent; however, the transient portion of the breakthrough curves is not necessarily expected to be identical for the two models, based on the difference between Eqs. 32 and 33. Thus, the apparently perfect agreement between the two models is something of a surprise. The exception to the apparent equivalence occurs when biological reaction inside the biofilm is slow. This is particularly evident in cases 7-9, where biological reaction is the rate-controlling process, and to a lesser degree in cases 10-12, where all three microscopic processes are significant. For these circumstances, the biofilm model predicts some accumulation of the contaminant inside the biofilm, a process that acts like sorption and therefore retards the breakthrough of the contaminant. The simple model does not account for this process.

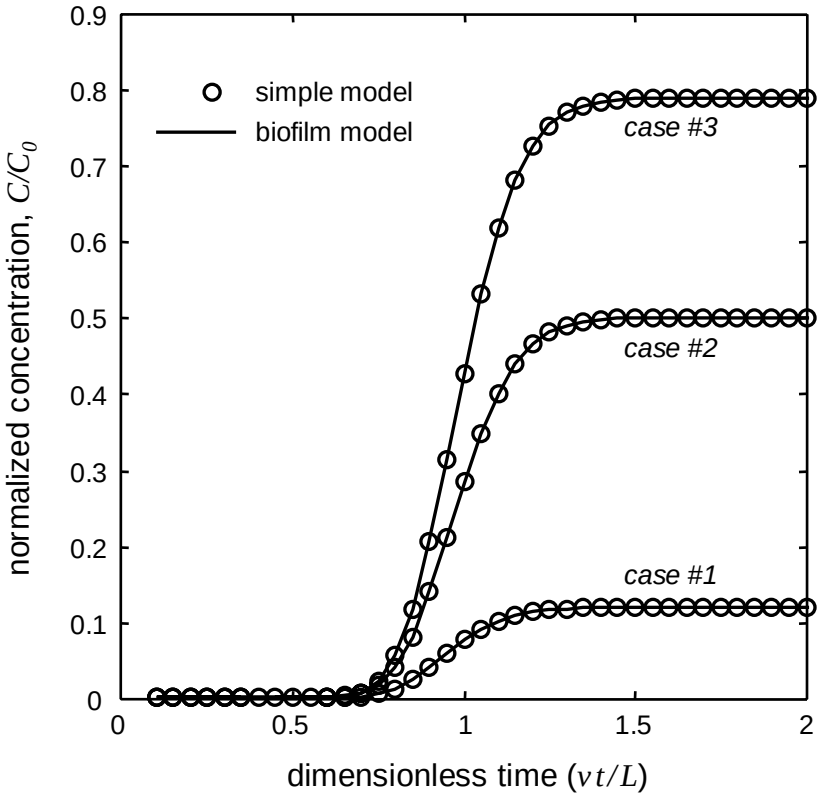

Fig. 3 Comparison of breakthrough curves predicted by the biofilm model and the simple model when external mass transfer is the rate controlling process.

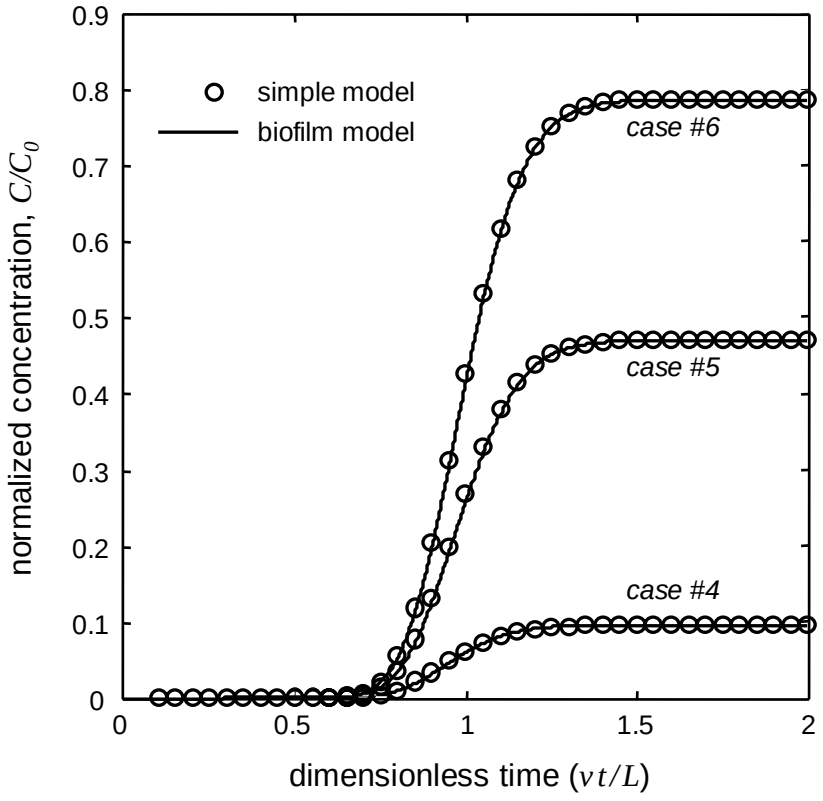

Fig. 4 Comparison of breakthrough curves predicted by the biofilm model and the simple model when diffusion within the biofilm is the rate controlling process.

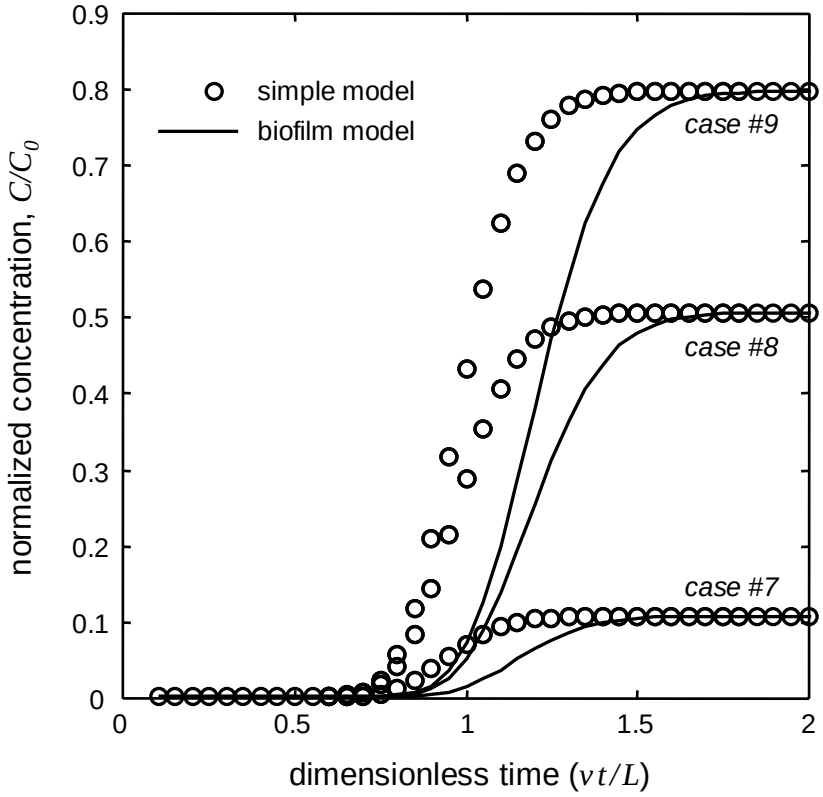

Fig. 5 Comparison of breakthrough curves predicted by the biofilm model and the simple model when biological reaction within the biofilm is the rate controlling process.

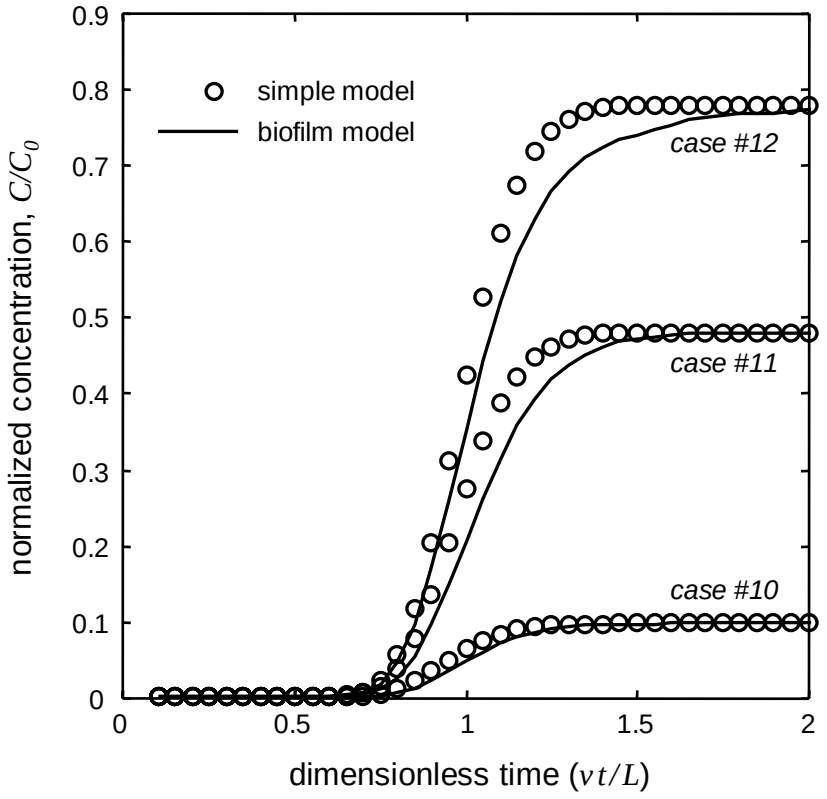

Fig. 6 Comparison of breakthrough curves predicted by the biofilm model and the simple model when all three microscopic processes are significant.

Discussion

Relation to Previous Research

As stated above, the purpose of this chapter is to compare Eq. 2 to a more sophisticated model of transport with biodegradation, and to determine when the "simple" model (Eq. 2) is valid. Similar endeavors have been undertaken in the past. Here the relation of the current work to some of the relevant previous studies is addressed. For instance, Baveye and Valocchi (1989) noted that there are essentially three distinct approaches to modeling biodegradation during transport, and they elucidated the relationship between the mathematical formulations of these three approaches. The stated objective of that work was to analyze critically "whether these three frameworks lead to fundamental differences in terms of model predictions," and the objective here is much the same.

However, the work presented here differs from that of Baveye and Valocchi (1989) in some important respects. First, Baveye and Valocchi (1989) assumed a steady-state concentration in the diffusion layer and in the biofilm, whereas here they are considered both steady-state and transient conditions. Second, Baveye and Valocchi (1989) neglected concentration gradients within the biofilm, restricting their analysis to situations where the biofilms (or microcolonies) are fully penetrated by the contaminant; in our current paper we allow for concentration gradients within the biofilm. Third, and most significantly, one of the important questions left unanswered by Baveye and Valocchi (1989) was resolved in the present chapter. It is clear to see that the "simple"' model invoked in this paper is a formulation of the model termed "Option A" by Baveye and Valocchi (1989). In their discussion, Baveye and Valocchi (1989) noted that "the

mathematical nature of the transport equations derived on the basis of Option A is fundamentally different from that of the equations derived on the basis of (microcolony or biofilm models). As a matter of fact, concentration profiles predicted by these latter models could be expected, in general, to differ from those predicted by Option A." This issue has now been addressed explicitly by showing when the concentration profiles predicted by the biofilm model differ (or do not differ) from those predicted by Option A. In this regard, the current work can be considered an extension of the previous work by Baveye and Valocchi (1989).

A different but complementary approach was taken by Dykaar and Kitanidis (1996), who considered that Eq. 2 might be a legitimate upscaled representation of hydrodynamic and microbiological processes that are occurring on a smaller scale, i.e., on a scale smaller than the representative elementary volume for which Eq. 2 is appropriate. The goal of Dykaar and Kitanidis (1996) was then to determine how the macroscopic parameters, such as k in Eq. 2, are related to the physical, chemical, and biological parameters describing the microscopic processes. In this chapter, a similar strategy has been followed in that k in Eq. 2 has been related to the parameters of a more sophisticated model. However, despite the philosophically similar approach, the microscopic model adopted here is quite different from that considered by Dykaar and Kitanidis (1996). The model adopted by Dykaar and Kitanidis (1996) does not lend itself to a closed-form expression for the macroscopic rate constant k (called $\gamma_\bullet$ by Dykaar and Kitanidis (1996)) in terms of the microscopic hydrodynamic and biological parameters. In contrast, the biofilm model presented in this chapter permits

an explicit representation of k in terms of the microscopic transport and degradation parameters. It is difficult to speculate which microscopic model -- that presented here, or that presented by Dykaar and Kitanidis (1996) -- is a better representation of the true biodegradation process. Both are based on the assumption of a continuous biofilm coating the surfaces of the aquifer solids. It would be interesting to compare the predictions of these two microscopic models, but that effort is clearly beyond the scope of the present chapter.

Contribution of this Chapter

Papers appearing in the literature have often invoked the simple model presented in this paper Eqs. 1 or 2 when describing transport with biodegradation. However, until now, the author is not aware of any investigation into the fundamental validity of these mathematical models. In fact, many of the papers that have considered the processes underlying biodegradation (Williamson and McCarty 1976; Rittmann and McCarty 1980; Suidan and Wang 1985) would seem to indicate that the simple model is not valid, because it relates the biodegradation kinetics to the contaminant concentration in the bulk aqueous phase; however, biodegradation occurs within a biofilm or microcolony (Molz et al. 1986; Baveye and Valocchi 1989; Rittmann 1993). Therefore, the contribution of the current chapter is twofold.

First, a conceptual basis for the simple first-order model is presented. The apparent first-order rate constant, k, can be thought of as a macroscopic representation of the microscopic processes that govern biodegradation. In the current chapter, a

framework was developed in which there are three such microscopic processes: diffusion across a boundary layer (external mass transfer), diffusion within the biofilm (internal mass transfer), and reaction within the biofilm. The macroscopic rate constant k is a somewhat complicated function of the rates that describe the three underlying microscopic processes.

Second, the conditions are presented under which this conceptual equivalence can be considered valid. Under steady-state conditions, the simple model is able to exactly reproduce the macroscopic concentration profile predicted by the more sophisticated biofilm model. The only restriction is that k must be chosen properly in order to ensure the equivalence of the two models. Under transient conditions, the two models are not strictly equivalent, but they are effectively indistinguishable when the rate-controlling process is either external mass transfer or internal mass transfer. Therefore, in either of these cases, the simple model should be considered valid, with the conceptual interpretation discussed above.

Not surprisingly, there are cases where the biofilm model can not be suitably replaced by the simple model. For instance, one limitation is that noted in this chapter, namely, the case where contaminant mass accumulates inside the biofilm because the biological reaction is slow compared to the external and internal mass transfer processes. Examples of such chemicals are xenobiotic compounds that are not easily recognized by existing degradative enzymes (Singleton 1994), as a result they present slow biological reaction kinetics. In that case, a retardation effect is seen in the contaminant transport, which is not predicted by the simple model. Other situations in which the simple model

would be inadequate include those where microscopic concentrations are significant. Hence, the biofilm model would be important for, say, understanding bacterial behavior, interpreting certain laboratory experiments, predicting pore clogging, and generally describing phenomena that occur at the pore scale or smaller. Some of these phenomena are explored in this dissertation.

It is worth noting that one assumption in this study is that the kinetics of biodegradation inside the biofilm can be described with a first-order kinetic model. Therefore, the analysis in this chapter should be considered valid only for low contaminant concentrations, when the first-order kinetic model is valid (Rittmann and McCarty, 2001). For many contaminants of environmental concern (e.g., chlorinated solvents), it is reasonable to expect groundwater concentrations low enough that this condition is satisfied.

In conclusion, there is indeed a theoretical basis for the validity of the simple model often employed previously by other researchers. However, when employing the simple model, one needs to recognize the limitations to its validity, which have been outlined herein.

CHAPTER III

EFFICIENT ALGORITHM FOR MODELING TRANSPORT IN POROUS MEDIA WITH MASS EXCHANGE BETWEEN MOBILE FLUID AND REACTIVE STATIONARY MEDIA*

Overview

In this chapter two approaches to numerically solve the mathematical model of reactive mass transport in porous media with exchange between the mobile fluid and the stationary medium were compared. The first approach, named the "monolithic algorithm," is the approach in which a standard finite-difference discretization of the governing transport equations yields a single system of equations to be solved at each time step. The second approach, named the "system-splitting algorithm," is here applied for the first time to the problem of transport with mass exchange. The system-splitting algorithm (SSA) solves two separate systems of equations at each time step: one for transport in the mobile fluid, and one for uptake and reaction in the stationary medium. The two systems are coupled by a boundary condition at the mobile-immobile interface, and are solved iteratively. Because the SSA involves the solution of two smaller systems compared to that of the monolithic algorithm, the computation time may be greatly reduced if the iterative method converges rapidly. Thus, the main objective of this chapter is to determine the conditions under which the SSA is superior to the monolithic algorithm in terms of computation time. We found that the SSA is superior

*Reprinted with kind permission of Springer Science and Business Media. Springer/Kluwer Academic Publishers Transport in Porous Media, 68, 2007,285-300, Efficient algorithm for modeling transport in porous media with mass exchange between mobile and reactive stationary media, Mendoza-Sanchez I. and Cunningham J.A., original copyright to Transport in Porous Media.

under all the conditions that we tested, typically requiring only 0.3% to 50% of the computation time required by the monolithic algorithm. The two methods are indistinguishable in terms of accuracy. Further advantages to the SSA are that it employs a modular code that can easily be modified to accommodate different mathematical representations of the physical phenomena (e.g., different models for reaction kinetics within the stationary medium), and that each module of the code can employ a different numerical algorithm to optimize the solution.

Introduction

During mass transport through porous media, one important phenomenon is often the transfer of mass from the mobile fluid to the stationary medium. Examples where that phenomenon is important include adsorption onto activated carbon, reaction in packed beds of catalyst, chemical transport in streambeds, and separations in chromatographic columns. Of particular interest in this dissertation is the transport of contaminants in groundwater aquifers. In that case, the exchange of contaminants between the mobile groundwater and the stationary aquifer grains is known to have an important influence on the contaminant plume behavior (Roberts et al. 1986), and may also control biodegradation of reactive contaminants (Cunningham and Mendoza-Sanchez 2006). Therefore, in order to design appropriate remedial technologies, it is essential that we understand and be able to efficiently model the exchange process.

In the present chapter, the mathematical model of mass transport in porous media with exchange between mobile fluid and reactive stationary media includes the

following processes: advection and dispersion in the bulk mobile fluid; diffusion and reaction taking place inside a film that coats the surface of the stationary medium; and mass transfer between the bulk mobile fluid and the film coating the stationary medium (cf. Dykaar and Kitanidis 1996; Cunningham and Mendoza-Sanchez 2006). This mathematical model is described more completely later in the paper.

It is challenging to solve the resulting system of equations in an efficient manner. To meet this challenge, different strategies have been implemented in the past. The most straight-forward approach is a standard finite-difference discretization of the governing transport equations, yielding a single system of equations to be solved at each time step (e.g., Cunningham et al., 1997). This method is called the "monolithic algorithm." The monolithic algorithm (MA) requires high central processing unit (CPU) storage if a large number of nodes are used for the spatial discretization. Furthermore, due to the number of operations needed to solve the discrete system, those numerical algorithms also require extensive CPU time. The CPU requirements become even more demanding if the system requires the consideration of multiple chemical species. Because of the relative inefficiency of this method, other approaches have been used. For instance, a semi-analytical solution can be obtained by Laplace transforms, with analytical solution of the transformed equations and numerical inversion back to the original domain (Chen and Wagenet, 1995; Haggerty and Gorelick, 1998). However, the Laplace-transform approach is not applicable for non-linear reaction kinetics or non-linear transport equations. Other researchers (Crittenden et al., 1986; Moe and Li, 2005) have solved the system of equations with the method of orthogonal collocation. However, the

orthogonal collocation method, like the monolithic algorithm, requires a large number of coupled equations to be solved simultaneously at each time step; therefore the method offers little advantage over the monolithic algorithm if a large number of collocation points are required for accuracy (Villadsen and Stewart 1967).

Sometimes, problems of transport with reaction are solved with splitting techniques. For instance, the operator-splitting method, sometimes called the time-splitting method, splits the governing equations into different processes and solves each process sequentially (e.g., Chiang et al. 1991; Valocchi and Malmstead 1992; Kaluarachchi and Morshed 1995; Barry et al. 2000; Barry et al. 1996a; Barry et al. 1996b; Barry et al. 1997; Barry et al. 2002; Lanser and Verwer 1999; MacQuarrie and Sudicky 2001; Kanney et al. 2003). An operator-splitting method might, for instance, solve the transport portion of the governing equations over a full time step, followed by a solution of the reaction portion of the equations over the same time step (e.g., Carrayrou et al. 2004). Operator-splitting methods are efficient for problems in which transport and reaction are described by a single equation. However, in this chapter, a system of equations that consists of multiple transport equations is used; hence, it does not appear that a traditional operator-splitting method can be applied here. Similarly, an alternating-direction splitting method that splits a multi-dimensional transport operator into individual orthogonal directions (e.g., Peaceman and Rachford 1955; Karaa and Zhang 2004) cannot be applied. Some other method is required to solve the system of equations in an efficient manner.

Therefore, in this chapter, an efficient algorithm to numerically integrate the mathematical model of mass transport with exchange between mobile fluid and a reactive stationary medium is presented. The algorithm is called the "system-splitting algorithm" (SSA): it solves the numerical problem iteratively by splitting the complete set of equations into two systems. One system accounts for transport in the mobile fluid along the bulk direction of flow, and the other system describes the diffusion and reaction inside the reactive film that coats the stationary medium. The two systems are coupled by a boundary condition at the interface between the mobile fluid and the stationary medium. This approach is not a time-splitting, operator-splitting, or alternating-direction approach; instead, the problem is split into two orthogonal directions, one along the direction of bulk transport, and one into the reactive film. Similar algorithms have been applied in solving models with coupled systems of equations in different areas of study, such as steady-state heat transfer in porous media (Karki and Patankar 2004). In this chapter, the SSA is applied to the problem of mass transport through porous media with exchange between a mobile fluid phase and a reactive stationary phase.

The original contributions of this chapter are twofold. First, to the best of the author's knowledge, this chapter represents the first time that the SSA has been applied to the problem of transport in porous media with mass exchange between the mobile fluid and the stationary porous medium. The SSA gains its computational efficiency by splitting a large system of equations into a set of small systems of equations, each of which can be solved rapidly. Second, the SSA is compared with the monolithic

algorithm (MA), which solves the complete (fully coupled) system involved in the physical representation of the reactive transport. The comparison will be presented in terms of calculation time efficiency and viability of applications. The efficiency of the SSA is evaluated in order to determine when the SSA is computationally superior to the MA, so that potential users of the new algorithm will know when it is most beneficial. A range of different possible physical scenarios has been considered, to quantify the conditions under which one algorithm is superior to the other.

Conceptual and Mathematical Model

The conceptual model of transport with mass exchange between mobile fluid and reactive stationary medium is depicted in Fig. 7. The stationary medium is comprised of spherical grains of homogeneous radius R_1. These grains are coated with a reactive film of constant thickness L_f. A diffusive boundary layer surrounds the coated grains. This conceptual model could describe, for instance, reactive biofilms coating the grains of an aquifer, or an "eggshell" coating of catalyst on an inert support material. In the mobile (bulk) fluid, advection and dispersion occur in the direction of macroscopic fluid flow. Chemical mass transfer occurs from the mobile fluid, through the diffusive boundary layer, to the surface of the reactive film. Within the reactive film, diffusion and reaction occur.

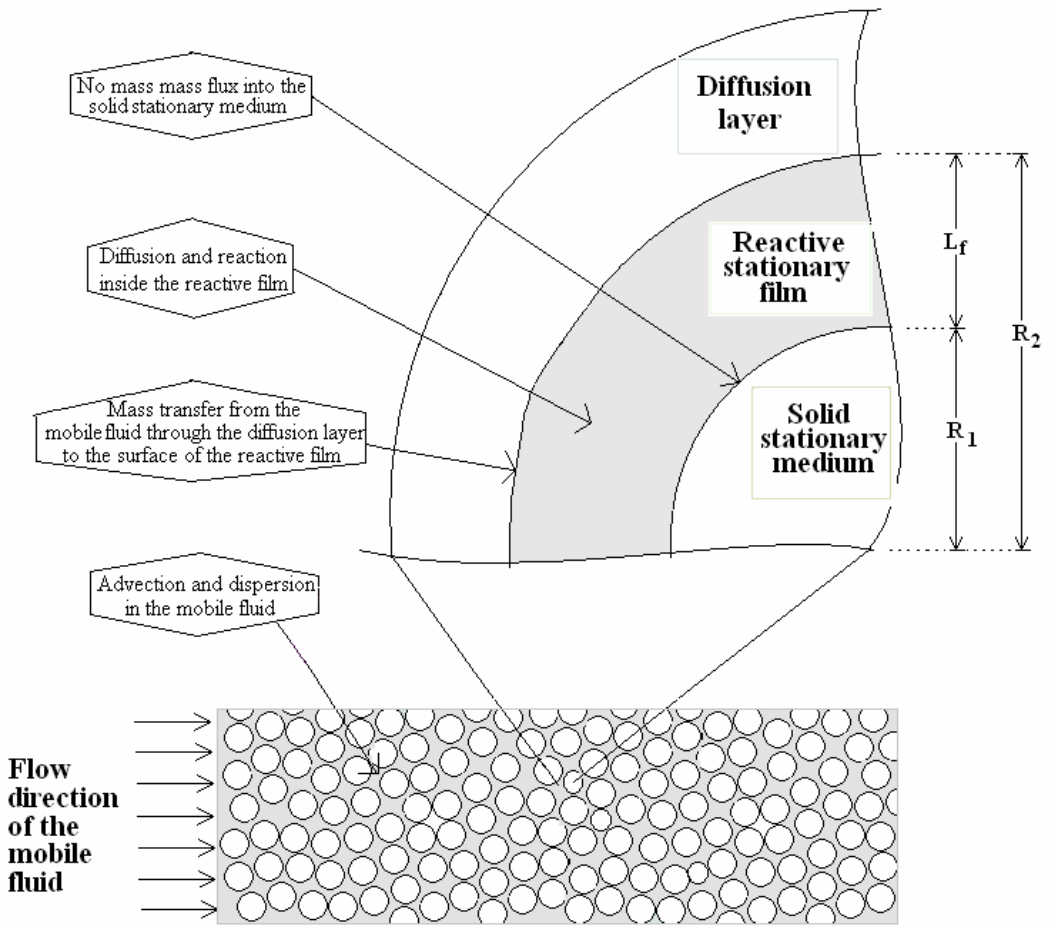

Fig. 7 Schematic representation of the conceptual model.

This model is actually a generalization of many other common models for transport in porous media. For instance, by setting the radius of the inert portion to $R_1 = 0$, but maintaining a reactive film thickness, we arrive at the case where the entire grain is reactive (e.g., a catalyst pellet). Or, by setting the reaction rate in the film equal to zero, we arrive at the case where contaminant absorption occurs without reaction (e.g., activated carbon). Therefore, the model considered in this paper is of wide potential applicability, as it may be reduced to other models as special cases.

Mathematical representation of the conceptual model is described by the following system of equations. The following equations were termed the "biofilm model" in Chapter II because these equations can describe the transport of a contaminant in groundwater with uptake and reaction in a biofilm that coats the aquifer grains.

Chemical diffusion and reaction within the reactive film are mathematically represented by Eq. (34):

$$n_f \frac{\partial C_f(x,r,t)}{\partial t} = n_f D_f \frac{1}{r^2}\frac{\partial}{\partial r}\left[r^2 \frac{\partial C_f(x,r,t)}{\partial r}\right] - n_f k_f C_f(x,r,t) \quad \text{for } R_1 \le r \le R_2 \qquad (34)$$

where x is the distance along the direction of the macroscopic fluid flow, t is the time, r is the radial direction inside a grain of the stationary medium, $C_f(x,r,t)$ is the chemical concentration within the pore space of the reactive film, n_f is the porosity of the reactive film, D_f is the diffusion coefficient within the reactive film, and k_f is the reaction rate constant inside the reactive film.

Equation (35) represents the mass balance in the mobile fluid, accounting for accumulation in the mobile fluid, advection, dispersion, and mass transfer through the diffusive layer to the reactive film:

$$n\frac{\partial C(x,t)}{\partial t} = n\,D\frac{\partial^2 C(x,t)}{\partial x^2} - n\,v\frac{\partial C(x,t)}{\partial x} - 3(1-n)\frac{\omega}{R_2}\left[C(x,t) - C_f(x,r=R_2,t)\right] \quad (35)$$

where $C(x,t)$ is the chemical concentration in the mobile fluid, n is the bulk porosity, D is the longitudinal dispersion coefficient, v is the flow velocity, and ω is the mass transfer coefficient for transport through the diffusive boundary layer.

Eqs. 34 and 35 are coupled through the boundary condition at the surface of the reactive film by Eq. 36.

$$n_f\ D_f\ \frac{\partial C_f(x,r=R_2,t)}{\partial x} = \omega\left[C(x,t) - C_f(x,r=R_2,t)\right] \quad (36)$$

Finally, the boundary condition indicating that there is no contaminant flux from the reactive film into the inert grains of the stationary medium is represented by Eq. 37.

$$\frac{\partial C_f(x,r=R_1,t)}{\partial r} = 0 \quad (37)$$

The important assumptions in the mathematical model are: there is no chemical sorption into the inert portion of the stationary medium, the solid matrix of the stationary medium is considered homogeneous and isotropic, and the reaction within the stationary phase follows first order reaction kinetics.

In order to simplify the analysis, the non-dimensional form of the mathematical model is obtained. The principal non-dimensional variables are:

$$\overline{C} = \frac{C}{C_0} \qquad \overline{C}_f = \frac{C_f}{C_0} \qquad \bar{x} = \frac{x}{L} \qquad \bar{t} = \frac{v\,t}{L} \qquad \bar{r} = \frac{r}{R_2} \tag{38}$$

where C_0 is the characteristic concentration of the chemical, and L is the characteristic length scale of the transport problem. Then, the following non-dimensional system of equations is obtained, analogous to Eqs. 34-38.

$$\frac{\partial \overline{C}_f(\bar{x},\bar{r},\bar{t})}{\partial t} = Ed\,\frac{1}{\bar{r}^2}\frac{\partial}{\partial \bar{r}}\left[\bar{r}^2\,\frac{\partial \overline{C}_f(\bar{x},\bar{r},\bar{t})}{\partial \bar{r}}\right] - Da_f\,\overline{C}_f(\bar{x},\bar{r},\bar{t}) \quad \text{on } r^* \le \bar{r} \le 1 \tag{39}$$

$$\frac{\partial \overline{C}(\bar{x},\bar{t})}{\partial \bar{t}} = \frac{1}{Pe}\frac{\partial^2 \overline{C}(\bar{x},\bar{t})}{\partial \bar{x}^2} - \frac{\partial \overline{C}(\bar{x},\bar{t})}{\partial \bar{x}} - 3\,\kappa\,St\left[\overline{C}(\bar{x},\bar{t}) - \overline{C}_f(\bar{x},\bar{r}=1,\bar{t})\right] \tag{40}$$

$$Ed\,\frac{\partial \overline{C}_f(\bar{x},\bar{r}=1,\bar{t})}{\partial \bar{x}} = St\left[\overline{C}(\bar{x},\bar{t}) - \overline{C}_f(\bar{x},\bar{r}=1,\bar{t})\right] \tag{41}$$

$$\frac{\partial \overline{C}_f(\bar{x},\bar{r}=r^*,\bar{t})}{\partial \bar{r}} = 0 \tag{42}$$

The non-dimensional system of equations is fully characterized by six dimensionless parameters, which are described in Table 3.

System-Splitting Algorithm (SSA)

To solve the mathematical model represented by Eqs. 39-42, it is first employed standard finite difference approximations to the spatial derivatives. By so doing, the partial differential equations (Eqs. 39 and 40) are each replaced by a system of ordinary

differential equations. For instance, the mobile fluid is discretized into N intervals in the longitudinal direction, resulting in N+1 nodal concentrations $\overline{C}(\bar{t})$ that must be determined (see Fig. 8). At each of these N+1 longitudinal nodes, the reactive film is discretized into N_F intervals, resulting in N_F+1 radial concentrations $\overline{C}_f(\bar{x},\bar{t})$ at each longitudinal node. Hence, for each time step, the total number of unknown concentrations is (N+1)*(N_F+2).

The monolithic approach, described more fully in a subsequent section, is to solve for all the unknowns simultaneously at each time step. In contrast, the system-splitting algorithm keeps the systems split, and solves each system separately. Thus, instead of solving one large system of equations at each time step, the SSA solves a number of smaller systems. Specifically, at each time step, a total of N+2 systems of equations are solved. One of these systems is for the mobile-fluid concentration $\overline{C}(\bar{t})$; the other N+1 systems are for the film concentrations $\overline{C}_f(\bar{x},\bar{t})$ at each of the N+1 axial nodes. All of the N+2 systems of equations are tri-diagonal, and may be solved efficiently with the tri-diagonal Thomas algorithm (Pinder and Gray 1977). The difficulty with this approach is that Eqs. 34 and 35 are inherently coupled. Therefore, in order to solve the systems while keeping them split, they must be solved iteratively until all the solutions converge.

Table 3. Definitions of dimensionless parameters

Dimensionless Parameter	Definition
$Pe = \frac{v\,L}{D}$	Peclet number: ratio of the rate of transport by advection to the rate of transport by axial dispersion
$\kappa = \frac{1-n}{n} n_f$	Capacity factor: capacity of the reactive film to store the contaminant
$r^* = \frac{R_1}{R_2}$	Dimensionless radius of the interface between the solid grain and the reactive film
$Da_f = \frac{k}{v/L}$	Damkohler number: ratio of the reaction rate inside the film to the advection rate
$Ed = \frac{D_f / R_2^{\,2}}{v/L}$	Diffusion modulus: ratio of the diffusion rate inside the film to the advection rate
$St = \frac{\omega/R_2}{n_f v/L}$	Stanton number: ratio of the external mass transfer rate across the diffusion layer to the advection rate

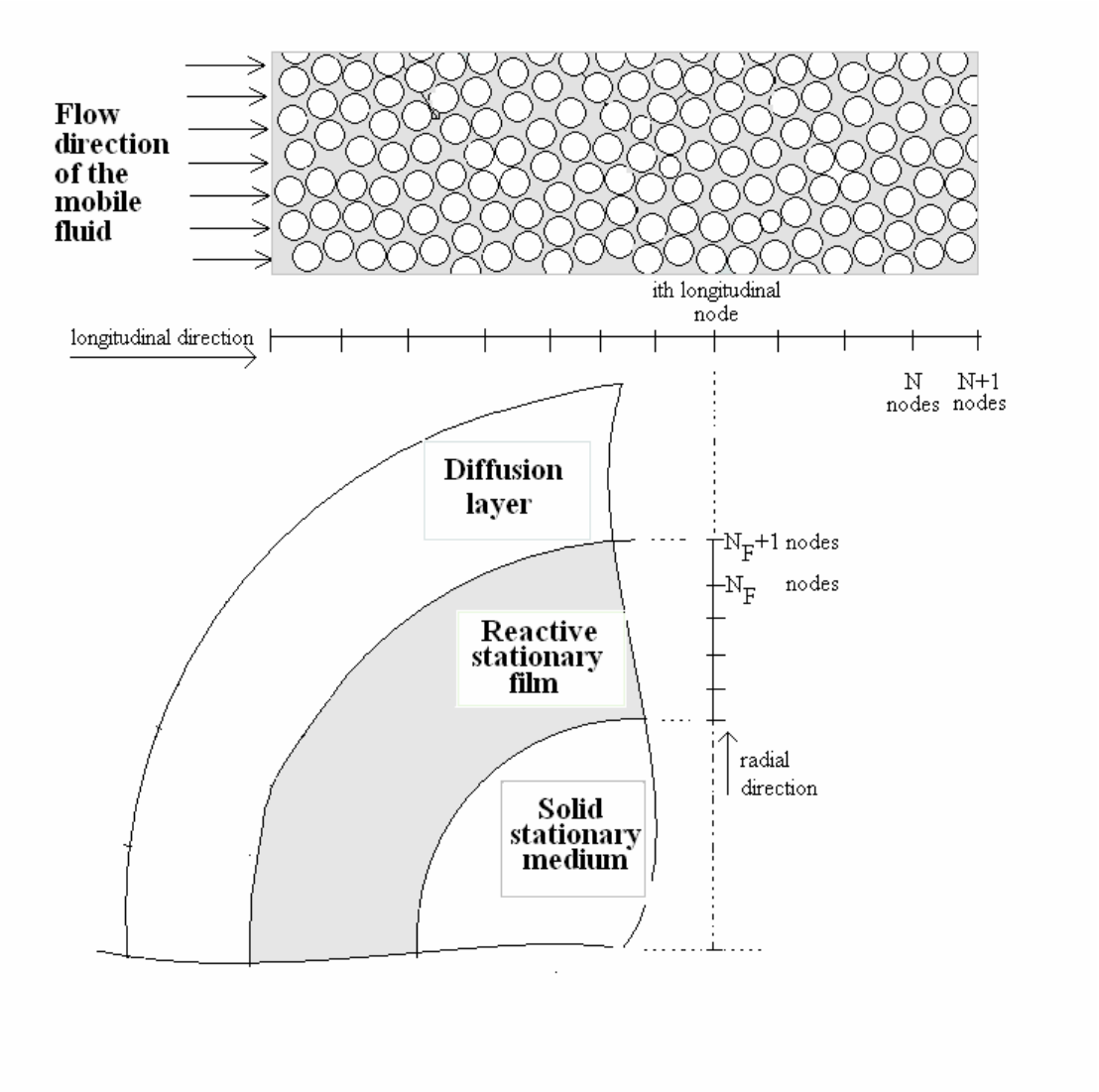

Fig. 8 Schematic representation of the discretization of the partial differential equations.

The schematic representation of the iterative procedure is shown in Fig. 9. Here the procedure is described in words. It is desired to take a time step from $\bar{t}$ to $\bar{t}+\Delta\bar{t}$, solving for the unknown concentrations $\overline{C}(\bar{x},\bar{t}+\Delta\bar{t})$ and $\overline{C}_f(\bar{x},\bar{r},\bar{t}+\Delta\bar{t})$. The SSA starts by making initial estimates of these unknown concentrations. In symbols, it is said that initial estimates $\overline{C}^{i=1}(\bar{x},\bar{t}+\Delta\bar{t})$ and $\overline{C}_f^{i=1}(\bar{x},\bar{r},\bar{t}+\Delta\bar{t})$ are made, where the superscript *i* denotes the i^{th} guess at the value. Specifically, the initial estimates are the concentrations obtained from the previous time step, i.e., it is started by setting $\overline{C}^{i=1}(\bar{x},\bar{t}+\Delta\bar{t})=\overline{C}(\bar{x},\bar{t})$ and $\overline{C}_f^{i=1}(\bar{x},\bar{r},\bar{t}+\Delta\bar{t})=\overline{C}_f(\bar{x},\bar{r},\bar{t})$.

The initial estimates of the concentrations at the surface of the reactive film, $\overline{C}_f^{i=1}(\bar{x},\bar{r}=1,\bar{t}+\Delta\bar{t})$, are used to solve the advection-dispersion-mass-transfer equation (Eq. 40). This yields an updated estimate of the mobile-fluid concentration: $\overline{C}^{i=2}(\bar{x},\bar{t}+\Delta\bar{t})$. Then, the mobile-fluid estimates are used to solve the diffusion-reaction equation (Eq. 39) inside the reactive film. This is done at each $\bar{x}$ location, i.e., *N*+1 different systems are solved. This yields new iteration values of the concentration inside the reactive film: $\overline{C}_f^{i=2}(\bar{x},\bar{r},\bar{t}+\Delta\bar{t})$.

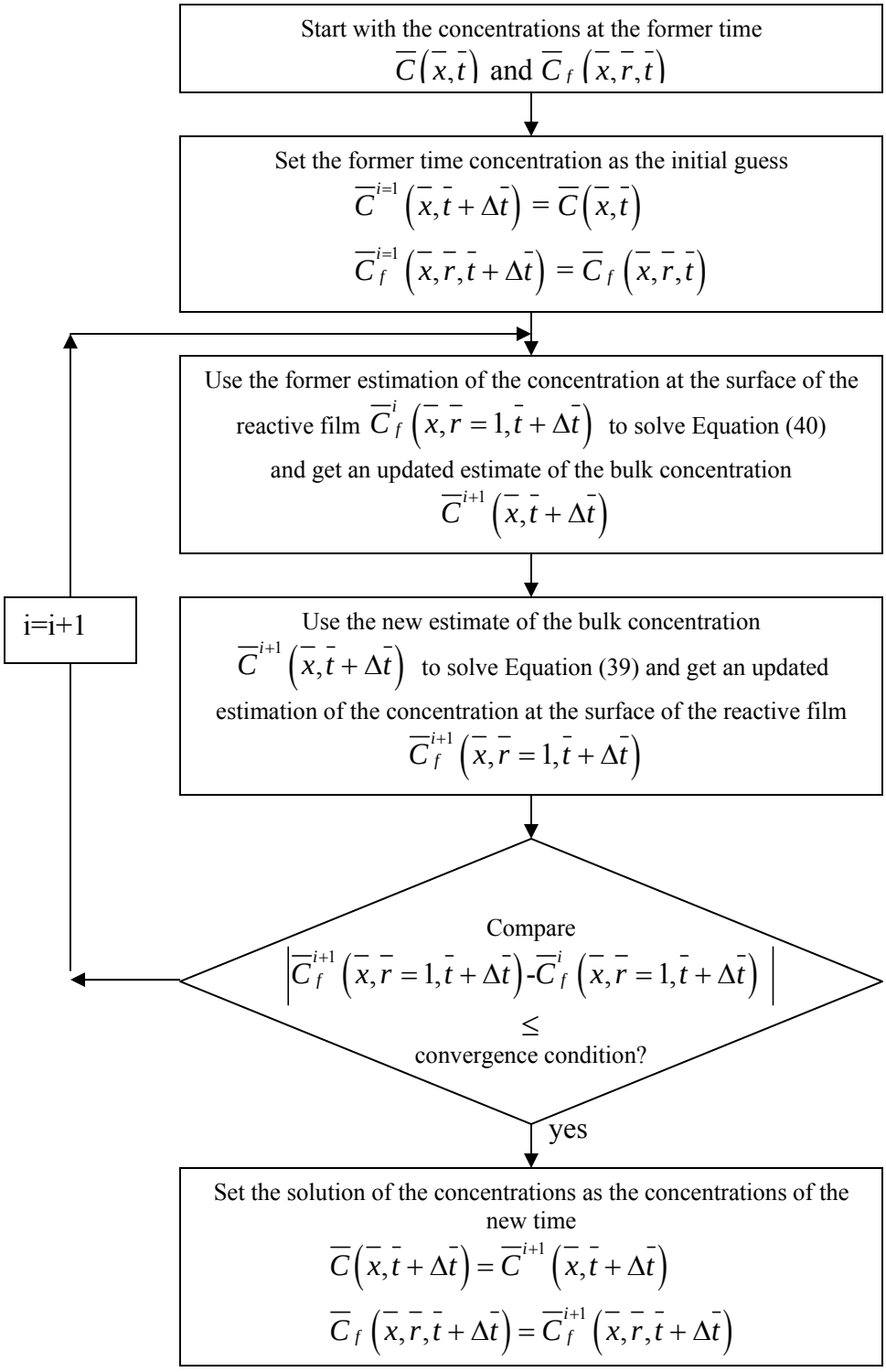

Fig. 9 Schematic representation of the SSA procedure.

Then the estimated values of film-surface concentration are compared from successive iterations, i.e., we compare $\overline{C}_f^{\,i}(\bar{x},\bar{r}=1,\bar{t}+\Delta\bar{t})$ to $\overline{C}_f^{\,i+1}(\bar{x},\bar{r}=1,\bar{t}+\Delta\bar{t})$. The difference between these two estimates is compared to a tolerance criterion, which is typically set at 10^{-9}. The iterative process continues until the difference meets the tolerance criterion, as shown in Fig. 9**.**

Monolithic Algorithm (MA)

As with the system-splitting algorithm, the monolithic algorithm (MA) is based on finite-difference approximations to the spatial derivatives in Eqs. 39-42. As described above, this results in a total of (N+1)*(N_F+2) unknown concentrations that must be determined at each time step. The monolithic algorithm solves for these unknown concentrations simultaneously, i.e., all the equations are fully coupled and solved simultaneously. Thus, if the equations are represented in matrix form, then the matrix of coefficients is a square matrix of size (N+1)(N_F+2)-by-(N+1)(N_F+2). This matrix of coefficients is sparse and banded. Figure 10 shows the structure of the banded matrix for the case of N = 3 axial intervals and N_F = 4 radial intervals; thus the matrix is size 24-by-24. In practice, one would always use many more intervals than 3 axial and 4 radial, but Fig. 10 is provided to show the structure of the matrix. At each time step, the matrix of coefficients is used to determine the unknown concentrations $\overline{C}(\bar{x},\bar{t}+\Delta\bar{t})$ and $\overline{C}_f(\bar{x},\bar{r},\bar{t}+\Delta\bar{t})$.

Since the objective of this chapter is to evaluate the efficiency of the SSA compared to the MA, the matrices should be solved with similar algorithms. Therefore,

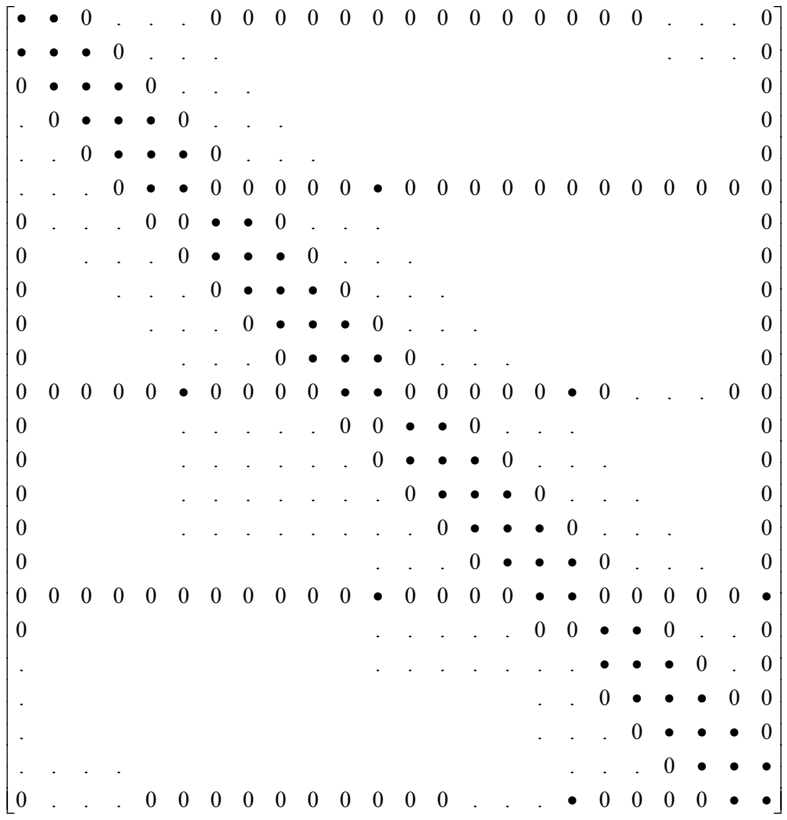

Fig. 10 Structure of the MA matrix for the case $N = 3$ axial intervals and $N_F = 4$ radial intervals.

the banded matrix was solved using a modified Gaussian elimination procedure developed by the author for the specific matrix structure, to take advantage of the sparse and banded structure. The modified Gaussian elimination procedure is similar to the Thomas algorithm and was found to be computationally far superior to solution by LU decomposition or by inversion of the original matrix. Since both the SSA equations and the MA equations are solved with algorithms that take advantage of their tri-diagonal or banded structure, it is appropriate to compare the two methods.

Results

The system of Eqs. 39-42 was solved for a hypothetical column with the following initial and boundary conditions. Initially, there is no chemical present in the mobile fluid or within the reactive film (Eq. 43).

$$\overline{C}(\bar{x},\bar{t}=0)=0$$
$$C_f(\bar{x},\bar{r},\bar{t}=0)=0 \tag{43}$$

There is a continuous source of chemical located at the column inlet, $\bar{x}=0$ (Eq. 44). At the effluent end of the column, there is no dispersive flux (Eq. 45).

$$\overline{C}\left(\bar{x}=0,\bar{t}\right)-\frac{1}{Pe}\frac{\partial\overline{C}\left(\bar{x}=0,\bar{t}\right)}{\partial\bar{x}}=1 \tag{44}$$

$$\frac{\partial\overline{C}\left(\bar{x}=1,\bar{t}\right)}{\partial\bar{x}}=0 \tag{45}$$

To evaluate the efficiency of the SSA compared to the MA, both methods were used to solve Eqs. 39-42 subject to the initial and boundary conditions of Eqs. 43-45. Solutions were obtained from time $\bar{t} = 0$ up $\bar{t} = 2.0$, i.e., for both transient and steady-state (long-time) conditions. Solutions were obtained for twelve different sets of simulated physical conditions. It has been shown previously (Chapter II) that the overall reaction rate can be controlled by the chemical diffusion across the diffusion boundary layer (external mass transfer), by diffusion within the reactive film (internal mass transfer), or by the reaction rate within the film. Thus, for the comparison of the SSA to the MA, three cases where external mass transfer is the controlling process, three cases where internal mass transfer is the controlling process, three cases where reaction in the film is the controlling process, and three cases where all three processes are important were considered. The purpose was to determine the conditions under which the SSA might be computationally superior to the MA. Conditions for the twelve cases are shown in Table 4.

Simulation results were compared for calculation time and accuracy. Both algorithms were evaluated with the same computational conditions, described as follows. The computer characteristics are: Pentium® 4 processor 2.8 GHz, 750 MB in RAM, and Windows XP® environment. The SSA and MA codes were developed and run in MATLAB® version 7.

To verify that the system-splitting algorithm and the monolithic algorithm were coded properly, and that the methods are valid, results from these two methods were compared and were found to agree to within 0.05% or better for all the cases tested.

Table 4. Conditions tested for comparison of SSA to MA

Case	*St*	*Ed*	Da_f	Controlling Process
1	0.500	1000.	100.	
2	0.143	1000.	100.	External mass transfer
3	0.0476	1000.	100.	
4	1000.	0.0272	100.	
5	1000.	0.0136	100.	Internal mass transfer
6	1000.	0.0091	100.	
7	1000.	1000.	10.	
8	1000.	1000.	3.	Reaction
9	1000.	1000.	1.	
10	1.25	0.100	20.	
11	0.369	0.050	6.	All three processes
12	0.125	0.025	2.	

Note: All simulations were performed using $r^* = 0.95$, $\kappa = 1.6$, and $Pe = 100$.

Also, the two methods were verified against a Laplace-transform solution of the equations (Chapter II). Hence, it is concluded that the SSA and the MA produce correct and equally accurate solutions to the model, in both the transient and steady-state portions of the solution.

To demonstrate this further, Fig. 11 shows the breakthrough curve at $\bar{x} = 1$ when external mass transfer is the condition controlling the process (cases 1–3 of the twelve cases tested). The steady-state concentration at $\bar{x} = 1$ does not approach a dimensionless concentration $C/C_0 = 1$; this is because some of the contaminant undergoes first-order decay, as indicated by Eqs. 34 or 39. The important point is that the SSA and the MA result in indistinguishable breakthrough curves. The same level of agreement is obtained for the rest of the conditions tested (cases 4–12; data not shown). In all cases tested, the results obtained by the SSA and the MA agree to within a relative difference of 0.05% or better.

When the external mass transfer is the rate-controlling process (cases 1–3), the CPU time required by the SSA is approximately 3% of the CPU time required by the MA (Fig. 12). This result is based on simulations conducted with $N = 100$ axial nodes and $N_F = 50$ radial nodes. Simulations were run to a maximum dimensionless time $\bar{t}_{\max} = 2.0$, with a time step $\Delta\bar{t} = 0.001$. Figure 13 shows that when the process is controlled by internal mass transfer (cases 4–6), the SSA requires approximately 0.3% of the CPU time required by the MA, based on $N = 100$, $N_F = 5000$, $\bar{t}_{\max} = 2.0$, and $\Delta\bar{t} = 0.001$. For cases 4–6, the computation time for the MA is estimated based on running the code only to $\bar{t}_{\max} = 0.01$, then extrapolating to $\bar{t}_{\max} = 2.0$. This was done

because, for cases 4–6, a very fine discretization is required for the reactive film ($N_F = 5000$), which makes the MA code run extremely slowly. For cases 7–9, in which the overall degradation rate is controlled by the reaction inside the film, the SSA requires about 50% of the CPU time required by the MA (Fig. 14), based on $N = 100$, $N_F = 50$, $\bar{t}_{\max} = 2.0$, and $\Delta\bar{t} = 0.001$. Finally, when all three processes are important (cases 10–12), the SSA requires approximately 0.4% of the CPU time required by the MA (Fig. 15), based on $N = 100$, $N_F = 500$, $\bar{t}_{\max} = 2.0$, and $\Delta\bar{t} = 0.001$. In summary, the computation time required by the SSA is lower than that of the MA for all 12 cases we tested. The time required by the SSA ranges from 0.3% to 50% of that required by the MA. It is concluded that the new system-splitting algorithm, introduced in this chapter, offers a significant computational savings over the monolithic method, with no sacrifice in accuracy.

The computation time of the SSA increases as more iterations per time step are needed for convergence. This can be noticed in the difference of computation time between cases with similar simulation conditions. For example, cases 1–3 and cases 7–9 were all based on simulations with $N = 100$ axial nodes and $N_F = 50$ radial nodes, run to a maximum dimensionless time $\bar{t}_{\max} = 2.0$, and run with a time step $\Delta\bar{t} = 0.001$. For cases 1–3, where the external mass transfer was the rate-limiting process, the average number of iterations per time step was 2. Meanwhile, for cases 7–9, where the reaction inside the film was the rate-limiting process, the average number of iterations per time step was 32. Thus, the CPU time required for cases 7–9 was about 16 times larger than the CPU time for cases 1–3.

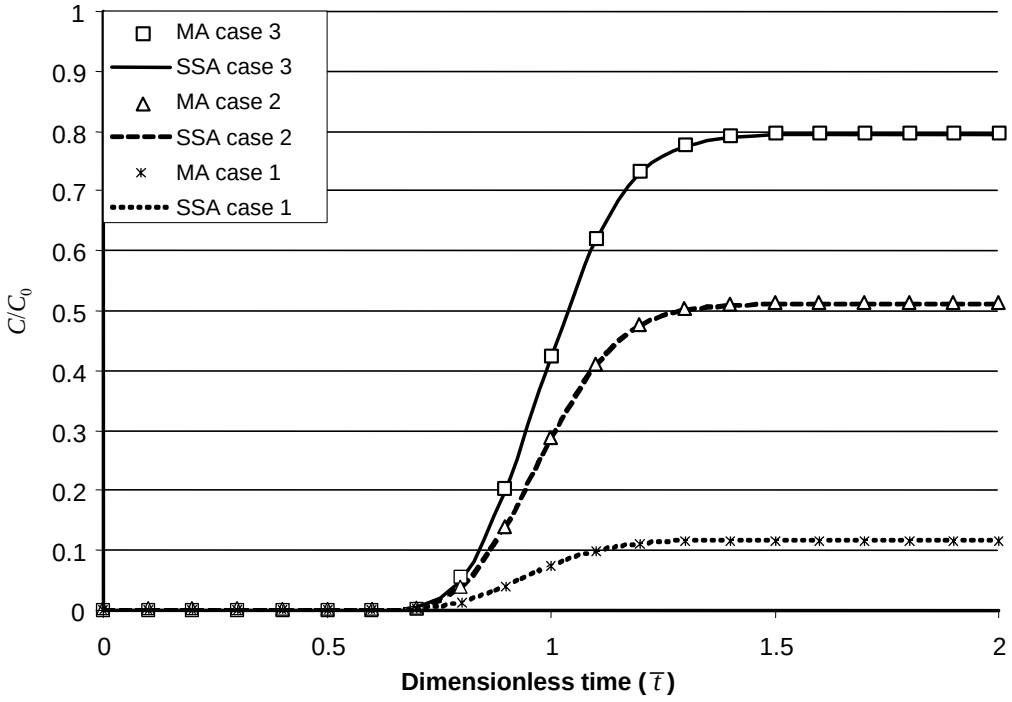

Fig. 11 Breakthrough curves at $\bar{x} = 1$ for the conditions in which external mass transfer is the controlling process.

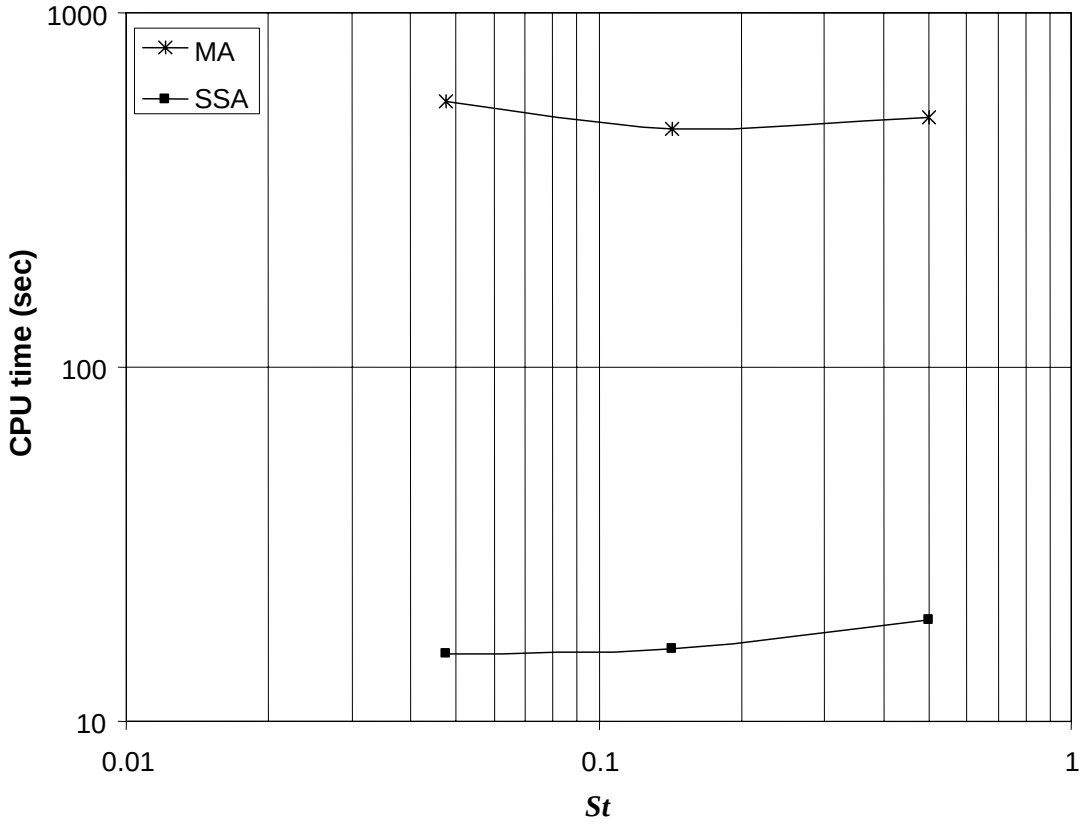

Fig. 12 Comparison of CPU time for the cases in which external mass transfer is the controlling process (cases 1–3).

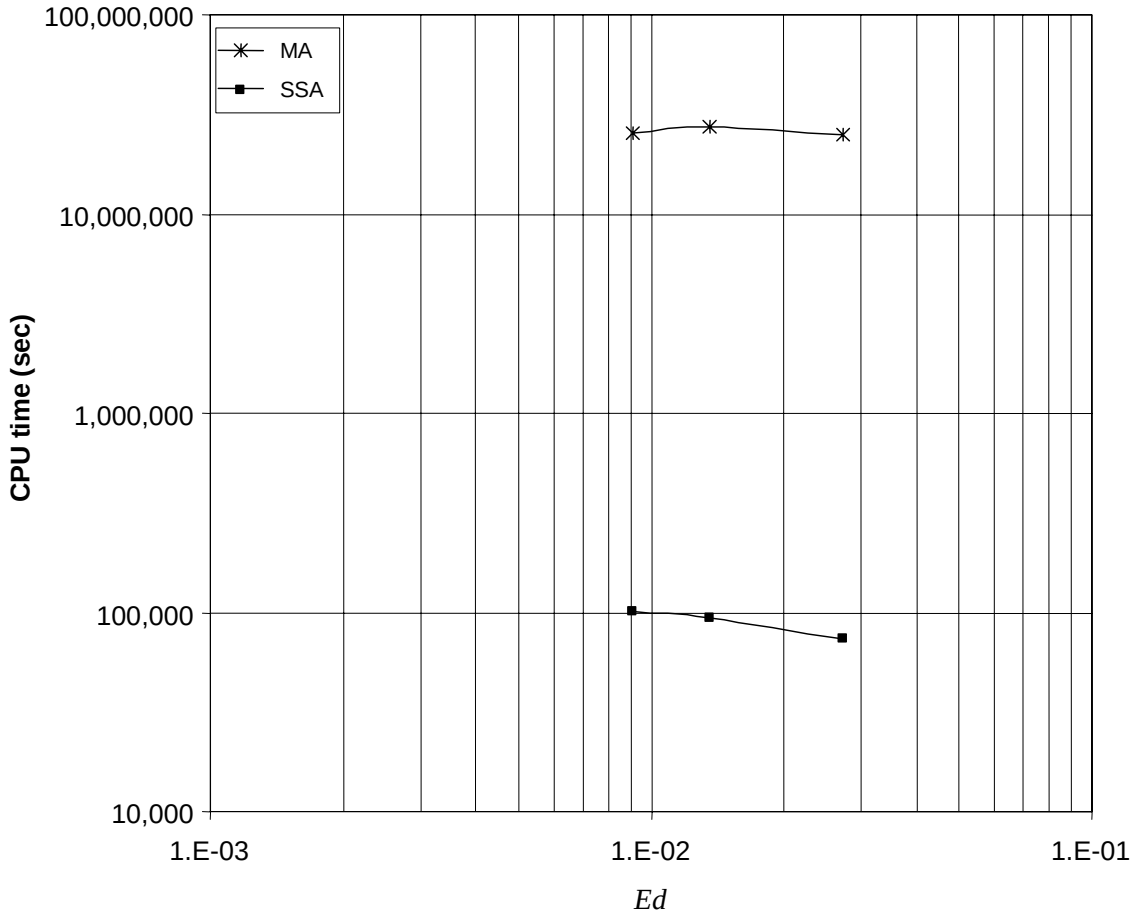

Fig. 13 Comparison of CPU time for the cases in which internal mass transfer is the controlling process (cases 4–6).

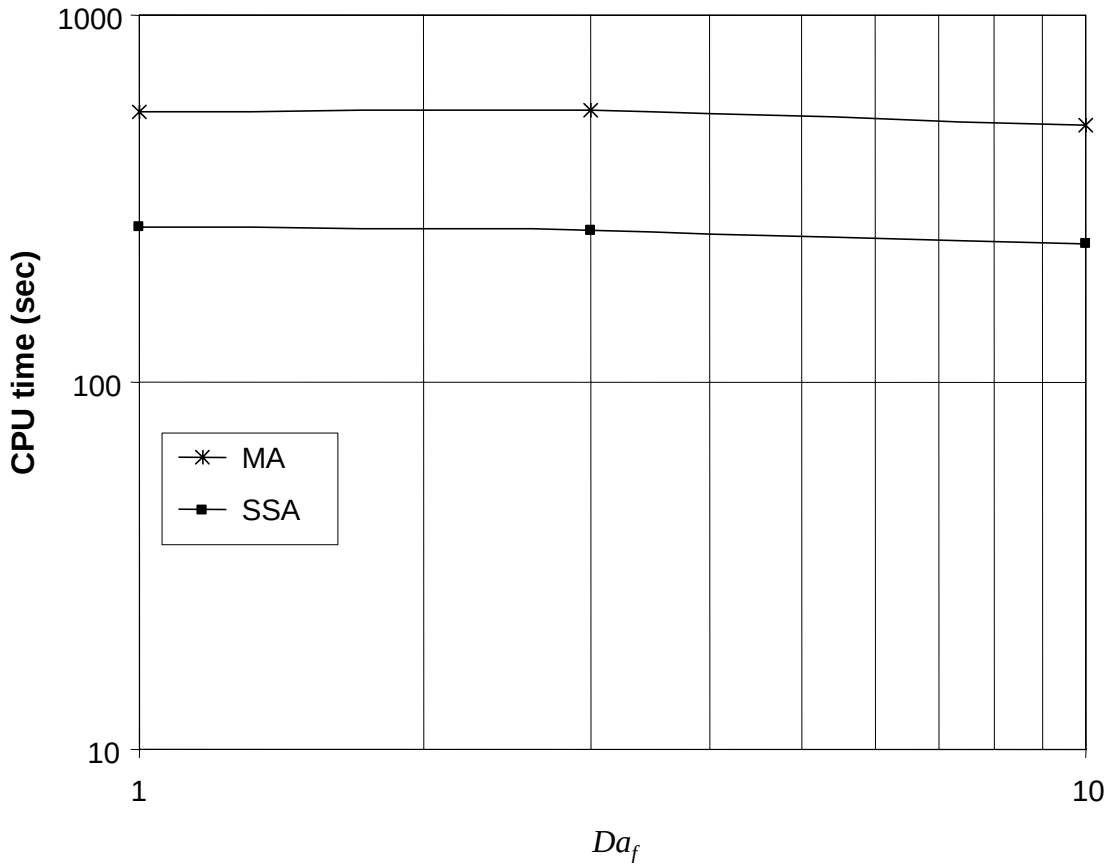

Fig. 14 Comparison of CPU time for the cases in which reaction inside the film is the controlling process (cases 7–9).

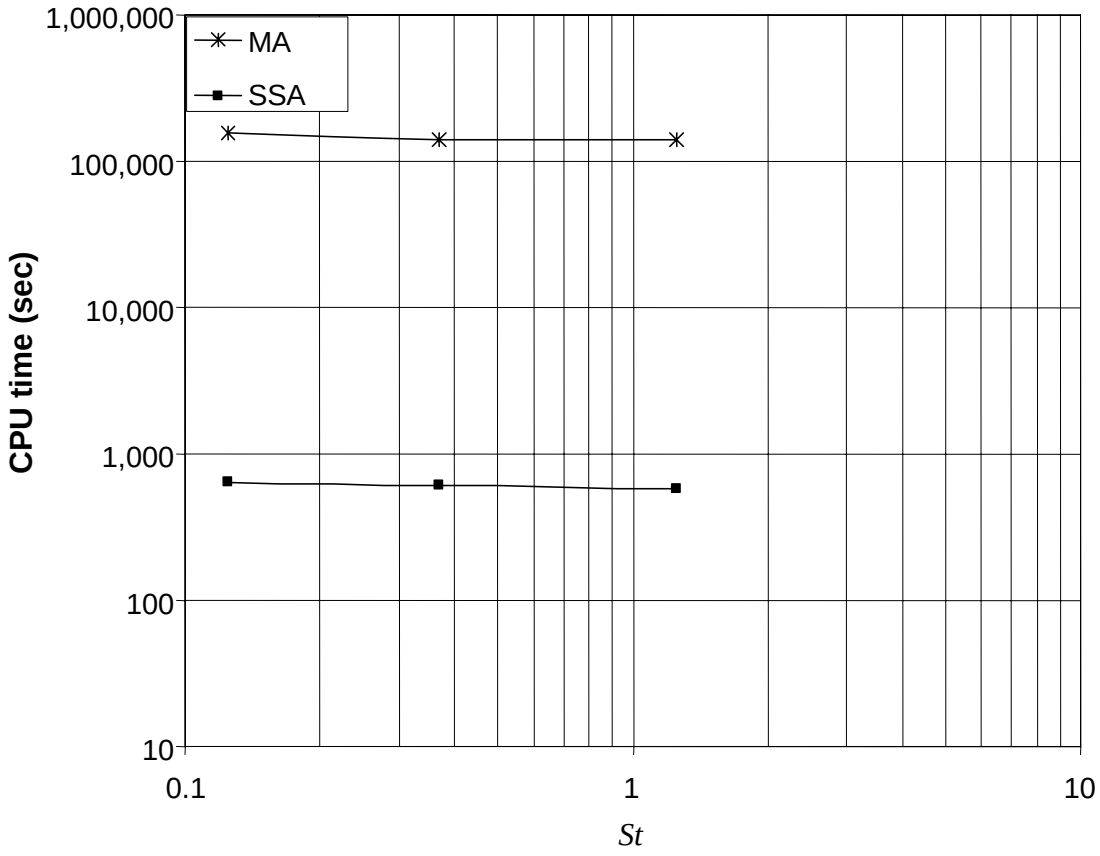

Fig. 15 Comparison of CPU time for the cases in which external mass transfer, internal mass transfer, and reaction inside the film are all significant processes (cases 10–12).

As the internal diffusion rate *Ed* decreases, the concentration profile within the reactive film becomes very steep. This requires an increase in the number of radial nodes (N_F) inside the film in order to accurately resolve the concentration profile. For the cases where the external mass transfer or the reaction in the film is the rate-controlling process, the value of *Ed* is high, and N_F is equal to 50. For cases 10–12, when *Ed* is decreased, N_F is increased to 500 to maintain accuracy. For cases 4-6, when internal diffusion is the controlling process, *Ed* is very low, and N_F is increased to 5000. The average CPU time was compared versus the number of radial nodes in Fig. 16**.** The SSA cases shown in Figure 16 all required about 30 iterations per time step in order to converge. It is noted that, for the SSA, the slope of this curve (on a log-log scale) is approximately 1.3. This means that the number of computations required by the SSA is approximately proportional to $(N_F)^{1.3}$. In contrast, the slope of the curve for the MA is approximately 2.3, so the number of computations required by the MA is proportional to $(N_F)^{2.3}$. This quantifies the superior computational efficiency of the SSA over the MA.

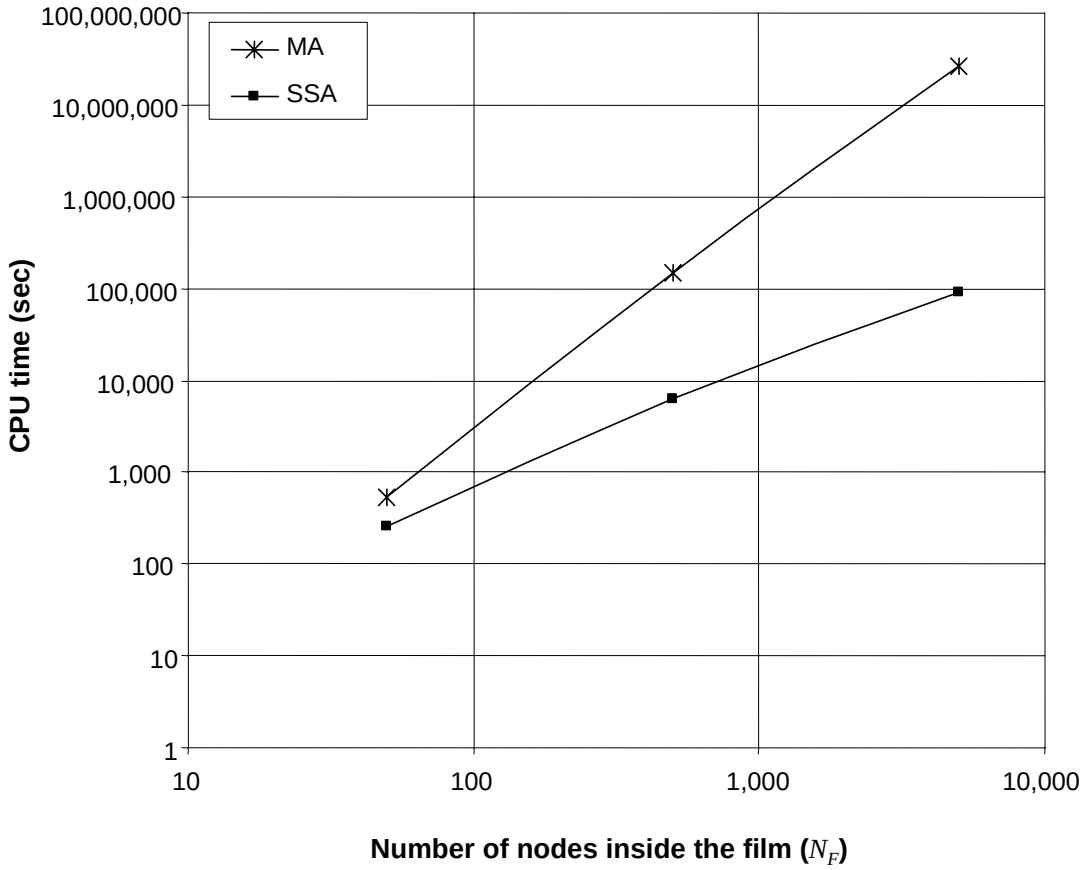

Fig. 16 Dependence of the CPU time on the number of radial nodes for the SSA and MA.

Discussion, Summary, and Conclusions

The results presented here provide a comparison of the SSA to the MA in terms of calculation time. Based on the assumption that the overall reaction rate is controlled by external mass transfer, internal mass transfer, and reaction rate within the film (Chapter II), 12 different cases that account for a range of possible physical scenarios were simulated. The SSA is seen to be superior in CPU time, with no sacrifice in accuracy, under all conditions tested. Therefore it is concluded that the SSA is computationally superior to the MA. The SSA is computationally efficient because it converts the original two-dimensional system of partial differential equations into two smaller one-dimensional systems, saving CPU time and storage.

The SSA also has some other attractive features for solving the system of partial differential equations. The solution is divided in two systems; each system can be solved using different numerical techniques. Similarly, the SSA permits the use of different time steps depending on the method employed to solve each system. These features have not yet been explored in the current chapter but should be relatively easy to implement. Overall, the solution procedure employs a practical modular code that can be easily modified as the mathematical representation of the physical phenomena changes.

For research focused on phenomena occurring inside the reactive film, it is appropriate to employ the SSA because the code is easily modified to account for any type of reaction kinetics. For example, when dealing with reactive biofilms coating the grains of an aquifer, the reaction kinetics are non-linear most of the time. Then, the SSA

is an appealing algorithm because the modular code gives flexibility in choosing the best numerical technique to solve the non-linear diffusion-reaction equation inside the reactive film. Additionally, the SSA can be easily modified to account for multiple species because the CPU storage requirements are less demanding than the MA.

Furthermore, the SSA will be useful when spatial or temporal discretizations in the computer code differ between the mobile fluid system and the stationary medium system. For example, in simulating groundwater contaminant transport and remediation, which is the original purpose of the present dissertation, the SSA is a practical tool to distinguish between the effects of macroscopic processes (along the mobile fluid) and microscopic processes (in the stationary medium). Different temporal or spatial grids can be used for the two scales.

In summary, the system-splitting algorithm presented in this chapter is a novel method for simulating transport in porous media with mass exchange between the mobile fluid and the stationary medium. The new method offers advantages in terms of computational efficiency and in terms of flexibility of application. In the next Chapter, I apply the SSA to multi-species transport and biodegradation in groundwater with non-linear reaction kinetics. A future application could be the removal of heavy metals from drinking water by adsorption in fixed beds of activated alumina. It is anticipated that the SSA will be found useful for many other porous-medium applications as well.

CHAPTER IV

MODELING MULTISPECIES NON-LINEAR REACTIVE TRANSPORT IN POROUS MEDIA WITH MASS EXCHANGE BETWEEN MOBILE FLUID AND STATIONARY MEDIUM

Overview

The applicability of a novel approach to numerically solve the mathematical model of non-linear reactive mass transport in porous media is evaluated. The main objective is to solve a system of equations describing multispecies transport with non-linear reaction, where the transfer of mass from the mobile fluid to the stationary medium is considered an important mechanism involved in the process. The new solution approach, named "system-splitting-operator-splitting approach" (SSOSA), is a combination of the system splitting approach (SSA) described in Chapter III and an operator-splitting approach (OSA). The SSA is used to separate the systems of differential equations: one for transport in the mobile fluid, and one for uptake and reaction in the stationary medium. In addition, the system of uptake and reaction in the stationary medium involves a non-linear system of equations, so it is solved using an operator splitting approach to overcome the complexity of the system. The operator splitting approach permits the solution of the non-linear system of equations (uptake and reaction inside the stationary medium) by using a different numerical scheme to solve each operator. The SSOSA contains intrinsic errors as a result of the operator splitting algorithm, so the SSOSA was evaluated for different cases to determine when the error is acceptably small. Overall, the solution procedure provides flexibility in combining different numerical tools to

efficiently solve the complex system of equations resulting from the mathematical description of biodegradation during transport in groundwater or porous media.

Introduction

Systems of multispecies non-linear reactive transport are sometimes required to describe contaminant fate and transport in groundwater or porous media. Solving this complex system of equations usually requires significant computational effort. Therefore, it is important to develop an efficient algorithm to solve the mathematical description of the relevant phenomena, and that algorithm must account properly for the non-linearities of the system of equations.

The mathematical model of multispecies non-linear reaction transport in porous media comprises a system of coupled non-linear partial differential equations. The solution is not trivial, thus different numerical approaches have been used to solve the complex system of equations (Brusseau et al. 1992; Li et al. 2001; Sun et al. 1998; Tsai et al. 2005). A sequential approach named operator-splitting has received good acceptance for solving real case scenarios (Clement et al. 1998; Phanikumar and McGuire 2004; Vencelides et al. 2007). Basically, the operator splitting approach splits the system of equations in two operators: one operator is the system of partial differential equations describing the transport phenomena, and the other operator is the non-linear partial differential system of equations describing the reaction kinetics. In the OS approach, the transport operator is solved first, and the reaction operator is solved second. This approach is appealing because it permits the solution of each operator using

the most suitable numerical scheme; the most appropriate time scale can be used to solve each operator; and the OSA can be easily modified to adapt to the different mathematical representation of the phenomena of interest. Since each operator is solved independently, parallelization is also possible (Valocchi and Malmstead 1992). Therefore, the OS approach is appealing for problems of transport with non-linear reaction because it permits the solution of more realistic mathematical representation of transport in porous media due to the flexibility for handling complex systems of equations (Odencratz et al. 1990).

To solve the system of coupled partial differential equations (describing the transport of the contaminant) and partial differential equations with non-linear terms (describing the reaction kinetics) describing the multispecies nonlinear transport, the system-splitting algorithm from Chapter III has been combined with an operator splitting (OS) method. The combined algorithm is named the "system-splitting operator-splitting algorithm" (SS-OSA). As described in Chapter III the SSA solves the numerical problem iteratively by splitting the complete set of equations into two systems. One system accounts for transport in the mobile fluid along the bulk direction of flow; and the other system describes the diffusion and reaction inside the reactive film that coats the stationary medium. The two systems are coupled by a boundary condition at the interface between the mobile fluid and the stationary medium. Furthermore, in this chapter, an operator splitting method is used to solve the system of diffusion and non-linear reaction inside the reactive film. The sequential operator-splitting method solves the transport (diffusion) portion of the governing equations over a full time step,

followed by a solution of the non-linear reaction portion of the equations over the same time step (Carrayrou et al. 2004).

However, the splitting procedure generates errors inherent to the time splitting (Carrayrou et al. 2004; Barry et al. 1996b; Barry et al. 1996a; Kaluarachchi and Morshed 1995; Kanney et al. 2003; Morshed and Kaliarachchi 1995). The nature of the errors has been studied elsewhere. Valocchi and Malmstead (1997) concluded that the sequential operator splitting method leads to a mass balance error associated with continuous mass input at the boundary condition for one dimensional first order problems. They introduced a criterion for reducing the error where the reaction rate multiplied by the time step must be smaller that 0.1. Kaluarachchi and Morshed (1995) concluded that the concentration prediction error of a given problem is larger than its overall mass balance error, so a reaction rate time step criterion must be smaller than the one used for the mass balance error criterion. In the second part of their work, Morshed and Kaluarachichi (1995) determined that the error is related to the reaction rate and the timelag verifying the observations from other error studies (Carrayrou et al. 2004; Barry et al. 1996b; Barry et al. 1996a; Kaluarachchi and Morshed 1995; Kanney et al. 2003; Morshed and Kaliarachchi 1995).

In the present chapter, a mathematical model has been developed for the purpose of modeling mass transport of chlorinated ethenes in groundwater with exchange between a mobile fluid phase and a reactive stationary phase. The reactive stationary phase is a reactive biofilm coating the grains of an aquifer. Diffusion and biodegradation (non-linear reaction) occur inside the biofilms that coat the aquifer grains

(Rittmann 1993). The reaction kinetics is described by Monod kinetics with competition between substrates. Therefore a non-linear system of partial differential equations has to be solved for each chemical species at each time step and each axial location. For this purpose the SSOSA has been applied to the problem of transport and biodegradation of chlorinated ethenes. Finally an evaluation of the SSOSA inherent errors has been attained.

The original contributions of this chapter are three. First, to the best of the author's knowledge, this paper represents the first time that the SSA is combined with an OS method to solve the problem of multispecies and nonlinear reaction transport in porous media with mass exchange between the mobile fluid and the stationary porous medium. Second, the SSOSA has been used to simulate transport and degradation of chlorinated ethenes through porous media. Third the error inherent to the splitting procedure has been evaluated. A range of different possible physical scenarios has been considered to evaluate the applicability and limitations of the SSOSA.

Conceptual and Mathematical Model

The conceptual model is described in Chapter III and Fig. 7 of Chapter III. Briefly, in the mobile (bulk) fluid, advection and dispersion occur in the direction of macroscopic fluid flow. The stationary medium is comprised of spherical grains coated with a biofilm. A diffusive boundary layer surrounds the coated grains, and chemical mass transfer occurs from the mobile fluid, through the diffusive boundary layer, to the surface of the biofilm. Within the biofilm, diffusion and reaction occur. The differences here are (1) that the

reaction is mathematically represented by nonlinear reaction and (2) multiple species are being transported through the porous media. Particularly in the present chapter, the non-linear sequential degradation of chlorinated ethenes is studied. The biodegradation of chlorinated ethenes is represented by a model based on Monod kinetics with competition between substrates (Cupples et al. 2004).

Mathematical representation of the conceptual model is similar to the one described in Chapter III, so some equations are not derived here. Chemical diffusion and reaction within the reactive film are mathematically represented by Eq. 46:

$$\phi_f \frac{\partial C_{nf}(x,r,t)}{\partial t} = \phi_f D_{nf} \frac{1}{r^2}\frac{\partial}{\partial r}\left[r^2 \frac{\partial C_{nf}(x,r,t)}{\partial r} \right] + f_n\left(C_{1f}(x,r,t),...,C_{nf}(x,r,t),...,C_{Nf}(x,r,t)\right) \quad \text{for } R_1 \le r \le R_2 \qquad (46)$$

where the subscript $n = 1...N$ indicates the n^{th} chemical species inside the biofilm, x is the distance along the direction of the macroscopic fluid flow, t is the time, r is the radial direction inside a grain of the stationary medium, $C_{nf}(x,r,t)$ is the concentration of the n^{th} chemical within the pore space of the reactive film, ϕ_f is the porosity of the reactive film, and D_{nf} is the diffusion coefficient of the n^{th} chemical species within the reactive film. The term $f_n()$ describes the rate of chemical reaction of the n^{th} species.

The reaction functions f_n for each chemical species are related to the sequential degradation of cis-Dichloroethene (cDCE) under anaerobic and substrate limiting conditions (low hydrogen and chlorinated ethene concentrations). Biodegradation of cDCE under anaerobic conditions (those of groundwater) is conducted by bacterially-

mediated sequential reductive dechlorination. That is, cDCE is converted sequentially to vinyl chloride (VC), and finally ethene, a benign end-product (McCarty 1998). The dechlorination reaction is modeled following the approach of Cupples et al. (2004). The reaction is represented by Monod kinetics with competitive inhibition between the multiple electron acceptors involved in the dechlorination for the case when electron donor is rate limiting (Cupples et al. 2004). Therefore, the reaction function comprises three different chemical species, namely cis-Dichloroethene (cDCE), vinyl chloride (VC) and ethene (ETH) (n=1,2,3 respectively). The system of equations representing the reaction functions are:

$$f_1 = -\left[\frac{\hat{q}_1 C_{1f}(x,r,t)}{C_{1f}(x,r,t) + K_1\left(1+\frac{C_{2f}(x,r,t)}{K_{i\_2}}\right)}\left[\frac{H_f(x,r,t)-H^*}{\left(H_f(x,r,t)-H^*\right)+K_h}\right]\right] X_a(r,t) \tag{47}$$

$$f_2 = \left[\left[\frac{\hat{q}_1\ C_{1f}}{C_{1f}(x,r,t) + K_1\left(1+\frac{C_{2f}(x,r,t)}{K_{i\_2}}\right)}\right] - \left[\frac{\hat{q}_2 C_{2f}}{C_{2f}(x,r,t) + K_2\left(1+\frac{C_{1f}(x,r,t)}{K_{i\_1}}\right)}\right]\right]\left[\frac{H_f(x,r,t)-H^*}{\left(H_f(x,r,t)-H^*\right)+K_h}\right] X_a(r,t) \tag{48}$$

$$f_3 = \left[\frac{\hat{q}_2 C_{2f}}{C_{2f}(x,r,t) + K_2\left(1 + \frac{C_{1f}(x,r,t)}{K_{i\_1}}\right)} \right] \left[\frac{H_f(x,r,t) - H^*}{\left(H_f(x,r,t) - H^*\right) + K_h} \right] X_a(r,t) \tag{49}$$

where $\hat{q}_1$ and $\hat{q}_2$ are the maximum utilization coefficients for each chemical species (μmol/cell day), K_1 and K_2 are the half-velocity coefficients (μM) for cDCE and VC respectively, K_{i_1} and K_{i_2} are the competitive coefficients for cDCE and VC respectively, H_f is the hydrogen concentration in the biofilm, K_h is the half-velocity coefficient (μM) for hydrogen, H^* is the hydrogen threshold concentration (μM), and X_a is the concentration of bacteria (cell/L). The growth of microorganisms is represented by Eq. 50.

$$\frac{dX_a(r,t)}{dt} = \left\{ \left[\begin{array}{l} \dfrac{\hat{\mu}\, C_{1f}(x,r,t)}{C_{1f}(x,r,t) + K_1\left(1 + \dfrac{C_{2f}(x,r,t)}{K_{i\_2}}\right)} \\ + \dfrac{\hat{\mu}\, C_{2f}(x,r,t)}{C_{2f}(x,r,t) + K_2\left(1 + \dfrac{C_{1f}(x,r,t)}{K_{i\_1}}\right)} \end{array} \right] \left[\frac{\left(H_f(x,r,t) - H^*\right)}{\left(H_f(x,r,t) - H^*\right) + K_h} \right] - b \right\} X_a(r,t) \tag{50}$$

where $\hat{\mu}$ is the maximum growth rate (1/day) and b is the decay rate (1/day) of the bacteria.

The values used for the coefficients in the reaction equations ($\hat{q}$, K_1, K_2, K_{i_1}, K_{i_2}, H_f, K_h, H^*, X_a, $\hat{\mu}$, and b) as well as the mathematical representation of the reaction kinetics follow Cupples et al. (2004).

Equation 51 represents the mass balance in the mobile fluid, accounting for accumulation in the mobile fluid, advection, dispersion, and mass transfer through the diffusive layer to the reactive film for each chemical species:

$$\phi \frac{\partial C_n(x,t)}{\partial t} = \phi D_n \frac{\partial^2 C_n(x,t)}{\partial x^2} - \phi v \frac{\partial C_n(x,t)}{\partial x} - 3(1-\phi)\frac{\omega_n}{R_2}\left[C_n(x,t) - C_{nf}(x, r = R_2, t)\right] \qquad (51)$$

where $C_n(x,t)$ is the concentration of the nth chemical species concentration in the mobile fluid, ϕ is the bulk porosity, D_n is the longitudinal dispersion coefficient of compound n, v is the flow velocity, and ω_n is the mass transfer coefficient for transport through the diffusive boundary layer as described in Chapter III.

The system of equations (Eqs. 47-50 and 51) are coupled through the boundary condition at the surface of the reactive film for each chemical species by Eq.52.

$$\phi_f \; D_{nf} \; \frac{\partial C_{nf}(x, r = R_2, t)}{\partial x} \quad = \quad \omega_n \left[C_n(x,t) - C_{nf}(x, r = R_2, t)\right] \qquad (52)$$

Finally, the boundary condition indicating that there is no contaminant flux from the reactive film into the inert grains of the stationary medium is represented by Eq. 53.

$$\frac{\partial C_{nf}(x, r = R_1, t)}{\partial r} = 0 \qquad (53)$$

In order to simplify the analysis, we obtain the non-dimensional form of the mathematical model using the principal non-dimensional variables described in Chapter III. Then, the following non-dimensional system of equations is obtained, analogous to Eqs. 47-53.

$$\frac{\partial \overline{C}_{nf}(\overline{x},\overline{r},\overline{t})}{\partial \overline{t}} = Ed_n \frac{1}{\overline{r}^2} \frac{\partial}{\partial \overline{r}}\left[\overline{r}^2 \frac{\partial \overline{C}_{nf}(\overline{x},\overline{r},\overline{t})}{\partial \overline{r}}\right] + \overline{f}_n\left(\overline{C}_{1f}(\overline{x},\overline{r},\overline{t}),...,\overline{C}_{nf}(\overline{x},\overline{r},\overline{t}),...,\overline{C}_{Nf}(\overline{x},\overline{r},\overline{t})\right) \quad \text{on } r^* \le \overline{r} \le 1 \tag{54}$$

$$\overline{f}_1 = -Da_1 \overline{X}_a(\overline{r},\overline{t})\left[\frac{\overline{C}_{1f}(\overline{x},\overline{r},\overline{t})}{\overline{C}_{1f}(\overline{x},\overline{r},\overline{t}) + \gamma_1 + \gamma_{1\_i2}\overline{C}_{2f}(\overline{x},\overline{r},\overline{t})}\right]\left[\frac{\left(\overline{H}_f(\overline{x},\overline{r},\overline{t}) - \overline{H}^*\right)}{\left(\overline{H}_f(\overline{x},\overline{r},\overline{t}) - \overline{H}^*\right) + \gamma_H}\right] \tag{55}$$

$$\overline{f}_2 = \overline{X}_a(\overline{r},\overline{t})\left[\begin{array}{l} Da_1\left[\dfrac{\overline{C}_{1f}(\overline{x},\overline{r},\overline{t})}{\overline{C}_{1f}(\overline{x},\overline{r},\overline{t}) + \gamma_1 + \gamma_{1\_i2}\overline{C}_{2f}(\overline{x},\overline{r},\overline{t})}\right] \\ -Da_2\left[\dfrac{\overline{C}_{2f}}{\overline{C}_{2f}(\overline{x},\overline{r},\overline{t}) + \gamma_2 + \gamma_{2\_i1}\overline{C}_{1f}(\overline{x},\overline{r},\overline{t})}\right] \end{array}\right]\left[\frac{\overline{H}_f(\overline{x},\overline{r},\overline{t}) - \overline{H}^*}{\left(\overline{H}_f(\overline{x},\overline{r},\overline{t}) - \overline{H}^* + \gamma_h\right)}\right] \tag{56}$$

$$\overline{f}_3 = \left[Da_2 \overline{X}_a(\overline{r},\overline{t})\left[\frac{\overline{C}_{2f}(\overline{x},\overline{r},\overline{t})}{\overline{C}_{2f}(\overline{x},\overline{r},\overline{t}) + \gamma_2 + \gamma_{2\_i1}\overline{C}_{1f}(\overline{x},\overline{r},\overline{t})}\right]\right]\left[\frac{\overline{H}_f(\overline{x},\overline{r},\overline{t}) - \overline{H}^*}{\left(\overline{H}_f(\overline{x},\overline{r},\overline{t}) - \overline{H}^* + \gamma_h\right)}\right] \tag{57}$$

$$\frac{d\overline{X}_a(\overline{r},\overline{t})}{d\overline{t}} = \overline{X}_a(\overline{r},\overline{t})\left\{\left[Da_{\hat{\mu}}\left(\frac{\overline{C}_{1f}(\overline{x},\overline{r},\overline{t})}{\overline{C}_{1f} + \gamma_1 + \gamma_{1\_i2}\overline{C}_{2f}} + \frac{\overline{C}_{2f}(x,r,t)}{\overline{C}_{2f} + \gamma_2 + \gamma_{2\_i1}\overline{C}_{1f}}\right)\right]\left[\frac{\overline{H}_f(x,r,t) - \overline{H}^*}{\gamma_h + \overline{H}_f(x,r,t) - \overline{H}^*}\right] - Da_b - Da_{Rs}\right\} \tag{58}$$

$$\frac{\partial \overline{C}(\overline{x},\overline{t})}{\partial \overline{t}} = \frac{1}{Pe}\frac{\partial^2 \overline{C}(\overline{x},\overline{t})}{\partial \overline{x}^2} - \frac{\partial \overline{C}(\overline{x},\overline{t})}{\partial \overline{x}} - 3\kappa St\left[\overline{C}(\overline{x},\overline{t}) - \overline{C}_f(\overline{x},\overline{r}=1,\overline{t})\right] \tag{59}$$

$$Ed\,\frac{\partial \overline{C}_f(\overline{x},\overline{r}=1,\overline{t})}{\partial \overline{x}} \;=\; St\left[\overline{C}(\overline{x},\overline{t})-\overline{C}_f(\overline{x},\overline{r}=1,\overline{t})\right] \tag{60}$$

$$\frac{\partial \overline{C}_f(\overline{x},\overline{r}=r^*,\overline{t})}{\partial \overline{r}}=0 \tag{61}$$

The non-dimensional system of equations is fully characterized by a number of dimensionless parameters per each chemical species, which are described in Table 5. Here it is noted that the dimensionless concentration of the n^{th} chemical $\overline{C}_{nf}$ is normalized with respect to the initial cDCE concentration (C_0), thus the sum of $\overline{C}_1+\overline{C}_2+\overline{C}_3$ should always be equal to 1 at steady state conditions ($\overline{C}_1+\overline{C}_2+\overline{C}_3=1$).

System-Splitting Operator Splitting Algorithm (SSOSA)

The schematic representation of the solution procedure is shown in Fig. 17. Here the procedure is described in words. It is desired to take a time step from $\overline{t}$ to $\overline{t}+\Delta\overline{t}$, solving for the unknown concentrations $\overline{C}_n(\overline{x},\overline{t}+\Delta\overline{t})$ and $\overline{C}_{nf}(\overline{x},\overline{r},\overline{t}+\Delta\overline{t})$. The SSOSA starts by making initial estimates of these unknown concentrations. In symbols, an initial estimate $\overline{C}_n^{i=1}(\overline{x},\overline{t}+\Delta\overline{t})$ and $\overline{C}_{nf}^{i=1}(\overline{x},\overline{r},\overline{t}+\Delta\overline{t})$ are set for each chemical species, where the superscript *i* denotes the i^{th} guess at the value and the subscript *n* the n^{th} chemical species. Specifically, the initial estimates are the concentrations obtained from the previous time step, i.e., it is started by setting $\overline{C}^{i=1}(\overline{x},\overline{t}+\Delta\overline{t})=\overline{C}(\overline{x},\overline{t})$ and $\overline{C}_f^{i=1}(\overline{x},\overline{r},\overline{t}+\Delta\overline{t})=\overline{C}_f(\overline{x},\overline{r},\overline{t})$ for all chemical species.

Table 5. Dimensionless parameters for multispecies transport and reaction

Dimensionless Parameter	Definition
$Pe_n = \frac{v\,L}{D_n}$	Peclet number: ratio of the rate of transport by advection to the rate of transport by axial dispersion
$\kappa = \frac{1-\phi}{\phi}\phi_f$	Capacity factor: capacity of the reactive film to store the contaminant
$r^* = \frac{R_1}{R_2}$	Dimensionless radius of the interface between the solid grain and the reactive film
$Da_n = \frac{\hat{q}_n X_a}{C_0 v/L}$	Damkohler number: ratio of the reaction rate inside the film to the advection rate
$Da_\mu = \frac{\mu}{v/L}, Da_b = \frac{b}{v/L}$	Damkohler number: ratio of the growth or decay of the biomass inside the film to the advection rate
$Ed_n = \frac{D_{nf}/R_2^{\,2}}{v/L}$	Diffusion modulus: ratio of the diffusion rate inside the film to the advection rate
$St_n = \frac{\omega_n/R_2}{\phi_f v/L}$	Stanton number: ratio of the external mass transfer rate across the diffusion layer to the advection rate
$\gamma_n = \frac{K_n}{C_0}$	Ratio of half velocity coefficient to initial concentration of cDCE
$\gamma_{2\_i1} = \frac{K_2}{K_{i\_1}}, \gamma_{1\_i2} = \frac{K_1}{K_{i\_2}}$	Ratio of half velocity coefficient to competitive coefficient

The initial estimates of the concentrations at the surface of the reactive film, $\overline{C}_f^{i=1}(\overline{x},\overline{r}=1,\overline{t}+\Delta\overline{t})$, are used to solve the advection-dispersion-mass-transfer equation (Eq. 59). This yields an updated estimate of the mobile-fluid concentration: $\overline{C}^{i=2}(\overline{x},\overline{t}+\Delta\overline{t})$ for each chemical species. Then, the mobile-fluid estimates are used to solve the diffusion equation that has been separated as the transport or diffusion operator inside the reactive film:

$$\frac{\partial \overline{C}_{nf}(\overline{x},\overline{r},\overline{t})}{\partial t} = Ed_n \frac{1}{\overline{r}^2} \frac{\partial}{\partial \overline{r}}\left[\overline{r}^2 \frac{\partial \overline{C}_{nf}(\overline{x},\overline{r},\overline{t})}{\partial \overline{r}}\right] \tag{62}$$

The next step is to use the result obtained from the solution of the transport operator (diffusion equation) (Eq. 62) as an initial condition to solve the reaction operator.

$$\frac{\partial \overline{C}_{nf}(\overline{x},\overline{r},\overline{t})}{\partial t} = +\overline{f}_n\left(\overline{C}_{1f}(\overline{x},\overline{r},\overline{t}),...,\overline{C}_{nf}(\overline{x},\overline{r},\overline{t}),...,\overline{C}_{Nf}(\overline{x},\overline{r},\overline{t})\right) \tag{63}$$

The solution of transport and reaction is done at each $\overline{x}$ location. The result from the reaction step yields the new iteration values of the concentration inside the reactive film: $\overline{C}_{nf}^{i=2}(\overline{x},\overline{r},\overline{t}+\Delta\overline{t})$.

It is then compared the estimated values of film-surface concentration from successive iterations, i.e., a comparison of $\overline{C}_{nf}{}^{i}\left(\overline{x},\overline{r}=1,\overline{t}+\Delta\overline{t}\right)$ to $\overline{C}_{nf}{}^{i+1}\left(\overline{x},\overline{r}=1,\overline{t}+\Delta\overline{t}\right)$. The difference between these two estimates is compared to a tolerance criterion, which is typically set at 10^{-9}. The iterative process continues until the difference meets the tolerance criterion, as shown in Fig. 17.

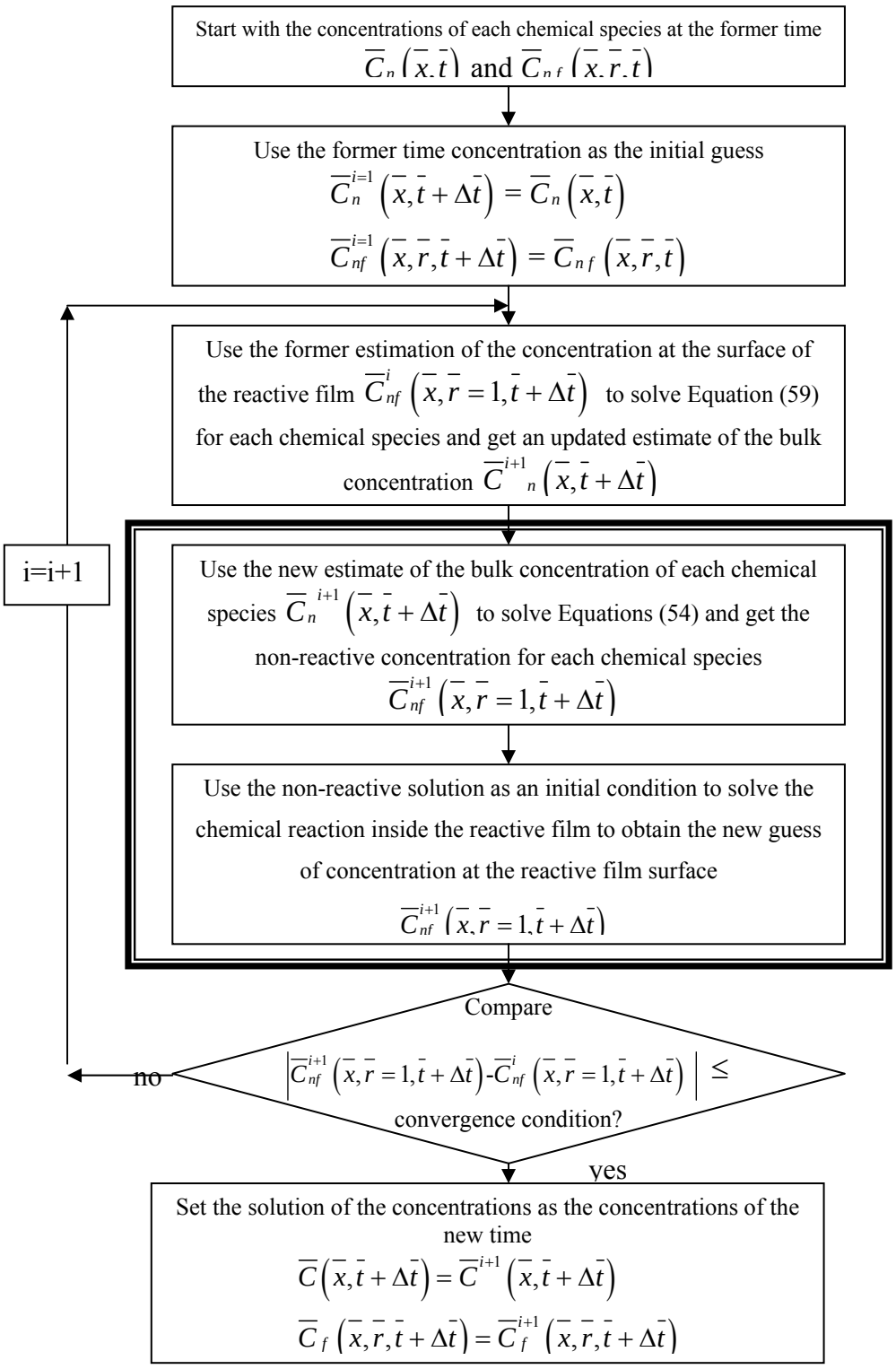

Fig. 17 Schematic representation of SSOSA procedure.

Results

The SSOS algorithm code was developed and run in MATLAB® version 7. The system of equations (Eqs. 54-61) was solved for a hypothetical column with the following initial and boundary conditions. Initially, there is no chemical present in the mobile fluid or within the reactive film (Eq. 64).

$$\begin{aligned} &\overline{C}_n(\overline{x},\overline{t}=0)=0 \\ &\overline{C}_{nf}(\overline{x},\overline{r},\overline{t}=0)=0 \end{aligned} \tag{64}$$

There is a continuous source of chemical number 1 located at the column inlet, $\overline{x}=0$ (Eq. 65). At the effluent end of the column, there is no dispersive flux (Eq. 66).

$$\overline{C}_n\left(\overline{x}=0,\overline{t}\right)-\frac{1}{Pe_n}\frac{\partial\overline{C}_n\left(\overline{x}=0,\overline{t}\right)}{\partial\overline{x}}=1 \text{ or } 0 \tag{65}$$

$$\frac{\partial\overline{C}_n\left(\overline{x}=1,\overline{t}\right)}{\partial\overline{x}}=0 \tag{66}$$

To evaluate the concentration error due to splitting, the SSOSA was run with quasi-linear conditions for different time steps. The conditions to obtain a quasilinear reaction are represented by Eq. 67.

$$\begin{aligned} &\overline{C}_{1f}\left(\overline{x},\overline{r},\overline{t}\right)<<\gamma_1 \\ &\gamma_{i\_2}<<\gamma_1 \\ &Da_2=0 \\ &\left[\frac{\overline{H}_f\left(\overline{x},\overline{r},\overline{t}\right)-\overline{H}^*}{\gamma_h+\overline{H}_f\left(\overline{x},\overline{r},\overline{t}\right)-\overline{H}^*}\right]\overline{Xa}\left(\overline{r},\overline{t}\right)=1=\text{constant} \end{aligned} \tag{67}$$

It is thereby obtained the following quasi-linear system of equations

$$\frac{\partial \bar{C}_{1f}(\bar{x},\bar{r},\bar{t})}{\partial t} = Ed_1 \frac{1}{\bar{r}^2} \frac{\partial}{\partial \bar{r}}\left[\bar{r}^2 \frac{\partial \bar{C}_{1f}(\bar{x},\bar{r},\bar{t})}{\partial \bar{r}}\right] - \frac{Da_1}{\gamma_1}\left(\bar{C}_{1f}(\bar{x},\bar{r},\bar{t})\right) \quad (68)$$

$$\frac{\partial \bar{C}_{2f}(\bar{x},\bar{r},\bar{t})}{\partial t} = Ed_2 \frac{1}{\bar{r}^2} \frac{\partial}{\partial \bar{r}}\left[\bar{r}^2 \frac{\partial \bar{C}_{2f}(\bar{x},\bar{r},\bar{t})}{\partial \bar{r}}\right] + \frac{Da_1}{\gamma_1}\left(\bar{C}_{1f}(\bar{x},\bar{r},\bar{t})\right) \quad (69)$$

The parameters used for the SSOSA quasilinear conditions are listed in Table 6. The results are compared to the SSA with linear conditions. The SSA was chosen because it does not involve an operator splitting method and has proven to give accurate results compared to an analytical solution (Mendoza-Sanchez and Cunningham 2007). Figure 18 shows the comparison of the results from SSOSA with different time steps against the SSA with a fixed time step of 1×10^{-4}. The SSOSA should give similar results as the SSA. In Fig. 18 as the time step (dt) decreases, the result from SSOSA approaches the result of the SSA, so it is concluded that the error decreases with decreasing time step size. A dimensionless time step of 1×10^{-6} is required for the SSOSA to give accurate results compared to the SSA.

The mass balance error was evaluated for 3 cases with non-linear reaction (Table 7). The 3 cases were run with the same dimensionless time step of $1x10^{-4}$. In the three cases (cases I, II, and III from Table 7) the diffusion within the biofilm is slow relative to external mass transfer (*Ed*<*St*), that is the internal diffusion is controlling the process. Figure 19 shows the results of the three cases. Since the concentration of all chemical species is normalized with respect to the initial concentration of cDCE, the sum of all chemical species (cDCE, VC and ETH) must be equal to 1, when steady state

is reached. When all the chemical species have the same transport and reaction parameters (case I) there is no apparent error in the mass balance. However the SSOSA will overestimate the concentration of reactants when $St_1<St_2<St_3$ (case II) and it will underestimate the concentration of the species involved when $St_1>St_2>St_3$ (case III).

The concentration error for the non-linear reaction was evaluated by comparing the results of case number IV from Table 7 to the results of a new approach developed for this specific purpose. Basically the new approach uses a Picard iteration approach (Vemuri and Karplus 1981) to solve the system of equations that describes the uptake and reaction in the stationary phase (Eqs. 54-58), therefore it has been named SSPIA. The difference between the SSOSA and the SSPIA is that the SSPIA does not use any operator splitting method; eliminating therefore the splitting error. The results (see Fig. 20) show that both approaches agree within 0.5% or better and the mass balance error is less than 0.001% when steady state is reached. It is reasonable to state that both codes are correct and that both methods are valid. Thus it can be concluded that the SSOSA gives accurate results if we make the time step small enough.

Table 6. Conditions for the quasi-linear system of equations to compare SSA to SSOSA

Parameter	Value
κ	2.419
r^*	0.95
Pe_n	18.143
St_n	9540.343
Ed_n	3513.4
Da_2	0.0
Da_1	76.2
γ_1	222.22
γ_{i_2}	0.0001

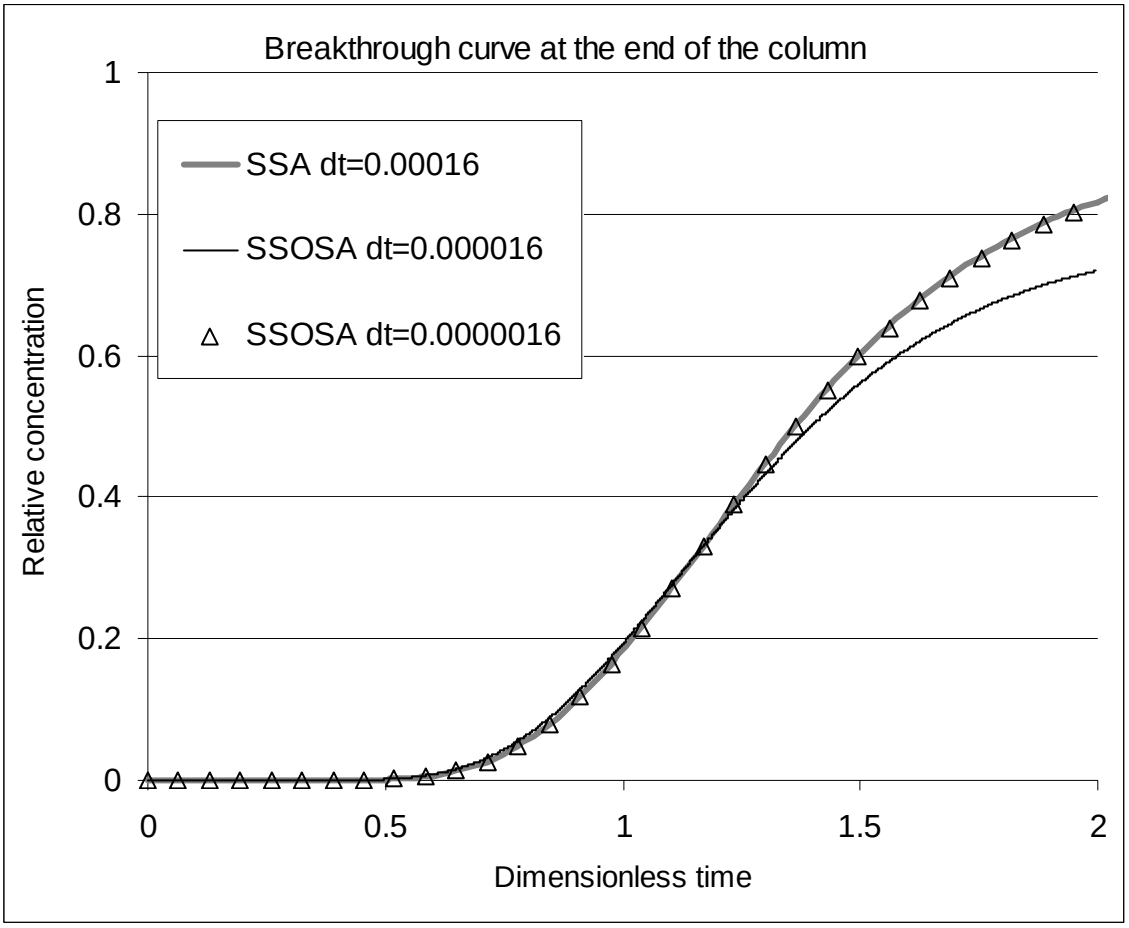

Fig. 18 Comparison of SSA to SSOSA for quasi-linear reaction where dt is the dimensionless time step.

Table 7. Conditions tested for calculating mass balance errors of SSOSA

Case	Species	*St*	*Ed*	*Pe*
Internal diffusion control				
I	cDCE (1)	1493.473	442.340	20.725
	VC (2)	1493.473	442.340	20.725
	ETH (3)	1493.473	442.340	20.725
II	cDCE (1)	1493.473	442.340	20.725
	VC (2)	1264.562	442.340	20.725
	ETH (3)	1024.062	442.340	20.725
III	cDCE (1)	1493.473	442.340	20.725
	VC (2)	1763.779	442.340	20.725
	ETH (3)	2177.984	442.340	20.725
External diffusion control				
IV	cDCE (1)	0.266	83.592	19.915
	VC (2)	0.297	98.720	19.900
	ETH (3)	0.346	121.900	19.870

Note: All simulations were performed using $r^* = 0.95$, $\kappa = 1.73$, $Da_1 = Da_2 = 0.16$, $Da_\mu = 0.48$, $Da_b = 0.11$, $Da_{rs} = 0$, $\gamma_1 = 0.11$, $\gamma_2 = 0.09$, $\gamma_{1\_i2} = 0.42$, $\gamma_{2\_i1} = 0.72$, $\bar{H} = 0.001$, $\bar{H}^* = 0.0003$, $\gamma_h = 0.0023$

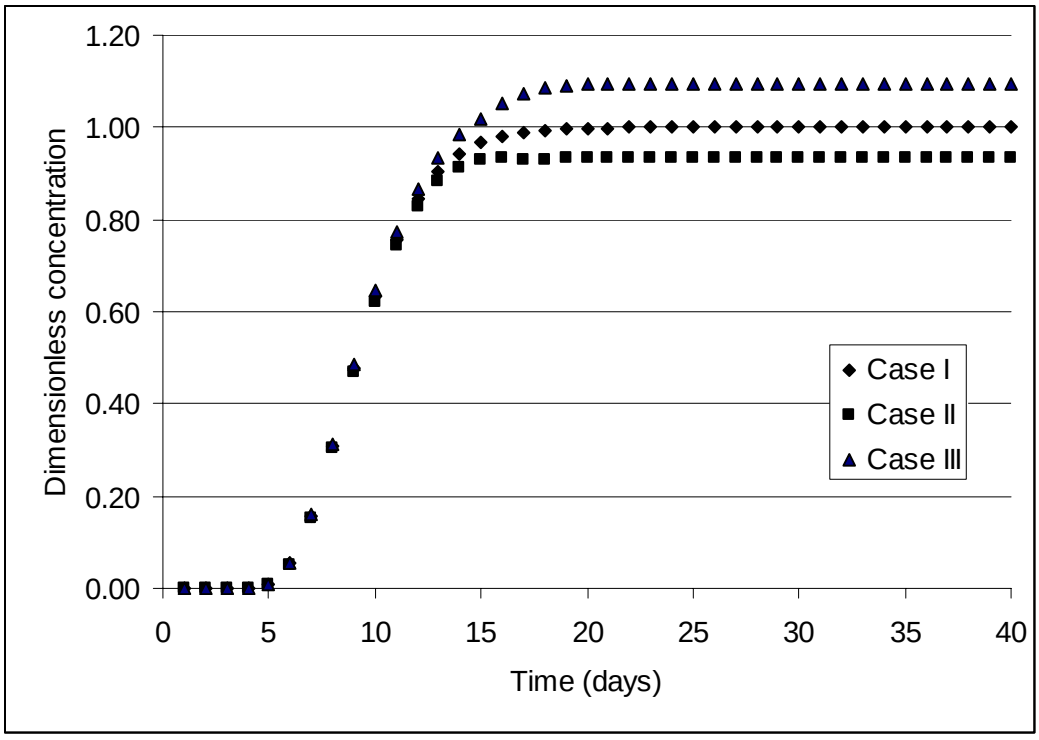

Fig. 19 Evaluation of SSOSA mass balance error for three sets of conditions. The dimensionless concentration in the y axis is the sum of all the chemical species. Since all the concentrations are normalized to the initial concentration the sum of all chemical species must be equal to 1 when steady state is reached.

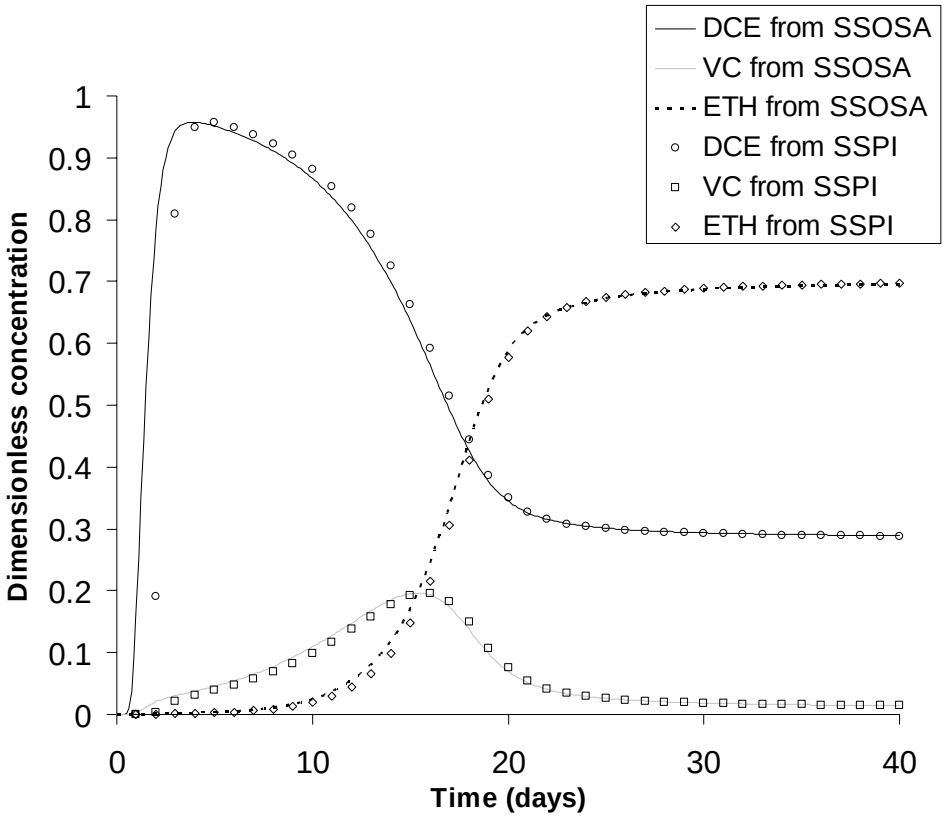

Fig. 20 Comparison of SSOSA and SSPI simulations of multispecies transport with non-linear reaction kinetics. Solid lines = results of SSOSA code; symbols = results of SSPI code.

Discussion, Summary, and Conclusions

The conceptual and mathematical model was developed to simulate groundwater contaminant transport and remediation. The mathematical model links microscopic processes to the macro-scale representation of contaminant transport. The model was originally developed in the present study to distinguish the effects of flow velocity on mass transport of chemicals from the mobile fluid to the biofilm. In particular the mathematical model represents the transport and degradation of cDCE in porous media, taking into account substrate limiting conditions and the degradation products of the parent compound (VC and ETH). A novel numerical approach to solve the mathematical model has been developed in this chapter. Additionally, the applicability and inherent errors of the numerical approach were evaluated.

The applicability and errors of the SSOSA were determined by evaluating different scenarios. The reaction kinetics of cDCE was studied elsewhere (Cupples et al. 2004), so one set of reaction constants available from the references was used for all the cases tested. Then we varied the values of the transport parameters to simulate 5 different cases of possible physical scenarios: one quasi-linear case; three cases where the overall process is controlled by internal mass transfer; and one case controlled by external mass transfer.

The quasi-linear case shows an error intrinsic to the operator splitting approach, consistent with previous research. The results show that the SSOSA give a negligible mass balance error (less than 0.001%) when the time step is sufficiently small. Under the

conditions tested, the dimensionless time step must be $1.6x10^{-6}$ to give acceptable results.

The evaluation of the concentration errors shows that the SSOSA is accurate if a small time step is used. This restriction affects the efficiency of the SSOSA. However, the SSPIA used to evaluate the concentration errors has shown to be more appealing because it did not presented as much restriction in the time step. The SSOSA could be improved by using an iterative operator splitting method. The iterative OS method has been evaluated elsewhere and proven to have a better accuracy than the non-iterative OS method (Carrayrou et al. 2004). These alternatives have to be studied in the future to determine the optimum efficiency of the SSOSA.

Overall, the SSOSA is attractive for different reasons. It converts the original two-dimensional system of partial differential equations into two smaller one-dimensional systems, saving CPU time and storage. Each system is solved using different numerical techniques (different numerical techniques have been implemented in this chapter: the SSOSA and the SSPI). The modular code permits the modification of the numerical approach to improve its efficiency when solving complex systems of equations. The SSOSA gives flexibility in choosing the best numerical technique to solve the non-linear diffusion-reaction equation inside the reactive film.

The SSOSA is useful when spatial or temporal discretizations in the computer code differ between the mobile fluid system and the stationary medium system. The SSOSA is a practical tool to solve different cases of the mathematical representation of the phenomena to distinguish between the effects of macroscopic processes (along the

mobile fluid) and microscopic processes (in the stationary medium). In the present chapter different temporal grids have been used for the two scales.

In summary, the system-splitting-operator-splitting algorithm presented in this chapter is a novel method for simulating multispecies non-linear reactive transport. The new method offers advantages in terms of computational adaptability for solving complex systems of equations employing different numerical approaches. The SSOSA gives accurate results when the time step condition is met. Future work will evaluate the efficiency of the SSOSA compared to other potential numerical approaches.

CHAPTER V

EFFECT OF PORE VELOCITY ON CONTAMINANT TRANSPORT AND DEGRADATION IN POROUS MEDIA

Overview

Column experiments were conducted to evaluate the effect of pore velocity on the extent of biodegradation of cis-Dichloroethylene (cDCE) during transport in porous media. The columns were filled with homogeneous glass beads and inoculated with the KB-1 culture (provided by SiREM, Guelph, Canada), which is capable of complete dechlorination of tetrachloroethylene to ethene. A constant concentration of cDCE was maintained in the feedstock solution. Three different pore flow velocities (0.04, 0.08 and 0.51 m/day) were tested in duplicate, subjecting each column to a specific constant flow velocity for the entire experiment. cDCE dechlorination to vinyl chloride (VC) and ethene (ETH) was monitored over time and space. Protein concentrations measured over time and space were used to relate cell growth to biodegradation efficiency. Additionally, denaturing gradient gel electrophoresis (DGGE) was used to determine differences in the microbial composition between the columns subjected to different flow velocities. The results show that the pore velocity has a strong influence on the microbial structure and the degree of dechlorination. At high flow velocity (0.51 m/day), degradation was nearly complete and the organism capable of cDCE dechlorination (*Dehalococcoides* sp.) was present. In contrast, at medium and low flow velocities (0.08 and 0.04 m/day respectively), incomplete dechlorination was observed with an absence or low

concentration of *Dehalococcoides* sp. These results demonstrate the importance of physical and biological processes and their interaction at the microscopic scale.

Introduction

In the United States, chlorinated ethenes (CE) are common groundwater contaminants. They are frequently found at National Priority List sites, with trichloroethylene (TCE) being the most prevalent contaminant followed by vinyl chloride (E.P.A. 2004). Due to the widespread groundwater contamination, a number of remediation technologies have been studied and implemented. Among these, bioremediation is particularly appealing due to its potential for low cost. However, many bioremediation technologies remain poorly understood and usually empirically controlled due to the lack of information describing the phenomena involved. A better understanding of the phenomena involved in the biodegradation process could lead to more efficient bioremediation technologies.

Biodegradation of tetrachloroethylene also named perchloroethylene (PCE) under anaerobic conditions is conducted by bacterially-mediated sequential reductive dechlorination. That is, PCE is converted sequentially to TCE, dichloroethylene (DCE), vinyl chloride (VC), and finally ethene, a benign end-product (McCarty 1998). Transformation of PCE to TCE and DCE is observed at almost all contaminated sites, but degradation of DCE to VC and ethene has been observed only at some sites (Hendrickson et al. 2002). Consequently, DCE and VC often accumulate at contaminated sites. VC is the most toxic and carcinogenic of all the chlorinated ethenes.

Several factors have been identified that may affect the degree of dechlorination observed in groundwater contaminated sites. These factors include: the presence or absence of dechlorinating species (Duhamel and Edwards 2006; Fennel et al. 2001; Hendrickson et al. 2002; Major et al. 2002); the presence and activity of fermentative bacteria to produce hydrogen for the dechlorinating species (Cabirol et al. 1998); a sufficient supply of electron-donating compounds (He et al. 2002); and competition among dechlorinating, sulfate-reducing, and methanogenic bacteria for nutrients and electron donors (Maymo-Gatell et al. 2001; Yang and McCarty 1998).

In the past, biological processes have typically not been related to physical phenomena at the microscopic (biofilm) scale. The interaction between biological and physical processes can be explained as follow. Biodegradation in groundwater occurs inside biofilms that coat the aquifer grains (Rittmann 1993). Accordingly, the degree of dechlorination may be a function of both the chemical mass transfer from the bulk solution to the surface of the biofilm, and the structure of the active biofilm layer. Chemical mass transfer is a physical process and depends on the thickness of a stationary layer formed immediately adjacent to the surface of the biofilm, named the diffusion layer. The active biofilm layer structure will depend on the biological processes involved during degradation such as chemical bioavailability and bacterial adherence characteristics. Therefore groundwater flow velocity may influence the degree of dechlorination because it may control two important structures at the microscopic (biofilm) scale: 1) the thickness of the diffusion layer, and 2) the microbial community structure. Hence, the main contribution of this chapter is to quantify the degree to which

inter-relationships between physical and biological phenomena at the microscopic scale affect the extent of dechlorination. In particular, the influence of groundwater flow velocity on the extent of dechlorination of cDCE to ETH was determined.

Materials and Methods

Chemicals

Liquid cis-1,2-dichloroethylene (cDCE) (99% Pfaltz and Bauer Inc., NM) was used to prepare stock solutions and standards. Vinyl chloride (VC, 2000 μg/ml) standard in methanol (Restek Corp.), and ethene (ETH, 1000μg/ml) standard in methanol (Spex CertiPrep) were used to prepare analytical standards. A gas mixture of 20% CO_2 / 80% N_2 was used for purging the anaerobic culture medium (Air liquid Houston, TX) to attain anaerobic conditions.

Culture

Commercially available KB1® Dechlorinator culture (SiREM, Guelph, Canada) was used to inoculate the columns. KB1® Dechlorinator was originally derived from a TCE-contaminated aquifer in southern Ontario, Canada (Duhamel and Edwards 2006).

Analytical Methods

Analysis of cDCE, VC and ETH was conducted using a HP 6890 series gas chromatograph (GC) equipped with a capillary column (Rt-QPLOT 30m x 320 μm x 10 μm) and a flame ionization detector (FID). The injector temp was set at 200^{o} C, and used in a splitless mode. The detector temperature was set at 250^{o}C with H_2 flow of 40 ml/min, air flow of 400 ml/min, and a make-up flow of He at 40 ml/min. The carrier

gas was He at a flow of 3 ml/min. The oven was programmed as follows: 35^{o}C for 2 min, increase at 60^{o}C/min to 110^{o}C, increase at 20^{o}C/min to 175^{o}C, increase at 2^{o}C/min to 180^{o}C, and held for 8 min.

Standards were prepared by adding known masses of cDCE, VC and ETH dissolved in methanol to 10 ml vials containing 2ml of deionized water. A maximum of 4µl of methanol solution was used to inject the dissolved cDCE,VC and ETH (0.02% of methanol) to avoid affecting the behavior of each species due to methanol presence. Standards were shaken for 1 hour and then allowed at least 12 hours of equilibration time. Then 1 ml of headspace was collected from the vials with a gas-tight syringe and manually injected in the GC.

Samples were prepared by adding 1ml sample to a 10 ml vial containing 1ml of acidified water (pH 2), followed by shaking for 1 hour and at least 12 hours of equilibration time. Then 1ml headspace was collected from the vial with a gas-tight syringe and injected manually onto the GC. The acidified water (pH2) was obtained by mixing a 0.2M boric acid and 0.05M citric acid solution with a 0.1M tertiary sodium phosphate solution to obtain a solution of 0.195M boric acid, 0.048M citric acid 0.0025M tertiary sodium phosphate.

Biomass was quantified by measuring the protein concentration in the samples was measured following a microassay kit (Bio-Rad) that uses the method of Bradford (Bradford 1976). Bovine serum albumin was used as a standard and the detection limit was lowered by first concentrating the sample by centrifugation.

Denaturing gradient gel electrophoresis (DGGE) was conducted to obtain information on the culture composition. At the end of the column experiment, the pore water in the column was collected (389 ml) and DNA was extracted with the Fast-DNA kit (BIO101 Systems). The DNA-extracted samples were frozen and sent to SiREM, Guelph, Canada, to be analyzed via DGGE. One KB-1 lane and three cloned KB-1 DNA lanes were run parallel to the samples to identify the bands in common with KB-1 in the DGGE results.

Experimental Set-up

Experiments were performed in glass columns (ACE Glass Inc, custom made) of 5 cm internal diameter and 60cm length, equipped with 5 equally distant sampling ports (10cm apart). The sampling ports were equipped with Mininert® valves (Valco Instruments Co) to allow for sampling while conserving the anaerobic conditions of the column. Each column was assembled with a Teflon adapter (ACE Glass Inc) at the top and bottom. Assembling of the adapter to the columns included a stainless steel mesh (2”OD mesh 100/0.0045, Purolator EFP) to retain the filling material and brass connectors to fit viton tubing at the inlet and outlet of the column. The columns were filled with soda lime glass beads of 0.8 to 1mm diameter (Grinding Media Depot). All tubing and connectors used were made of viton, Teflon®, brass, or stainless steel to reduce sorption of chlorinated ethenes to the material. All columns were wrapped in aluminum foil to avoid the growth of photosynthetic bacteria.

The columns were continuously fed in an upflow mode. The sampling ports of each column were numbered following the direction of the flow, thus port number 1 referred to the port at the bottom of the column and port number 5 referred to port at the top of the column. A schematic representation of the set-up of one column is depicted in Fig. 21. The columns were connected to a peristaltic pump (Masterflex) equipped with a large cartridge pump head (Masterflex) that allowed 9 tubes to be connected at a time. The pump was run at a defined speed (1.6RPM). Different tubing sizes were used to obtain the different flow rates tested. The tubes used have internal diameters (ID) of 0.89, 1.6, and 3.1 mm. The pump was calibrated for the speed of 1.6 RPM for tubing sizes of 0.89, 1.6, and 3.1 mm ID; their respective flow rate values were $0.016 \pm 8 \times 10^{-6}$, $0.036 \pm 2 \times 10^{-4}$, and $0.23 \pm 2 \times 10^{-4}$ ml/min. The column diameter was 5 cm and column porosity of 0.33 was measured. Therefore, the pore velocities calculated are: 0.04, 0.08, and 0.51 m/day for 0.016, 0.036 and 0.23 ml/min respectively. These values represent a realistic range of velocities in a groundwater system.

The columns were tested under substrate limiting conditions. The anaerobic medium was prepared prior to connection to the columns in a glass container. The container was filled with basal medium described in Yang and McCarty (1998) containing 50mg/L of yeast extract (as a limited substrate for hydrogen production). Then the medium in the container was purged with a gas mixture of 80% N_2 and 20% CO_2 to attain anaerobic conditions and a stable pH of 6.9 to 7.2. The container was closed with a three valve cap (ACE Glass Inc) to permit delivery of the anaerobic medium from the container. Two valves of the cap were closed and the other valve was

fitted with a septum to permit injection of cDCE to the anaerobic medium. Pure cDCE (2.5 µl per liter of anaerobic medium) was injected with a gas tight syringe through the septum to attain the cDCE concentration (30µM) desired. Then the three valves of the cap were fitted with viton tubing. One valve of the cap was connected to a foil gas bag (SKC Inc). The foil gas bag contained the same gas mixture used for purging the culture medium. The gas bag was filled with N_2/CO_2 gas mixture to keep anaerobic conditions in the feeding medium as the level in the glass container drains. The container-gas bag system was allowed to equilibrate for at least 12 hours and then connected to the columns. Then two valves of the cap were connected to two columns to maintain the same cDCE influent concentration and anaerobic conditions in duplicate. A schematic representation of the set-up procedure is depicted in Fig. 22.

During the experiment, a total of eleven column settings were arranged at different flow rates corresponding to specific pore velocities. Six column settings were used to measure the transport and biodegradation of cDCE at three different pore velocities (each conducted in duplicate); three column settings were used as controls for abiotic transport of cDCE at the three different pore velocities; and two more column settings were used as controls to measure biological products with no cDCE at two different pore velocities. The three different pore velocities tested were named slow, medium, and fast (0.04, 0.08 and 0.51 m/day respectively).

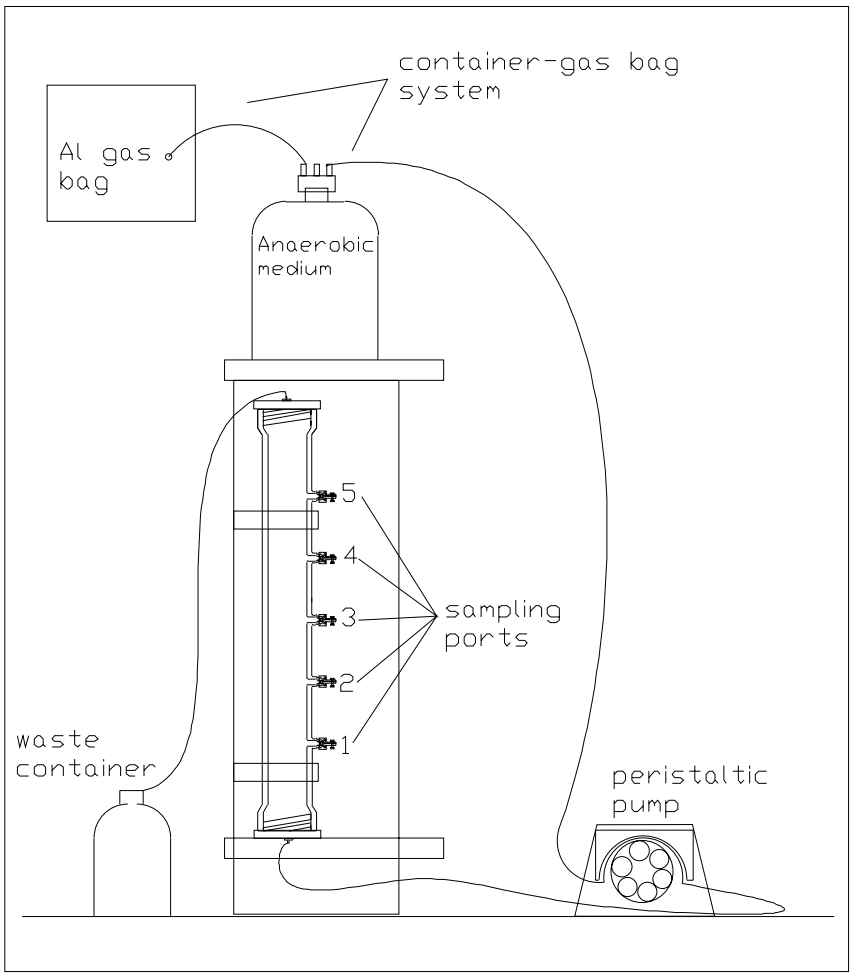

Fig. 21 Schematic representation of the set-up of one column. An arrangement of eight similar columns was used during the experiments.

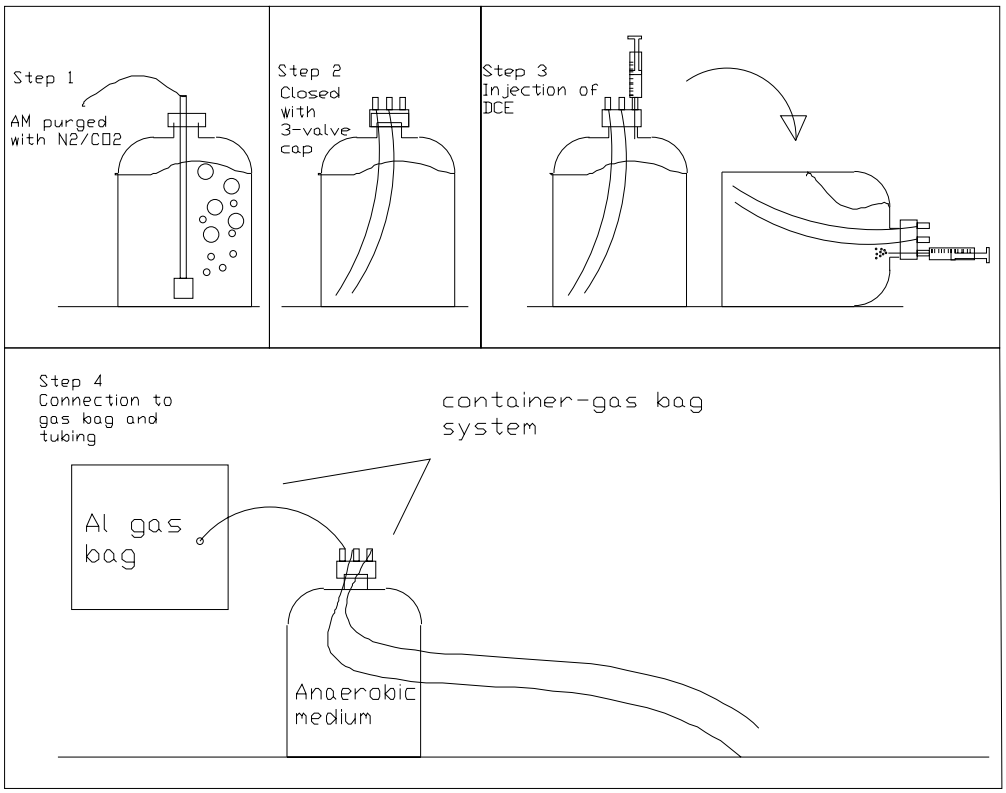

Fig. 22 Schematic representation of the procedure followed to attain anaerobic conditions in the culture medium. The container-gas-bag system was then connected to two columns to assure similar conditions in duplicate experiments.

Column Experiments

Prior to inoculation, the columns were conditioned by purging them with N_2 for at least 5 pore volumes followed by a 5-pore volumes purge with anaerobic medium (prepared as above) without cDCE.

The columns used for transport and biodegradation were run in duplicates, therefore six columns were set-up for this purpose. After conditioning, each column was inoculated with KB1® Dechlorinator culture. One ml of the culture was injected through each sampling port. The columns remained static for 24 hours with no flow through the column. Then, the column experiment was initiated after connecting the container-gas bag system containing anerobic medium with cDCE to the pump and column.

The columns used as abiotic controls received the same anaerobic medium as above with cDCE but they were not inoculated. The abiotic controls were initiated after connecting the container-gas bag system to the pump and column. Two columns were used to test a total of three different velocities, as follows. The first setting employed one column run at the slow pore velocity for 38 days. The second setting employed one column at the fast velocity for 7 days; then the same column was purged with at least 8 pore volumes of anaerobic medium to remove all the cDCE remaining in the column; and finally it was set at the medium pore velocity for 22 days.

At the end of the abiotic control experiments, the same two columns were also used to measure the biological products when no cDCE was present in the column. For this purpose, the abiotic columns were stopped and purged with 8 pore volumes of anaerobic medium to remove all the cDCE in the column. After purging, each column

was inoculated with KB1® Dechlorinator culture. One ml of the culture was injected through each sampling port. The columns remained static for 24 hours with no flow through the column. Then, the column experiment was initiated after connecting the container-gas bag system with anaerobic medium that contained no cDCE to the pump and column. These represented another type of control experiment.

All the columns were sampled at different times, depending on the flow rate tested, as shown in figures of results. The same samples were used to conduct both protein analysis and headspace analysis for cDCE, VC and ETH. At the end of the experiments, the pore water of the columns (388 ml) was collected by gravity for further DNA extraction and DGGE analysis.

Results

The columns that were subjected to low pore velocity showed an initial degradation of cDCE (Fig. 23). However, after 10 to 20 days the degradation rate slowed and an increase in cDCE concentration was observed in the breakthrough curves at the different sampling ports (Fig. 23). Near the inlet of the column, the concentration of cDCE was equal to the same as the injected concentration (30μM), and no VC production was observed at subsequent samples. Similar results were observed for the medium flow rate columns. The cDCE was degraded initially, but after days 14 to 20 days the degradation rate slowed. At later times an increase in cDCE concentration was observed accompanied by a decrease in VC concentrations. The effect was especially pronounced in sample port 1. Hence it can be concluded that dechlorination failed over time in the

low and medium flow rate. In contrast, the high flow rate columns efficiently degraded the cDCE. The cDCE concentration decreased in time and space as shown in Fig.23. The observed concentration of cDCE and VC indicate sustained dechlorination in the high flow columns.

During the data collection, ethene concentrations were higher than expected assuming stoichiometric conversion of cDCE to ETH (Fig. 24). The high concentrations of ETH were not observed in batch experiments (data not shown). Typically batch experiments showed good mass balance (30 μM of cDCE transformed to 30 μM of ETH). These batch results suggest that the calibration curves for ETH were correct. However, one set of batch experiments containing glass beads showed similar behavior as the column experiments, i.e., ETH was measured at higher concentrations than expected. A possible explanation for the high concentrations of ETH was that the glass beads enhanced ETH formation. To test this possibility, two columns were used as controls to measure biological products with no cDCE at two different pore velocities. Since no ETH was observed in these columns, a reliable explanation for the anomalous concentration of ETH remains unresolved. Alternatively, if ETH gas was trapped in the voids of the glass beads ETH could have been accumulated, but ETH still had be produced from a specific source. Nevertheless, the increase of ETH concentrations was positively related to cDCE disappearance suggesting that ETH was produced due to degradation of cDCE.

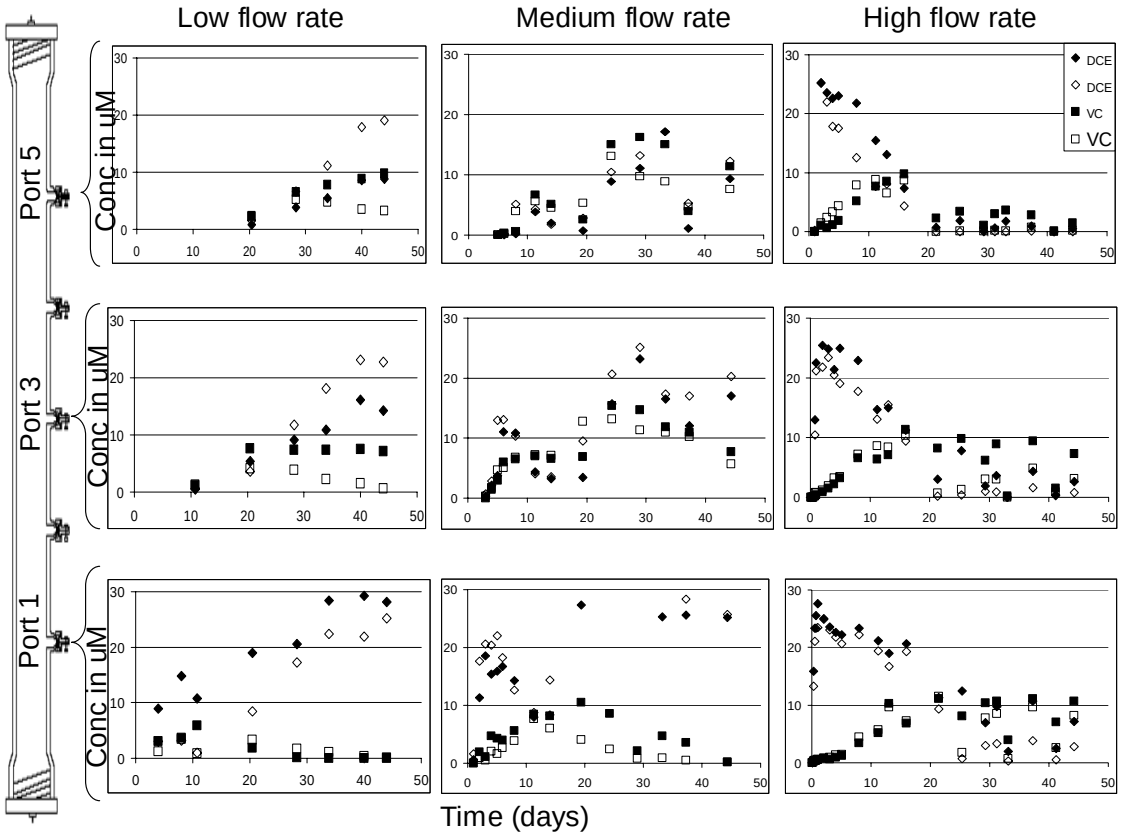

Fig. 23 Concentration of c-DCE and VC in the low-,medium-, and high-flow-rate columns as a function of both time and position. Solid and open diamonds (◊) are for cDCE, solid and open squares (□) are for VC from duplicated column experiments. All concentrations are given in μM. Injected concentration of cDCE was 30 μM.

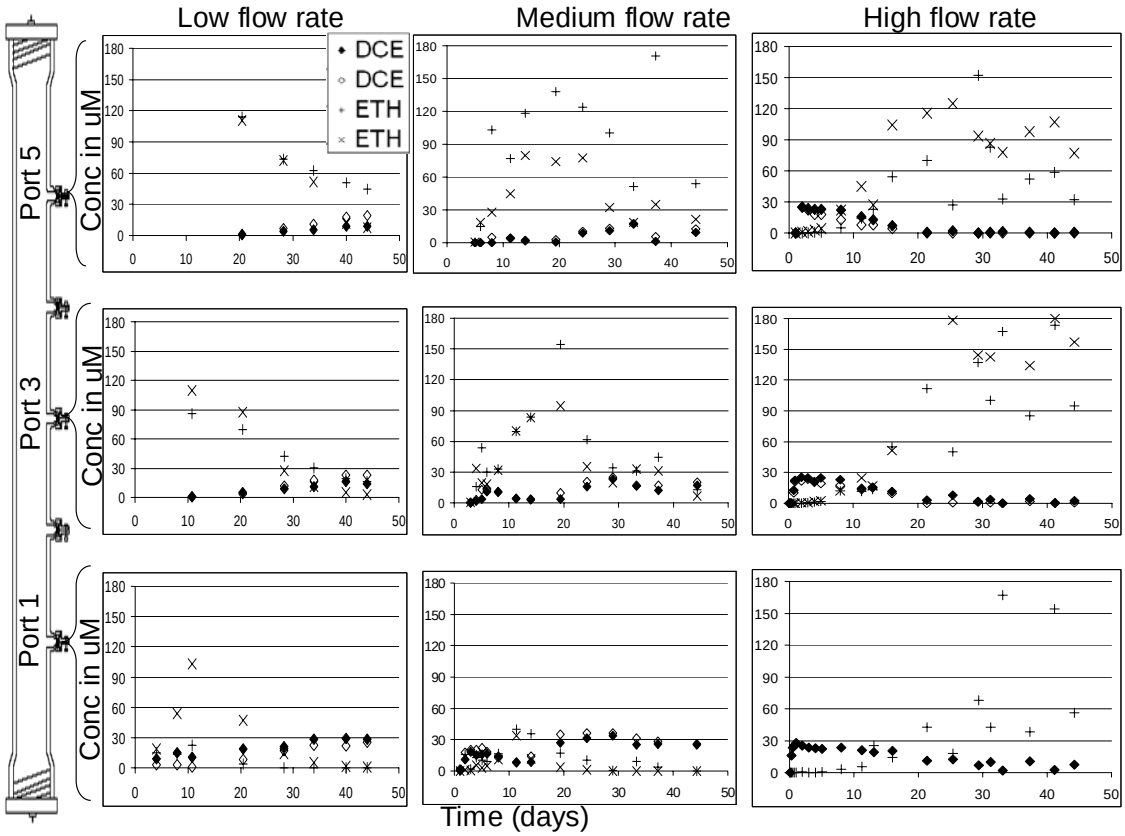

Fig. 24 Measured concentrations of ETH in low-,medium-, and high-flow rate columns. Soilid and white diamonds (◊) are for cDCE, X and + symbols are for ETH. All concentrations are given in μM. Injected concentration of cDCE was 30 μM.

Protein concentration was measured to relate growth of organisms (increment in protein concentration) with the extent of degradation. Since the same samples obtained for cDCE, VC and ETH analysis were used for protein analysis, it was possible to obtain a breakthrough curve (BTC) of protein concentration at the same positions as BTCs for cDCE, VC and ETH. In general the protein results show a weak trend related to the degradation measured. A slightly positive trend (growth in time) is observed in the high flow rate columns, where the degradation of cDCE was completed during the experiment (see Fig. 25). A slightly negative trend is also observed at the low flow rate ports 3 and 5, and in the medium flow rate at port 1, where the degradation failed.

When the columns were disassembled, the glass beads at the bottom of the low-flow-rate columns presented a yellowish color. Dark spots of the culture were found at the sampling ports were the culture was injected initially. Similar observations were made at the medium-flow-rate columns; the glass beads at the bottom of the column had a similar yellowish color. This coloration suggests that the culture was not transported with the flow through the column. However, the high flow rate columns presented a dark color spread all around the column, suggesting that the culture was transported with the flow and distributed in throughout the column. A comparison of the beads from the low-flow rate column and high flow rate columns disassembled is shown in Fig. 26.

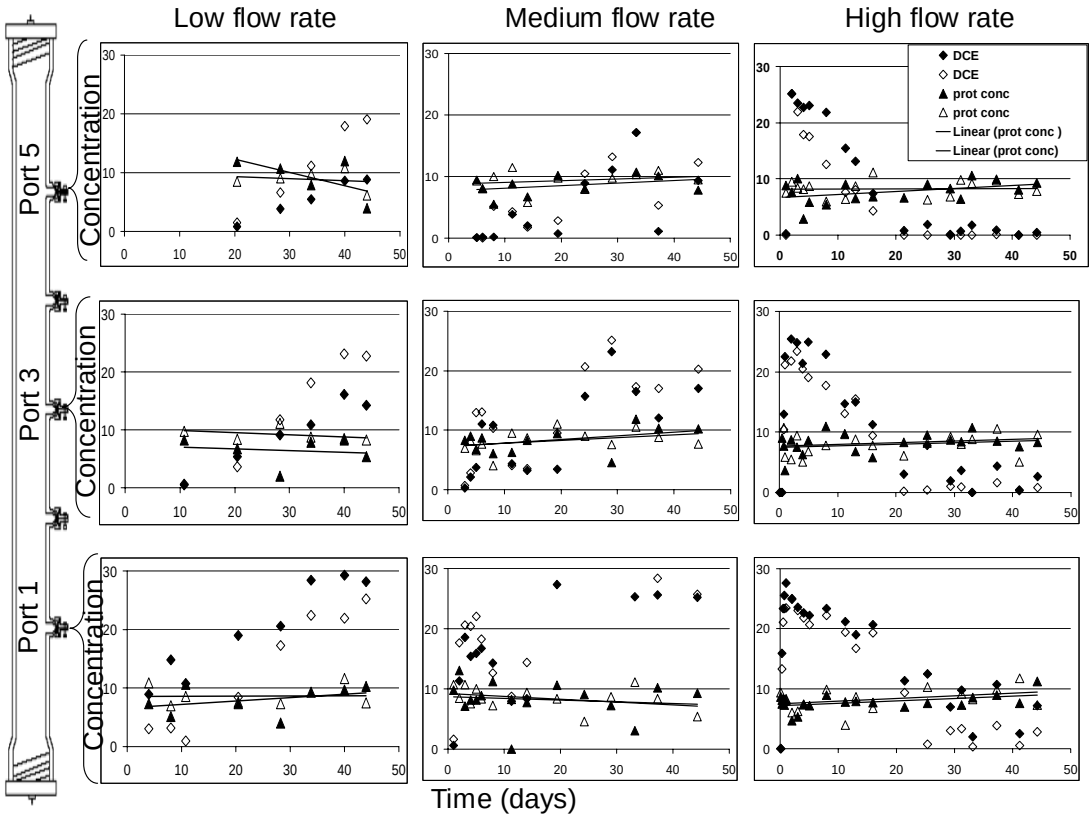

Fig. 25 Measured concentration of protein in low-, medium-, and high-flow rate columns. Solid and white diamonds (◊) are for cDCE concentration in μM. Solid lines is the trend of the protein concentration measured. Solid and white triangles (Δ) are for protein concentration multiplied by a factor of 10 in μg/ml.

The DGGE results provided evidence of culture viability and quantity. Figure 27 shows the result of the DGGE analysis. Each column of the figure represents a lane of each culture assayed. Lanes A, B, and C are KB-1 DNA clones; KB-1 is the lane for the KB-1 culture used for inoculation; the H1,H2, M1,M2 and L1, L2 lanes are the lanes from the duplicated columns with high flow rate (H1 and H2), medium flow rate (M1 and M2), and low flow rate (L1 and L2), respectively. Each lane is comprised of a number of bands, each band represents a specific microbial organism and the intensity of each band is related to the concentration of the microbial organism. Comparing the DGGE intensity and position of the bands, the intensity of the *Dehalococcoides* sp. band (band number 22 on lane D) is higher for H1 and H2 than the intensity at the M1 and M2 lanes, and a very low intensity is observed in L1 and L2 lanes. Results from the quantitative PCR analysis targeting *Dehalococcoides* sp. show that the ennumeration of *Dehalococcoides* in the high flow rate is $9x10^7$/liter whereas in the medium flow rate is $1x10^7$/liter and in the low flow rate is $2x10^7$/liter. The percentage of *Dehalococcoides* related to the whole microbial community is 2 – 5 %, 0.3 – 0.8 %, and 0.5 – 2 % for high-, medium- and low-flow rate respectively. The six lanes that correspond to the columns subjected to the three different flow rates showed similar strong intensities of two bands that were not originally present or were present at small concentrations in the KB1 culture. These are believed to be from background contamination in the laboratory. It is also observed that H1 and H2 lanes have more visible bands than the M1, M2, L1, and L2 lanes, suggesting that the high flow rate columns contained a more diverse microbial community than the medium and low flow rate columns.

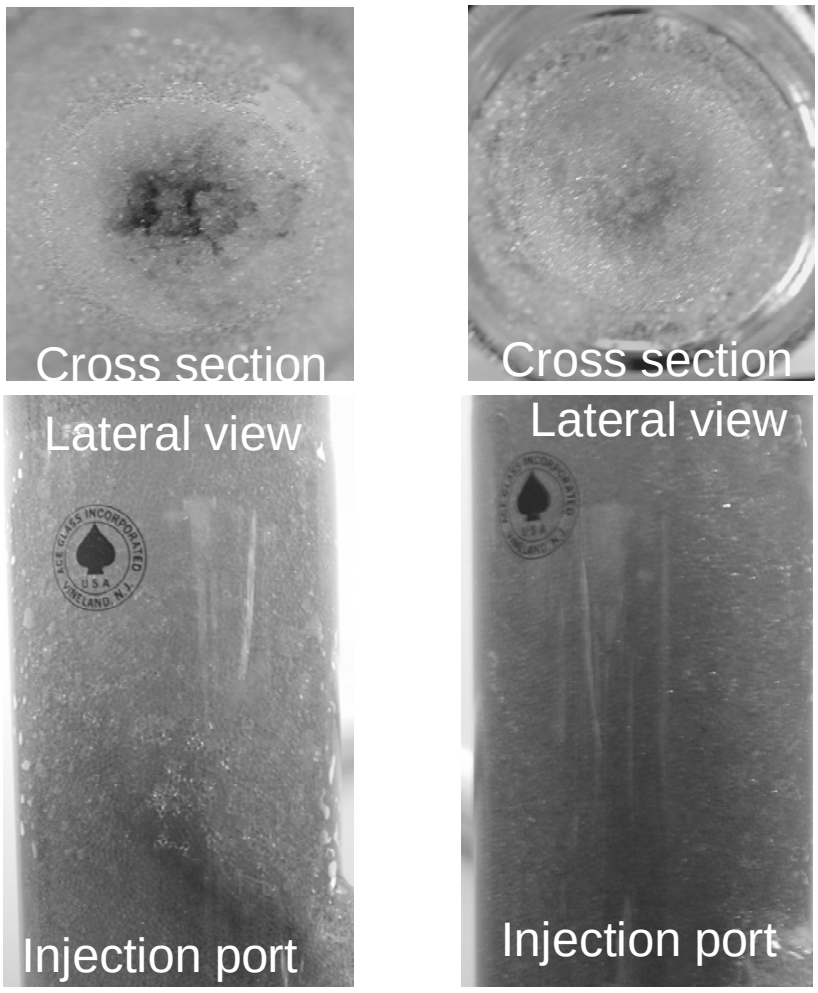

a) low flow rate b) high flow rate

Fig. 26 Cross section at the sampling port and lateral view of two columns subjected to different flow rates. In the (a) low flow rate the culture stayed concentrated at the sampling port or injection port. In the (b) high flow rate the culture was not concentrated at the port of injection, but rather was transported all along the column.

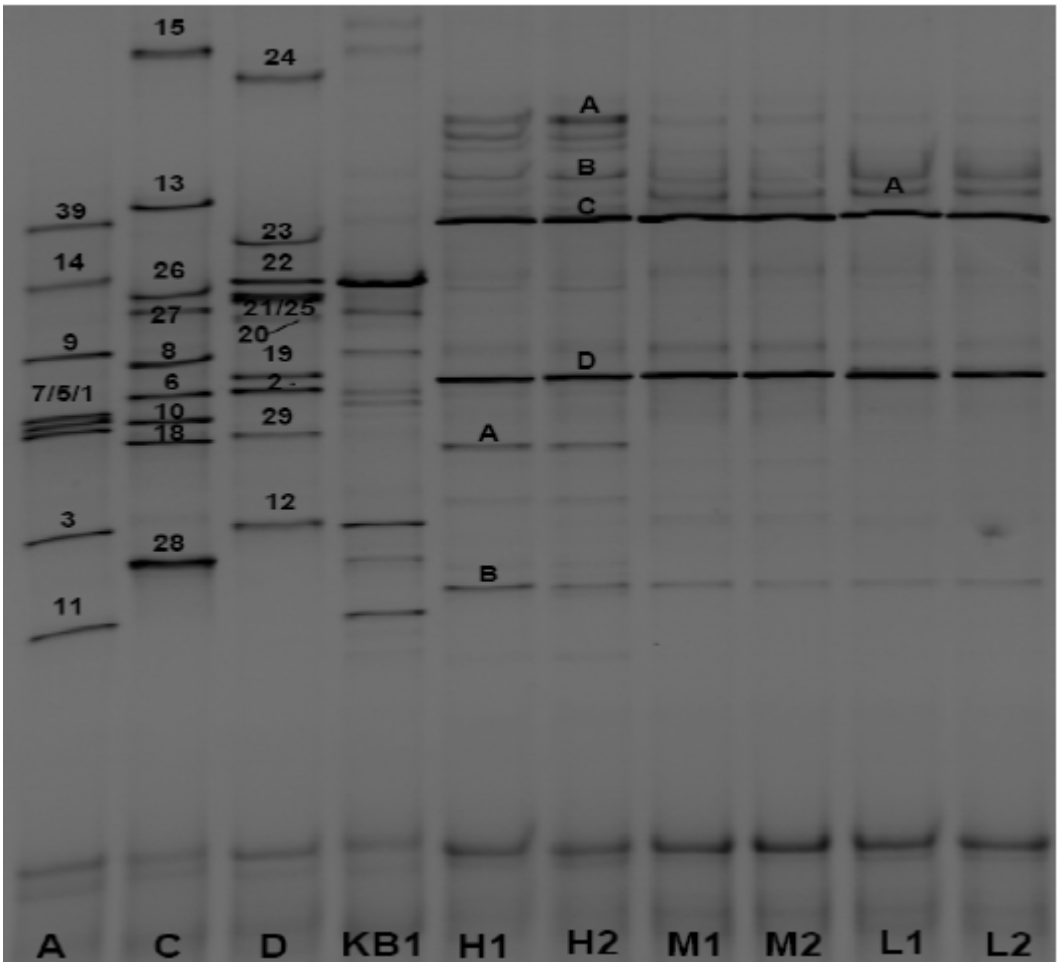

Fig. 27 DGGE results. Lanes H1 H2 M1 M2 L1 L2 are from the columns at high (H), medium (M) and low (L) flow rate. Band 22 has been identified as *Dehalococcoides* and is visualized with high intensity in lane KB-1, less intense in H1 and H2, and very low intensity in M and L, lanes.

Conclusions

It was demonstrated that the velocity is an important factor affecting the extent of biodegradation of cDCE. While high pore velocity in the columns induced nearly complete dechlorination of cDCE, medium and low flow velocity failed to dechlorinate cDCE. The microbial community also showed a shift in its composition, suggesting that the flow velocity has an important effect on the microbial community structure. These results indicate the importance of studying the interaction of physical and biological phenomena at the microscopic scale.

Results show that the flow velocity has a strong influence on the environmental conditions for attaining degradation of cDCE. Depending on the flow velocity conditions the culture was either transported through the entire column or remained close to the site of inoculation. In those columns where the culture was transported through the entire column, degradation was complete, which implies that favorable environmental conditions were established. At high flow rate the feeding substrate was not limited, and then cell growth was sustained, leading to a self-sufficient microbial community. Previous studies on the KB-1 culture reported that the community is robust and able to generate acetate and hydrogen for dechlorinating species as well as provide trace nutrients to *Dehalococcoides* (Duhamel and Edwards, 2007). However, perhaps the culture lost its self-sufficient capabilities (shift in microbial community) in the columns with lower flow rate. In those columns the culture was not transported through the entire column, the feeding substrate was limited, and cell growth was not sustained.

Additionally, the flow velocity appears to affect the microbial community composition. DGGE analysis shows that more bands are present in the lane for the high velocity columns, suggesting that the microbial community composition is more diverse in these columns compared to the medium-and low-flow- columns. It may be that the community has to maintain a level of diversity to achieve complete degradation of cDCE to ETH, and that the flow velocity affects the diversity.

The DGGE results show that all the columns contained two bands with high intensity indicating that the flow velocity selected for two different organisms present in high concentrations. Compared to the KB-1 lane the organisms were not present at the inoculation time or were present at low concentrations. These organisms are believed to come from background contamination in the laboratory.

Further studies have to be conducted on the main processes that affect the degradation abilities. It is necessary to measure the microbial structure change in time and space, as well as the changes in velocity and biofilm geometry at the pore scale to be able to study the interrelation between mass transfer and microbial community structure. In that way it could be explained the relationship between physical and biological phenomena.

The column studies presented in this study could be used in the future as a tool to physically alter community composition and study the biological implications. For example, perhaps one could use the velocity to select for certain microbes and evaluate their degradation potential or their role in the community.

CHAPTER VI

SUMMARY AND CONCLUSIONS

In the present study I have (partially) evaluated how micro-scale physical phenomena affect micro-scale biological phenomena. Specifically I have assessed if the pore flow velocity is a controlling process on the degradation potential of contaminants in groundwater. For this purpose, I have developed a mathematical model that links microscopic processes to the macro-scale representation of contaminant transport; I have developed efficient numerical approaches to solve the mathematical model; and I have quantified the influence of groundwater flow velocity on the biodegradation potential of specific contaminants. The target chemicals studied were chlorinated ethenes because they are commonly found in contaminated ground water sites.

The results of this investigation contribute to the bioremediation technology in groundwater with new insights on the effect of flow velocity on degradation potential of chlorinated ethenes.

The biofilm model employed in this study is important for understanding the phenomena that occur at the pore scale or smaller. It includes the following processes: advection and dispersion in the bulk mobile fluid; diffusion and reaction taking place inside a film that coats the surface of the stationary medium; and mass transfer between the bulk mobile fluid and the film coating the stationary medium. This will be useful for evaluating the interaction of physical and biological processes at the microscopic scale. Additionally the mathematical model has a broad application in different problems where reactive transport in porous media is employed.

The biofilm model resulted in a complex system of equations that is challenging to solve. For this purpose, two numerical approaches have been developed to efficiently solve the system of equations. The numerical approach SSA has proven to be computationally efficient when biodegradation kinetics are linear. The SSOSA was used to solve the mathematical model that included non-linear reaction, a more realistic description of reaction inside the biofilm. The SSOSA gives accurate results if the certain conditions are met. Both approaches are attractive because they employ a modular code that can easily be modified to represent the reaction kinetics of different problems. Additionally, they are flexible in terms of numerical techniques that can be used to solve the non-linear diffusion-reaction equation inside the reactive film.

Experimental results showed that the flow velocity is an important factor affecting the degradation potential of cDCE. It may be that the flow velocity affects the environment surrounding the active bacteria. Different bacteria are selected depending on the general conditions. Further investigation is recommended for evaluating the effect of flow velocity on the microbial behavior. For instance, it could be evaluated if the flow velocity affects the following: the morphology of the biofilms; the mass transfer of chemicals inside the biofilm; and the role of bacteria attached to the grains and floating with the mobile liquid.

The main question that inspired the present study is: How do micro-scale *physical* phenomena affect the micro-scale *biological* phenomena? Within this broad question, there are a lot of sub-questions that remain to be studied, for example, the morphology of biofilms, how biofilm morphology depends upon the surface properties

of the aquifer grains, and the role of different bacteria on the consortium for attaining favorable environmental conditions given different physical phenomena.

REFERENCES

Bahr, J.M., and Rubin, J.: Direct comparison of kinetic and local equilibrium formulations for solute transport affected by surface reactions. Water Resour. Res. **23**, 438-452 (1987)

Barry, D.A., Bajracharya, K., and Miller, C.T.: Alternative split operator approach for solving chemical reaction groundwater transport models. Adv. Water Resour. **19**, 261-275 (1996a)

Barry, D.A., Miller, C.T., and Culligan-Hensley, P.J.: Temporal discretisation errors in non-iterative split operator approaches to solving chemical reaction groundwater transport models. J. Contam. Hydrol. **22**, 1-17 (1996b)

Barry, D.A., Miller, C.T., Culligan, P.J., and Bajracharya, K.: Analysis of split-operator methods for non-linear and multi-species groundwater chemical transport models. Math. Comput. Simul. **43**, 331-341 (1997)

Barry, D.A., Bajracharya, K., Crapper, M., Prommer, H., and Cunningham, C.J.: Comparison of split-operator methods for solving coupled chemical non-equilibrium reaction/groundwater transport models. Math. Comput. Simul. **53**, 113-127 (2000)

Barry, D.A., Prommer, H., Miller, C.T., Engesgaard, P., Brun, A., and Zheng, C.: Modelling the fate of oxidisable organic contaminants in groundwater. Adv. Water Resour. **25**, 945-983 (2002)

Baveye, P., and Valochi, A.: An evaluation of mathematical models of the transport of biologically reacting solutes in saturated soils and aquifers. Water Resour. Res. **25**, 1413-1421 (1989)

Bekins, B.A., Warren, E., and Godsy, E.M.: A comparison of zero-order, first-order, and Monod biotransformation models. Ground Water **36**, 261-268 (1998)

Bjerg, P.L., Brun, A., Nielsen, P.H., and Christensen, T.H.: Application of a model accounting for kinetic sorption and degradation to in situ microcosm observations on the fate of aromatic hydrocarbons in an aerobic aquifer. Water Resour. Res. **32**, 1831-1841 (1996)

Bradford, M.A.: A rapid sensitive method for the quantitation of microgram quantities of protein utilizing the principle of protein-dye binding. Anal. Biochem. **72**, 248-254 (1976)

Brusseau, M.L., Jessup, R.E., and Rao, P.S.C.: Modeling solute transport influenced by multiprocess nonequilibrium and transformation reactions. Water Resour. Res. **28**, 175-182 (1992)

Brusseau, M.L., Xie, L.H., and Li, L.: Biodegradation during contaminant transport in porous media: 1. Mathematical analysis of controlling factors. J. Contam. Hydrol. **37**, 269-293 (1999)

Cabirol, N., Jacob, F., Perrier, J., Fouillet, B., and Chambon, P.: Interaction between methanogenic and sulfate-reducing microorganisms during dechlorination of a high concentration of tetrachloroethylene. J. Gen. Appl. Microbiol. **44**, 297-301 (1998)

Carrayrou, J., Mosé, R., and Behra, P.: Operator-splitting procedures for reactive transport and comparison of mass balance errors. J. Contam. Hydrol. **68**, 239-268 (2004)

Celia, M.A., Kindred, J.S., and Herrera, I.: Contaminant transport and biodegradation: A numerical model for reactive transport in porous media. Water Resour. Res. **25**, 1141-1148 (1989)

Chang, C.M., Kemblowski, M.W., and Urroz, G.E.: Transient stochastic analysis of biodegradable contaminant transport: First-order decay. Transp. Porous Med. **35**, 1-14 (1999)

Chiang, C.Y., Dawson, C.N., and Wheeler, M.F.: Modeling of in situ biorestoration of organic compounds in groundwater. Transp. Porous Med. **6**, 667-702 (1991)

Clement, T.P., Sun, Y., Hooker, B.S., and Petersen, J.N.: Modeling multispecies reactive transport in ground water. Groundwater Mon. Rem. **18**, 79-92 (1998)

Crittenden, J.C., Hutzler, N.J., Geyer, D.G., Oravitz, J.L., and Friedman, G.: Transport of organic compounds with saturated groundwater flow: model development and parameter sensitivity. Water Resour. Res. **22**, 271-284 (1986)

Crump, K.: Numerical inversion of Laplace transforms using a Fourier series approximation. J. Assoc. Comput. Mach. **23**, 89-96 (1976)

Cunningham, J.A., Werth, C.J., Reinhard, M., and Roberts, P.V.: Effects of grain-scale mass transport of volatile organics through sediments 1. Model development. Water Resour. Res. **33**, 2713-2726 (1997)

Cunningham, J.A., and Mendoza-Sanchez, I.: Equivalence of two models for biodegradation during contaminant transport in groundwater. Water Resour. Res. **42**, W02416 doi:02410.01029/02005WR004205 (2006)

Cupples, A.M., Spormann, A.M., and McCarty, P.L.: Vinyl chloride and cis-Dichloroethylene dechlorination kinetics and microroganisms growth under substrate limiting conditions. Environ. Sci. Technol. **38**, 1102-1107 (2004)

Duhamel, M., and Edwards, E.A.: Microbial composition of chlorinated ethene-degrading cultures dominated by *Dehalococcoides*. FEMS Microbiol. Ecol. **58**, 538-549 (2006)

Dykaar, B.B., and Kitanidis, P.K.: Macrotransport of a biologically reacting solute through porous media. Water Resour. Res. **32**, 307-320 (1996)

E.P.A.: Bioremediation of chlorinated solvent contaminated groundwater. E.P.A., Washington, D.C. (1998)

E.P.A.: Cleaning up the Nation's waste sites: Markets and technology trends. N.S.C.E.P., Cincinatti (2004)

El-Farhan, Y., Scow, K.M., de Jonge, L.W., Rolston, D.E., and Moldrup, P.: Coupling transport and biodegradation of toluene and trichloroethylene in unsaturated soils. Water Resour. Res. **34**, 437-445 (1998)

Fennel, D.E., Carroll, A.B., Gossett, J.M., and Zinder, S.H.: Assessment of indigenous reductive dechlorination potential at a TCE-contaminated site using microcosms, polymerase chain reaction analysis and site data. Environ. Sci. Technol. **35**, 1830-1839 (2001)

Fry, V.A., and Istok, J.D.: Effects of rate-limited desorption on the feasibility of in situ bioremediation. Water Resour. Res. **30**, 2413-2422 (1994)

Gargiulo, G., Bradford, S., Simunek, J., Ustohal, P., Vereecken, H., and Klumpp, E.: Bacteria transport and deposition under unsaturated conditions: The role of the matrix grain size and the bacteria surface protein. J. Contam. Hydrol. **doi:10.1016/j.jconhyd.2007.01.09** (2007)

Hall, J.A., Mailloux, B.J., Onstott, T.C., Scheibe, T.D., Fuller, M.E., Dong, H., and DeFlaun, M.F.: Physical versus chemical effects on bacterial and bromide transport as determined from on site sediment column pulse experiments. J. Contam. Hydrol. **76**, 295-314 (2005)

He, J., Sung, Y., Dollhopf, M.E., Fathepure, B.Z., Tiedje, J.M., and Loffler, F.E.: Acetate versus hydrogen as direct electron donors to stimulate the microbial reductive dechlorination process at chloroethene-contaminated sites. Environ. Sci. Technol. **36**, 3945-3952 (2002)

Hendrickson, E.R., Payne, J.A., Young, R.M., Starr, M.G., Perry, M.P., Fahnestock, S., Ellis, D.E., and Ebersole, R.C.: Molecular analysis of Dehalococcoides 16S ribosomal DNA from chloroethene-contaminated sites throughout North America and Europe. Appl. Env. Mocrobiol. **68**, 485-495 (2002)

Horn, H., Reiff, H., and Morgenroth, E.: Simulation of growth and detachment in biofilm systems under defined hydrodynamic conditions. Biotechnol. Bioeng. **81**, 608-617 (2003)

Kaluarachchi, J.J., and Morshed, J.: Critical assessment of the operator-splitting technique in solving the advection-dispersion-reaction equation: 1. First-order reaction. Adv. Water Resour. **18**, 89-100 (1995)

Kanney, J.F., Miller, C.T., and Kelley, C.T.: Convergence of iterative split-operator approaches for approximating nonlinear reactive transport problems. Adv. Water Resour. **26**, 247-261 (2003)

Karaa, S., and Zhang, J.: High order ADI method for solving unsteady convection-diffusion problems. J. Comput. Phys. **198**, 1-9 (2004)

Karapanagioti, H.K., Gossard, C.M., Strevett, K.A., Kolar, R.L., and Sabatini, D.A.: Model coupling intraparticle diffusion/sorption, nonlinear sorption and biodegradation processes. J. Contam. Hydrol. **48**, 1-21 (2001)

Karki, K.C., and Patankar, S.V.: Application of the partial elimination algorithm for solving the coupled energy equations in porous media. Num. Heat Transfer, Part A **45**, 539-549 (2004)

Kasten, P.R., Lapidus, L., and Amundson, N.R.: Mathematics of adsorption in beds, V, Effect of intra-particle diffusion in flow systems in fixed beds. J. Phys. Chem. **56**, 683-688 (1952a)

Kasten, P.R., Lapidus, L., and Amundson, N.R.: Mathematics of adsorption in beds: V, Effect of intraparticle diffusion in flow systems in fixed beds. J. Phys. Chem. **56**, 683-688 (1952b)

Lanser, D., and Verwer, J.G.: Analysis of operator splitting for advection-diffusion-reaction problems from air pollution modelling. J. Comput. Applied Math. **111**, 201-216 (1999)

Li, L., Yolcubal, I., Sandrin, S., Hu, M.Q., and Brusseau, M.L.: Biodegradation during contaminant transport in porous media:3. Apparent condition-dependency of growth-related coefficients. J. Contam. Hydrol. **50**, 209-223 (2001)

MacQuarrie, K.T., Sudicky, E.A., and Frind, E.O.: Simulation of biodegradable organic contaminants in groundwater, 1: Numerical formulation in principal directions. Water Resour. Res. **26**, 207-222 (1990)

MacQuarrie, K.T.B., and Sudicky, E.A.: Multicomponent simulation of wastewater derived nitrogen and carbon in shallow unconfined aquifers, 1, Model formulation and performance. J. Contam. Hydrol. **47**, 53-84 (2001)

Major, D.W., McMaster, M.L., Cox, E.E., Edwards, E.A., Dworatzev, S.M., Hendrickson, E.R., Starr, M.G., Payne, J.A., and Buonamici, L.W.: Field demonstration of successful bioaugmentation to achieve dechlorination of tetrachloroethene to ethene. Environ. Sci. Technol. **36**, 5106-5116 (2002)

Maymo-Gatell, X., Nijenhuis, I., and Zinder, S.H.: Reductive dechlorination of cis-1,2 Dichloroethene and vinyl chloride by Dehaloccoides ethenogens. Environ. Sci. Technol. **35**, 516-521 (2001)

McCarty, P.L.: Breathing with chlorinated solvents. Science **276**, 1521-1526 (1998)

Mendoza-Sanchez, I., and Cunningham, J.A.: Efficient algorithm for modeling transport in porous media with mass exchange between mobile fluid and reactive stationary media. Transp. Porous Med. **68**, 285-300 (2007)

Michaelis, L., and Menten, M.L.: Die Kinetic der Invertinwirkung. Biochem. Z. **49**, 333-369 (1913)

Miller, C.T., and Webber, W.J.: Sorption of hydrophobic organic pollutants in sturated soil systems. J. Contam. Hydrol. **1**, 243-261 (1986)

Miralles-Wilhem, F., and Gelhar, L.W.: Stochastic analysis of transport and decay of a solute in heterogeneous aquifers. Water Resour. Res. **32**, 3451-3459 (1996)

Molz, F.J., Widdowson, M.A., Benefield, L.D.: Simulation of microbial growth dynamics coupled to nutrient and oxygen transport in porous media. Water Resources Research **22**, 1207-1216 (1986)

Monod, J.: The growth of bacterial cultures. Annu. Rev. Microbiol. **3**, 371-394 (1949)

Morshed, J., and Kaliarachchi, J.J.: Critical assessment of the operator-splitting technique in solving the advection-dispersion-reaction equation: 2.Monod kinetics and coupled transport. Adv. Water. Resour. **18**, 101-110 (1995)

Murphy, E.M., Ginn, T.R., Chilakapati, A., Resch, C.T., Phillips, J.L., Wietsma, T.W., and Spadoni C.M.: The influence of physical heterogeneity on microbial degradation and distribution in porous media. Water Resour. Res. **33**, 1087-1103 (1997)

N.A.S.: Water for the future: The West Bank of Gaza Strip, Israel, and Jordan. The National Academy Press, Washington, D.C. (1999)

N.A.S.: Watershed management for potable water supply: Assessing the New York City strategy National Academies Press, Washington, D.C. (2000)

N.R.C.: Our common journey: A transition toward sustainability. National Academy of Sciences, Washington, D.C. (2000)

Odencratz, J., Valocchi, A.J., and Rittman, B.E.: 1990, Modeling two-dimensional solute transport with different biodegradation kinetics, *Petroleum hydrocarbons and organic chemicals in groundwater: Prevention, prediction and restoration*, American Petroleum Institute, Houston, Texas.

Okoh, A.I., and Trejo-Hernandez, M.R.: Remediation of petroleum hydrocarbon polluted systems: Exploiting the bioremedation strategies. African J. Biotechnol. **5**, 2520-2525 (2006)

Overmiere, A., Lens, P., and Verstraete, W.: Mass transfer limitation of sulfate in methanogenic aggregates. Biotechnol. Bioeng. **44**, 387-391 (1994)

Oya, S., and Valocchi, A.J.: Characterization of traveling waves and analytical estimation of pollutant removal in one-dimensional subsurface bioremediation modeling. Water Resour. Res. **33**, 117-1127 (1997)

Peaceman, D.W., and Rachford, H.H.: The numerical solution of parabolic elliptic differential equations. J. Soc. Ind. App. Math. **3**, 28-41 (1955)

Phanikumar, M.S., and McGuire, J.T.: A 3D partial-equilibrium model to simulate coupled hydrogeochemical, microbiological, and geochemical processes in subsurface systems. Geophys. Res. Letters (2004)

Pinder, G.F., and Gray, W.G.: Finite element simulation in surface and subsurface hydrology, pp. 23-25. Academic Press, New York (1977).

Quindoz, H.A., and Valocchi, A.J.: Stochastic analysis if the transport of kinetically sorbing solutes in aquifers with randomly heterogeneous hydraulic conductivity. Water Resour. Res. **29**, 3227-3240 (1993)

Rasmuson, A., and Neretniecks, I.: Migration of radionuclides in fissured rock: The influence of micropore diffusion and longitudinal dispersion. J. Geophys. Res. **86**, 3749-3758 (1981)

Rittmann, B.E., and McCarty, P.L.: Model of steady-state-biofilm kinetics. Biotechnol. Bioeng. **22**, 2343-2357 (1980)

Rittmann, B.E.: The significance of biofilms in porous media. Water Resour. Res. **29**, 2195-2202 (1993)

Rittmann, B.E., and McCarty, P.L.: Environmental biotechnology: Principles and Applications. New York (2001)

Roberts, P.V., Goltz, M.N., and Mackay, D.M.: A natural gradient experiment on solute transport in a sand aquifer .3. Retardation estimates and mass balances for organic solutes. Water Resources Research **22**, 2047-2058 (1986)

Rosen, J.B.: Kinetics of a fixed-bed system for solid diffusion into spherical particles. J. Chem. Phys. **20**, 2047-2058 (1952)

Sandrin, S., Jordan, F.L., Maier, R.M., and Brusseau, M.L.: Biodegradation during contaminant transport in porous media: 4. Impact of microbial lag and bacterial cell growth. J. Contam. Hydrol. **50**, 225-242 (2001)

Singleton, I.: Microbial metabolism of xenobiotics: Fundamental and applied research. J. Chem. Tech. Biotechnol. **59**, 9-23 (1994)

Suidan, M.T., and Wang, Y.T.: Unified analysis of biofilm kinetics. J. Env. Eng. **111**, 634-646 (1985)

Suflita, J.M., Gibson, S.A., and Beeman, R.E.: Anaerobic biotransformation of pollutant chemicals in aquifers. J. Ind. Microbiol. **3**, 179-194 (1988)

Sun, A.K., Hong, J., and Wood, T.K.: Modeling trichloroethylene degradation by a recombinant pseudomonad expresing toluene ortho-monooxygenase in a fixed-film bioreactor. Biotechnol. Bioeng. **59**, 40-51 (1998)

Sun, Y., Lu, X., Petersen, J.N., and Buscheck, T.A.: An analytical solution of tetrachloroethylene transport and biodegradation. Transp. Porous Med. **55**, 301-308 (2004)

Sun, Y., and Lu, X.: A screening model for evaluating the degradation and transport of MTBE and other fuel oxygenates in groundwater. Transp. Porous Med. **60**, 75-88 (2005)

Tsai, H.-H., Ravindran, V., and Pirbazari, M.: Model for predicting the performance of membrane dioadsorber reactor process in water treatment applications. Chem. Eng. Sci. (2005)

Valocchi, A.J., and Malmstead, M.: Accuracy of operator splitting for advection-dispersion-reaction problems. Water Resources Research **28**, 1471-1476 (1992)

Vemuri, V., and Karplus, W.J.: Digital computer treatment of partial differential equations. Prentice Hall, New Jersey (1981)

Vencelides, Z., Sracek, O., and Prommer, H.: Modelling iron cycling and its impact on electron balance at a petroleum hydrocarbon contaminated site in Hnevice, Czech Republic. J. Contam. Hydrol. **89**, 270-294 (2007)

Villadsen, J.V., and Stewart, W.E.: Solution of boundary-value problems by orthogonal collocation. Chem. Eng. Sci. **22**, 1483-1501 (1967)

Williamson, K., and McCarty, P.L.: A model of substrate utilization by bacterial films. J. Water Pollut. Control Fed. **48**, 9-24 (1976)

Yang, Y., and McCarty, P.L.: Competition for hydrogen within a chlorinated solvent dehalogenating anaerobic mixed culture. Environ. Sci. Technol. **32** 3591-3597 (1998)

Zhang, K., and Woodbury, A.D.: A Krylov finite element approach for multi-species contaminant transport in discretely fractured porous media. Adv. Water. Resour. **25**, 705-721 (2002)

VITA

Name:	Itza Mendoza Sanchez
Address:	Escuela Superior de Ingeniería y Arquitectura, Instituto Politécnico Nacional, Mexico City, Mexico
Email Address:	itzam@hotmail.com
Education:	B.A., Civil Engineering, Instituto Politécnico Nacional, Mexico City, Mexico, 1999 M.S., Civil Engineering, Texas A&M University, 2002 Ph.D., Civil Engineering, Texas A&M University, 2007